Yield Point Phenomena in Ultrafine Grained Materials

2016

Si Gao

Yield Point Phenomena in Ultrafine Grained Materials

by

Si Gao

A Dissertation submitted to Kyoto University for

Doctor of Philosophy (PhD)

Department of Materials Science and Engineering

Graduate School of Engineering

Kyoto University

2016

Contents

Chapter 1 Background and purpose

1.1 Continuous yielding and discontinuous yielding in metallic materials

Plastic yielding normally starts uniformly when the metallic materials are subjected to tensile or compressive load, which is called continuous yielding. In the tensile or compression stress-strain curve the continuous yielding is characterized by a smooth transition from the elastic region to the plastic region, followed by a steadily strain hardening region before necking and failure occurs, as shown in **Figure 1.1 (a)**. In contrast to the continuous yielding, the yield point phenomena (also refer to as discontinuous yielding) have been found in some materials, which exhibits an abrupt transition from the elastic to plastic region with a drop of stress followed by a region of constant nominal stress or stress fluctuations, as can be seen in **Figure 1.1 (b)**.

Within the yield plateau after the yield-drop in the discontinuous yielding, plastic deformation takes place non-uniformly, by the formation and propagation of the localized deformation bands, - so-called Lüders band, as shown in **Figure 1.2 (a) and (b)**. The stress at the peak just before the load drop is called upper yield stress and the stress corresponds to the plateau is called lower yield stress. After the Lüders bands have propagated and spread the whole specimen gage, the normal strain hardening begins uniformly.

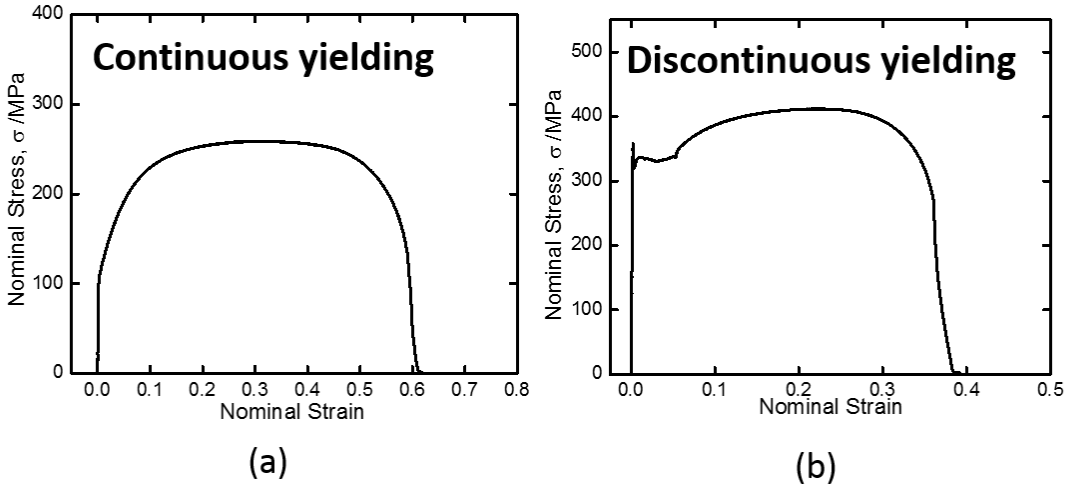

Figure 1.1 Illustrations of the tensile stress-strain curves exhibiting (a) continuous yielding and (b) discontinuous yielding.

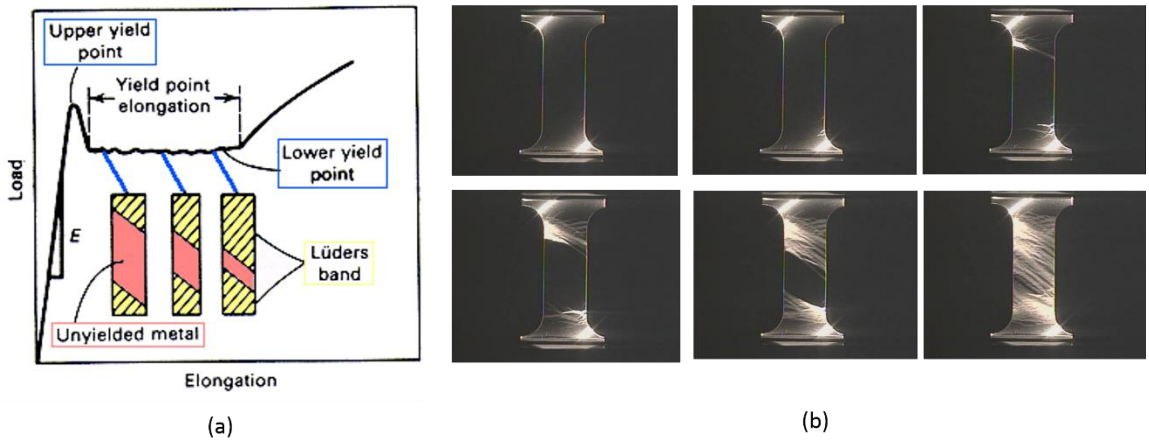

Figure 1.2 (a) An illustration of the tensile stress-strain curve exhibiting yield drop and propagation of Lüders band, and [1] (b) The Lüders band propagation during a tensile test in a low carbon steel, captured by a camera [2].

The yield point phenomena are usually found in low carbon steels, some copper alloys and aluminum alloys. It was firstly explained by Cottrell and Bilby [3] by pointing out that the yield point phenomena were attributed to the dislocation locking by solute atoms in the materials. The solute atoms, such as interstitial C and N in steels, or substitutional Zn in copper alloys and Mg in aluminum alloys having their strain fields around them, tend to segregate to the strain field of dislocations so that the total strain energy can be reduced. This leads to the formation of the atmosphere of the solute atoms around the dislocations, so-called Cottrell atmosphere, as illustrated in **Figure 1.3**. When the materials is subjected to the external load, a high stress is needed to release the dislocations from the Cottrell atmosphere which corresponds to the upper yield stress. As the dislocations have been "freed" from the atmosphere, the stress required to move dislocations is much smaller than that to release them, resulting in the yield drop. The lower yield stress corresponds to the stress required to move dislocations.

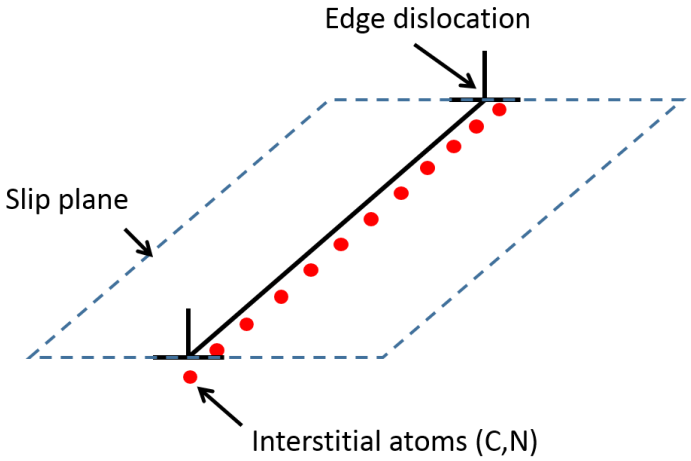

Figure 1.3 Illustration of interstitial solute atoms segregating on an edge dislocation lying on the slip plane in a low carbon steel.

Inspired by the fact that yield point phenomena were also found in ionic crystals and even in whisker, Hahn [4] proposed another mechanism to explain the yield point phenomena by the density of mobile dislocations. Based on Johnston and Gilman's work on LiF crystals [5], the relation between the external stress and dislocation velocity during plastic deformation of the crystalline materials can be described in following equation:

$$\nu = \left(\frac{\tau}{\tau_0}\right)^n \tag{1.1}$$

where ν is the velocity of dislocations, τ the resolved shear stress applied, τ_0 the resolved shear stress corresponding to unit velocity of dislocations, and n is a material constant. Meanwhile, the plastic strain rate of the material is expressed by the well-known Taylor equation:

$$\dot{\varepsilon} = b\rho_m\nu \tag{1.2}$$

where $\dot{\varepsilon}$ is the plastic strain rate, b the burgers vector and ρ_m the mobile dislocation density. By combining equations (1.1) and (1.2), it is seen that the mobile dislocation density is inverse proportional to the dislocation velocity at a constant plastic strain rate. For a material having small amount of initial mobile dislocation density, a large external stress is required to move the mobile dislocations at a high velocity in order to maintain the plastic strain rate. As the mobile dislocation density increases by multiplication with the plastic strain, the dislocation velocity will decrease, resulting in a lower external stress. Therefore, a sudden multiplication of the dislocations (an abrupt increase in ρ_m) will result in a drop of the external stress— the yield point phenomena.

In low carbon steels, the amount of initial mobile dislocations is sufficiently small due to the dislocations locked by interstitial atoms. In the whisker having little amount of lattice

defects, the initial mobile dislocation density is extremely small, resulting in a very high yield stress for nucleating dislocations and a dramatic yield drop phenomena during the tensile test. The ionic crystal usually have a very small *n* because of the high Peierls-Nabarro stress, thus it is also common to observe the yield point phenomena in the ionic crystalline. The effect of the mobile dislocation density on the yielding behavior of a low carbon steel is well captured by Hahn's model, as illustrated in **Figure 1.4**. It is seen that the difference between the upper yield stress and the lower yield stress becomes significant as the initial mobile dislocation decreases from $10^8 cm^{-2}$ to $10^2 cm^{-2}$, indicating that a more prominent yield point phenomenon can occur by decreasing the initial mobile dislocation density.

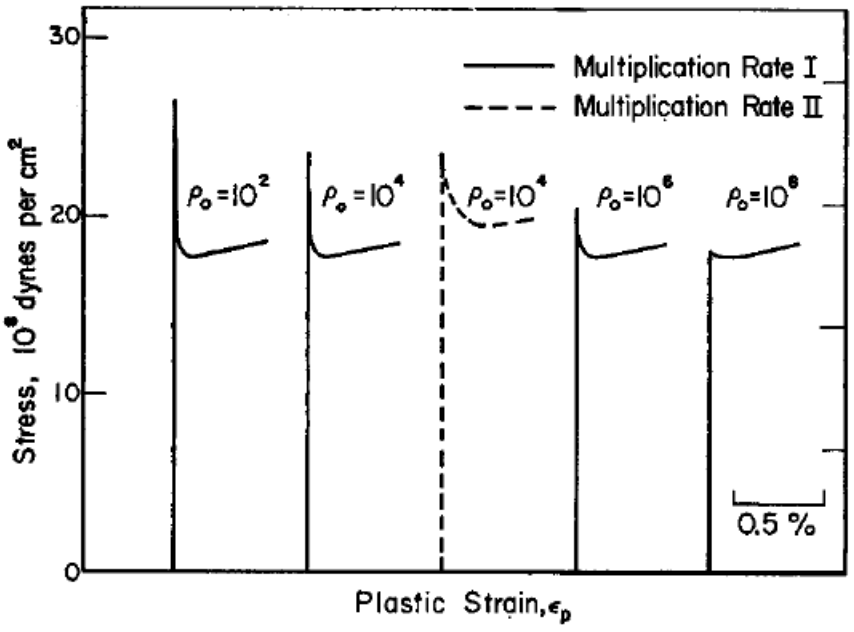

Figure 1.4 Calculated stress-strain curves by Hahn's model showing the influence of the initial dislocation density on the yield drop in a low carbon steel. ρ_0 is the initial dislocation density in an unit of cm^{-2} [4]. The corresponding initial dislocation density ρ_0 is $10^2 cm^{-2}$, $10^4 cm^{-2}$, $10^4 cm^{-2}$, $10^6 cm^{-2}$, $10^8 cm^{-2}$ from left hand side to right hand side, respectively.

1.2 Explanation of the Lüders band deformaton

Besides the above mentioned materials, the Lüders band deformation was also well-known to occur in shape memory alloys (SMA) [6], whose deformation mechanism is not based on the dislocations slip but the martensitic transformation. Moreover, in recent decades researchers realized that a variety of materials can exhibit Lüders band deformation, such as metallic glass [7], intermetallic compounds [8], even polymers [9] and rocks [10]. Therefore, it is believed that the explanation of this material phenomenon should not be only limited to the dislocation based mechanism. A general explanation of the Lüders band deformation is required from the aspect of the materials mechanics. Van Rooyen [11] realized that in order to propagate a Lüders band, the local stress at the head of the Lüders band should be equal to the upper yield stress, as illustrated in **Figure 1.5**. The local stress at the region right behind the Lüders band front is even lower than the lower yield stress because this region has just yielded and not yet being strain-hardened. At the tail of the Lüders band, the material has been gradually strain hardened to the level of the lower yield stress. Such a mechanically unstable state will facilitate the propagation of the band. Under those assumptions, Van Rooyen also depicted the strain distribution at the Lüders band in a low carbon steel.

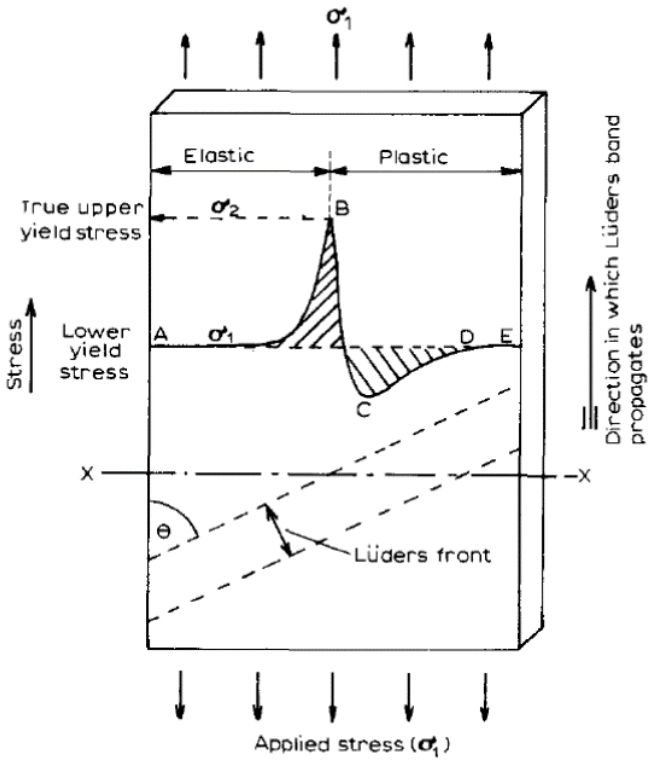

Figure 1.5 Schematic illustration of the transverse stress distribution across the Lüders band [11].

Schwab [12] further more emphasized that the true material behavior (the upper yield stress, lower yield stress and Lüders deformation) is different from what we observed in the tensile test. In his FEM modelling work, the true mechanical behavior of the material was assumed to follow a "hardening-softening-hardening" type, as shown in **Figure 1.6**. The appearance of the Lüders band deformation is just due to hardening-softening-hardening behavior of the material. By using the FEM analysis, the strain and stress distribution at the Lüders band has been well explained, as shown in **Figure 1.6 (b)**. Schwab emphasized that any materials having the intrinsic "hardening-softening-hardening" type stress-strain behavior should exhibit Lüders band deformation, which can explain the universality of this interesting mechanical behavior in various kinds of materials.

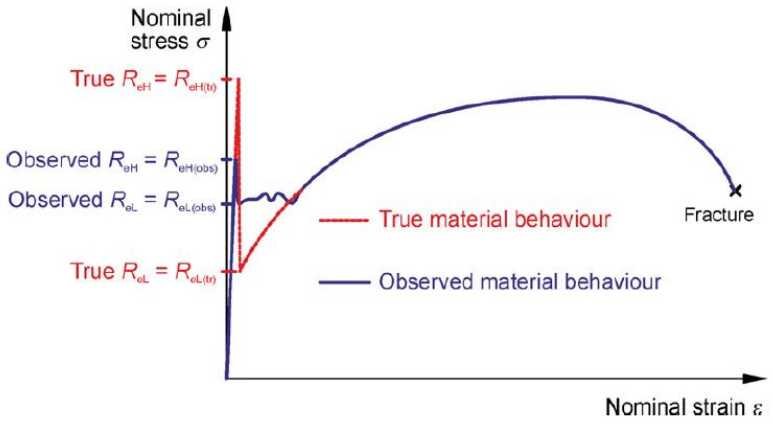

(a)

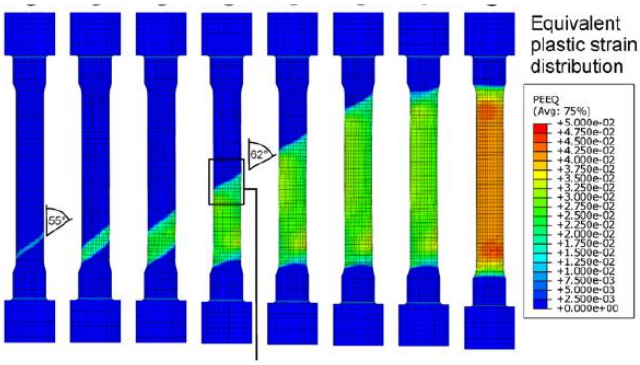

(b)

Figure 1.6 (a) Schematic representation of the observed stress-strain curve and the intrinsic true stress-strain behavior of the low-carbon steel, and (b) the propagation of Lüders band, simulated by the FEM analysis [12].

1.3 Yield point phenomena and related mechanical properties in ultra-fine grained materials

According to the well-known Hall-Petch relationship, the yield stress of polycrystalline materials increases with decreasing the average grain size [13] [14]:

$$\sigma_y = \sigma_0 + k_y d^{-1/2} \tag{1.3}$$

where σ_y is the yield stress, σ_0 the friction stress, k_y a constant (Hall-Petch slope), and d the mean grain size. Significant grain size refinement could be recently achieved by severe plastic deformation (SPD) processes [15], which has led to a very high strength according to the Hall-Petch relationship. Those materials having mean grain sizes smaller than 1~2 μm are called ultra-fine grained (UFG) materials. The UFG materials have superior strength and toughness due to the extreme small grain size. However, they usually exhibit a poor tensile ductility, especially a small uniform elongation, which greatly limits their applications in the industry.

The uniform elongation of the material during tensile test is determined by the plastic instability condition, typically like the Considére criteria for strain-rate non-sensitive materials[16]:

$$\sigma \geq \frac{\partial \sigma}{\partial \varepsilon} \tag{1.4}$$

where σ is the flow stress, and ε the corresponding true strain. According to the Considere criteria, plastic instability (necking) will occur when the flow stress becomes smaller than the strain hardening rate ($\partial\sigma/\partial\varepsilon$). It is believed that the UFG materials have poor capability

of the strain hardening, thus the Considére criteria is easily satisfied at a small strain during the tensile test, so-called early plastic instability. However, the effect of the yielding behavior on the tensile elongation in the UFG material is more or less neglected. Many studies showed that as the grain size became smaller than 1~3 μm, the materials exhibit the yield point phenomena immediately followed by necking, as shown in **Figure 1.7** [17].

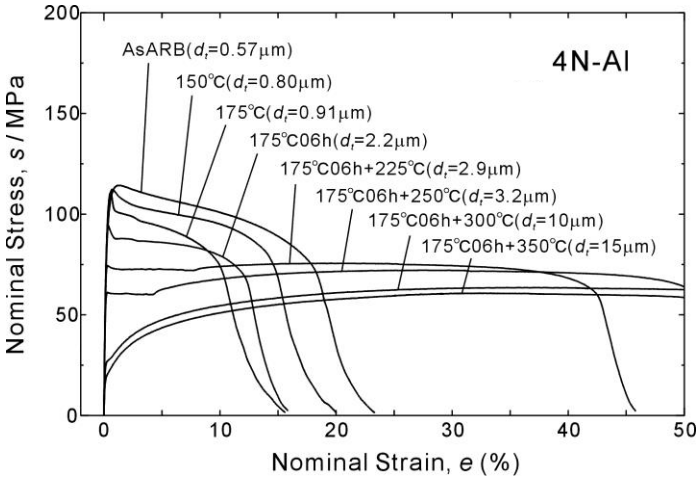

Figure 1.7 Stress-strain curves of the 4N-Al having different grain sizes, fabricated by the ARB and subsequent annealing processes [17].

In recent years the yield point phenomena have been frequently found in many UFG materials, although it was well-known that their coarse grain-sized counterpart exhibit continuous yielding during the tensile test. The variety of those UFG materials spans all the common lattice structures (BCC [18], FCC [17] and HCP [19]), pure metals and alloys [20][21][22], in which the dislocation locking mechanism does not usually occur. They are fabricated by various kinds of processes including SPD processes, powder metallurgy [23] or even conventional deformation and heat treatment processes [24]. Therefore, it is reasonable to consider that the yield point phenomena in the UFG materials do not depends on specific processing methods or on specific materials having strong dislocation locking

effects, but are the universal mechanical behavior in all of the materials having fine grain sizes. In addition, it has been found that sometimes the Hall-Petch slope k*y* is significantly larger in the UFG material than that in their coarse grain sized counter-part [17], although it is believed that the k_y should be a constant for a specific material and does not depend on the grain size. The increase of the k_y value shows a quite synchronization with the appearance of the yield point phenomena when the grain size decreases to the UFG range, but the reason is still unclear.

Several explanations have been proposed to explain the yield point phenomena in the UFG materials. The most frequently used explanation is based on Hahn's mobile dislocation density theory. It is believed that the mobile dislocation density in the UFG material is inherently small, especially after sufficient annealing process [25]. The scarcity of the mobile dislocations can be realized from two aspects: firstly, many experimental results have showed that fully annealed UFG materials have very "clean" microstructures with only few dislocations being observed in the grain interior by transmission electron microscopy (TEM), as can be seen in an ultra-low carbon interstitial free (IF) steel [26] and commercial purity Al [17] shown in **Figure 1.8**. In most cases, even though the dislocation density is comparable between the coarse grain sized specimen and the UFG specimen, the number of dislocations per grain is still significantly smaller in the UFG specimen than in the coarse-grained counterparts.

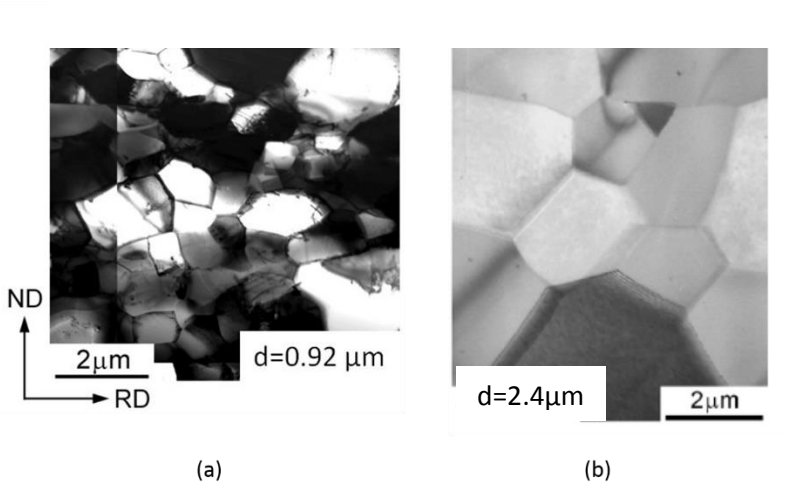

Figure 1.8 TEM micrographs showing the "clean" microstructures in the (a) IF steel [26] and (b) 4N-Al [17] having fine grain sizes, fabricated by ARB and subsequent annealing process. The mean grain sizes are indicated in the figure.

Secondly, it is expected that not only the mobile dislocation density but also the dislocation sources is inherently small in the UFG materials [25]. In the polycrystalline material, dislocation multiplication takes place mainly by the activation of the Frank-Read source. The Frank-Read source can be formed by the double cross-slip of dislocations, as shown in **Figure 1.9 (a)**, or by a portion of an immobile dislocation which is impeded by other forest dislocations, as shown in **Figure 1.9 (b)**. In the UFG materials the very small grain interior space greatly limits the possibilities of the double cross-slip or the interactions between dislocations, so that the density of dislocation sources is considered to be very small. Therefore, in the UFG materials a high external stress is needed to drive those mobile dislocations or to activate the dislocation sources to accommodate the plastic strain rate at the beginning of the tensile test, and then the stress will decrease as the mobile dislocation density increases, leading to the yield point phenomena.

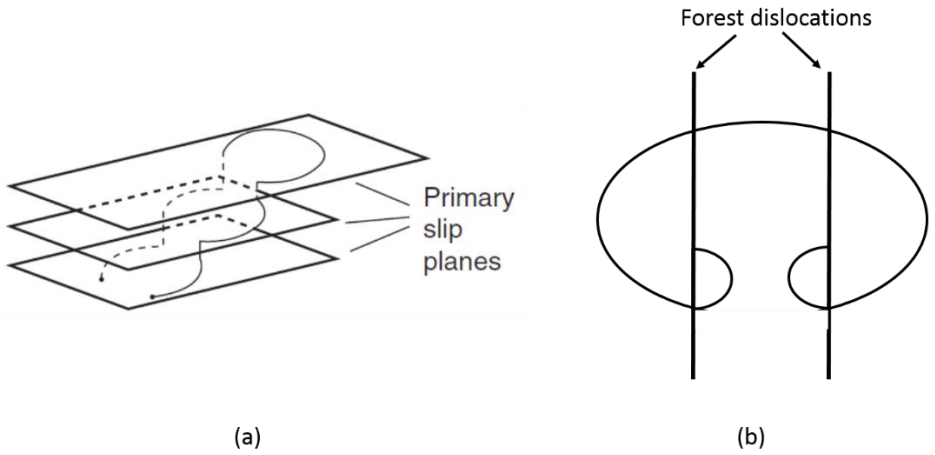

Figure 1.9 Illustration of the dislocation multiplication by (a) double cross-slip and (b) dislocation segment acting as a Frank-Read source.

On the other hand, Yu [27] proposed that mobile dislocations were largely impeded and absorbed by the excess grain boundaries in the UFG materials. As a result, a high stress is necessary to drive mobile dislocations at a high velocity to accommodate the plastic strain rate at the beginning of the tensile test. More importantly, the absorption of dislocations at grain boundaries also causes an enhanced dynamic recovery rate and a reduction in the strain hardening rate. At a critical strain stage during the tensile test, the decrease in the strain hardening rate will cause a stress drop. It is noted that the dynamic recovery by the dislocation absorption at grain boundaries is the reason for the stress drop in Yu's proposal, which is totally different from Hahn's theory.

The previously described explanations are more or less based on the Hahn's mobile dislocation density theory. However, both of them are not capable of explaining a very important experiment results: the directionality of the yield point phenomena. It is well-known that in low carbon steels, when the tensile test was stopped during straining and a low temperature heat treatment is given the specimen, the yield point will appear again in

the subsequent tensile deformation of the specimen again. It is the called strain aging effect and was well explained by Cottrell's dislocation locking mechanism. However, Orawan [28] found that in a low carbon steel the yield point did not appear if the re-strain direction was reversed to the pre-strain direction after aging treatment, as shown in **Figure 1.10**. According to Cottrell's theory, the strain aging effect is expected even if the direction is reversed, as the impurity atoms will re-segregate on dislocations by the aging treatment. Orawan's result seemed contradictory to Cottrell's theory, and because of that reason it had not been published until 2002. In recent years, the directionality of the yield point phenomena was studied by Taupin [29] and it is believed that the disappearance of the yield point in reverse straining is due to the internal stress.

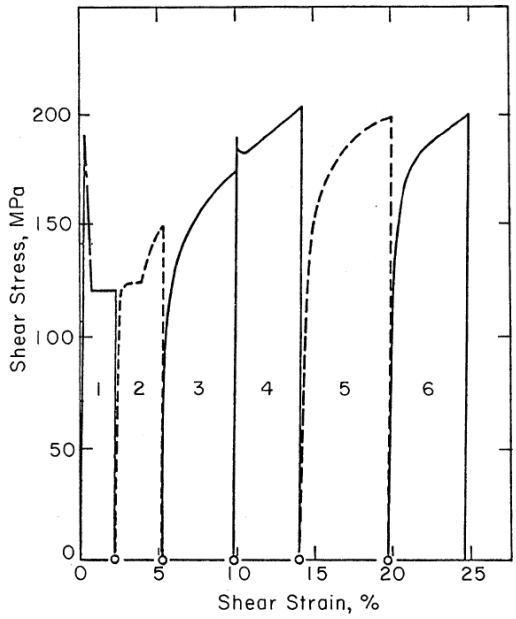

Figure 1.10 Stress-strain curves in torsion test showing the absence of the yield point phenomena even after ageing treatment when the strain direction was reversaled. (1: Forward straining, 2: aging + reverse straining, 3: aging + reverse straining after 2, 4: aging +forward straining after 3, 5: aging + reverse straining after 4, 6: aging +forward straining after 5) [28]

Another explanation for the yield point is related to the strain hardening of the UFG materials. Sinclair [30] proposed a physical model to explain the strain hardening behavior of the UFG copper. In his model, the strain hardening of the polycrystalline copper was composed of mainly two parts: the back-stress hardening coming from dislocation pile-ups and the dislocation forest hardening. At a small strain, dislocations are blocked by grain boundaries and piled up at grain boundaries, developing a back stress. The back stress increases with increasing the plastic deformation at small strains and the degree of the back stress is inversely proportional to the mean grain size. As the plastic strain further increases, the stress field given by the dislocation pile-up is "screened" by the dislocations in the adjacent grain or on the other slip systems, resulting in a decrease in the back stress. The increasing and decreasing of the back stress at small strain becomes significantly large when the mean grain size is decreased from a coarse grain size to a fine grain size, as illustrated in **Figure 1.11**. As a result, a dramatic drop in the tensile stress – a yield point phenomenon can be expected. It is noted that according to Sinclair's model, a large internal stress (back stress) can be expected in the UFG materials, which is supported by several experimental results [31,32]. However, systematic study on the back stress in the UFG materials has not been done yet.

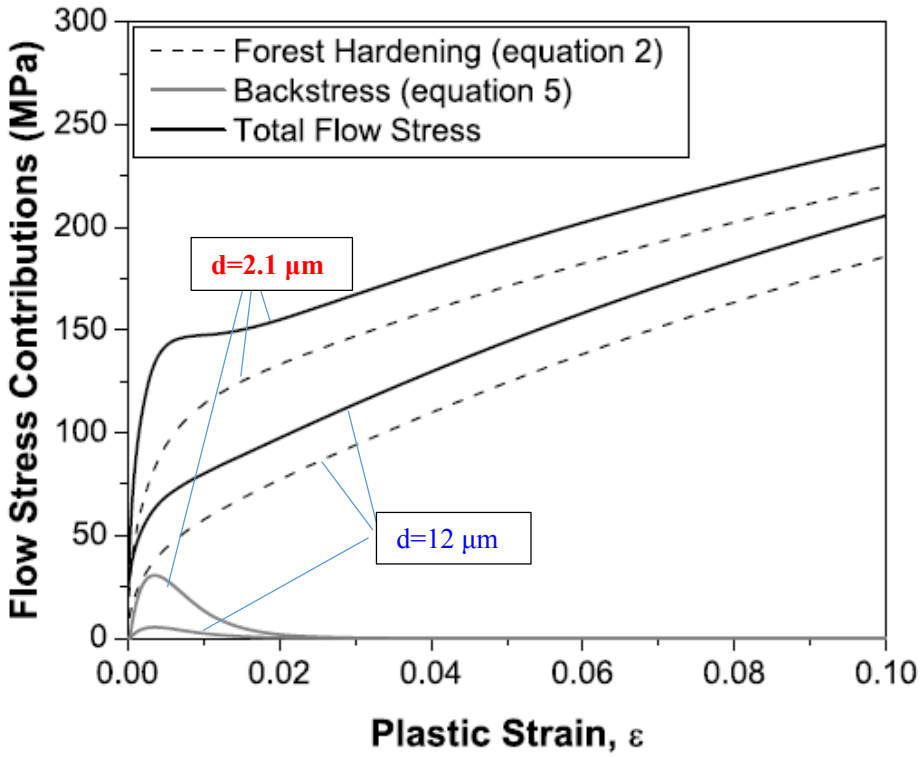

Figure 1.11 Evolution of the back stress, forest hardening and total flow stress of the copper with d=2.1 μm and d=12 μm, calculated by Sinclair's model [30].

1.4 Purpose of the present study

The main purpose of the present study is to systematically investigate the yield point phenomena in materials with a special focus on the UFG microstructures, in order to understand the grain size effect on the yielding behavior, the relation between the yielding behavior and the Hall-Petch relationship and the mechanism of the yield point phenomena in the UFG materials universally.

1.5 Outline of the dissertation

The thesis is composed of five chapters.

Chapter 1 introduces the background and purpose of the study.

In chapter 2, the effect of interstitial impurity atoms on the yielding behavior in an ultra-low carbon steels (high purity iron) is studied. It is shown that the ultra-low carbon steel with the same mean grain size can exhibit either continuous yielding or discontinuous yielding in the tensile test by simply changing the cooling process after annealing. The mechanism of the discontinuous yielding is discussed based on the dislocation locking mechanism by interstitial atoms such as carbon and nitrogen. Relation between the yielding behavior and Hall-Petch relationship is also discussed.

Chapter 3 studies the grain size effect on the yielding behavior in an interstitial free (IF) steel with various mean grain sizes from conventional range (larger than tens micron-meters) to ultrafine range, which is fabricated by the ARB process and subsequent annealing. It ss found that discontinuous yielding appeares in the IF steel when the mean grain size is decreases down to smaller than 2 μm. Meanwhile, the yield stress deviates from the Hall-Petch relationship extrapolated from the conventional grain size range and the uniform elongation of the material abruptly decreases to less than 2%. Digital image correlation (DIC) analysis shows that it is because the Lüders strain is larger than the uniform strain in the fine grained specimens. It is shown that the discontinuous yielding plays an important role in the elongation of the fine grained IF steel.

In Chapter 4 the mechanism of the yield point phenomena in UFG 2N-Al is investigated by measuring the back stress in Bauschinger tests. Bauschinger tests are conducted by

tension-compression for dumbbell-typed 2N-Al specimens, fabricated by the ECAP and annealing process. It is concluded that the yield point phenomena in UFG Al are attributed to the increase-decrease-increase of the back stress, given by the dislocation pile-up.

Chapter 5 summarizes the conclusion and achievements of the PhD thesis.

References

[1] Mechanics of Materials, 4th Ed., by J.M. Gere and S.P. Timoshenko, PWS Publishing, 1997, pp. 835-42.

[2] https://vimeo.com/4586024

[3] Cottrell A, Bilby B (1949) Dislocation theory of yielding and strain ageing of iron. Proc.Phys. Soc. A 49: 49-62.

[4] Hahn GT (1962) A model for yielding with special reference to the yield-point phenomena of iron and related bcc metals. Acta Metall 10: 727-738.

[5] Johnston, W. G., & Gilman, J. J. (1959). Dislocation Velocities, Dislocation Densities, and Plastic Flow in Lithium Fluoride Crystals. *Journal of Applied Physics*, *30*(2), 129.

[6] Sittner, P., Liu, Y., & Novak, V. (2005). On the origin of Lüders-like deformation of NiTi shape memory alloys. *Journal of the Mechanics and Physics of Solids*, *53*(8), 1719–1746.

[7] Sergueeva, V., Mara, N., Kuntz, J. D., Lavernia, E. J., & Mukherje, K. (2005). Shear band formation and ductility in bulk metallic glass. *Philosophical Magazine*, *85*(23), 2671–2687.

[8] Kuwabara, T., Kurishita, H., & Hasegawa, M. (2006). Development of an ultra-fine grained V–1.7mass% Y alloy dispersed with yttrium compounds having superior ductility and high strength. *Materials Science and Engineering: A*, *417*(1-2), 16–23.

[9] Li, J. C. M. (1984). Behavior and properties of shear bands. *Polymer Engineering and Science*, *24*(10), 750–760.

[10] Olsson, A. (2000). Origin of Liiders ' bands in deformed rock, *105*, 5931–5938.

[11] G. Van Rooyen,. (1971). Basic factors which influence the Lüders strain during discontinuous yielding. *Materials Science and Engineering*. Retrieved from http://www.sciencedirect.com/science/article/pii/0025541671900590

[12] Schwab, R., & Ruff, V. (2012). On the nature of the yield point phenomenon. *Acta Materialia*.

[13] Hall EO (1951) The deformation and ageing of mild steel. Proc.Phys. Soc. B 64: 747-753.

[14] Petch NJ (1953) The cleavage strength of polycrystals. J Iron Steel Inst 174: 25-28.

[15] Sabirov, I., Murashkin, M. Y., & Valiev, R. Z. (2013). Nanostructured aluminium alloys produced by severe plastic deformation: New horizons in development. *Materials Science and Engineering: A*, *560*, 1–24.

[16] M. Mayers, Mechanical behavior of materials, Cambridge University Press, 2009.

[17] Kamikawa, N., Huang, X., Tsuji, N., & Hansen, N. (2009). Strengthening mechanisms in nanostructured high-purity aluminium deformed to high strain and annealed. *Acta Materialia*, *57*(14), 4198–4208.

[18] Tsuji N, Ito Y, Saito Y, Minamino Y (2002) Strength and ductility of ultrafine grained aluminum and iron produced by ARB and annealing. Scripta Mater 47: 893-899.

[19] Li, Z., Fu, L., Fu, B., & Shan, A. (2013). Yield point elongation in fine-grained titanium. *Materials Letters*, *96*, 1–4.

[20] Fu, L., Li, Z., Wang, H., Wang, W., & Shan, A. (2012). Lüders-like deformation induced by delta-ferrite-assisted martensitic transformation in a dual-phase high-manganese steel. *Scripta Materialia*, *67*(3), 297–300.

[21] Hodge, a. M., Wang, Y. M., & Barbee, T. W. (2008). Mechanical deformation of high-purity sputter-deposited nano-twinned copper. *Scripta Materialia*, *59*(2), 163–166.

[22] Huang, C. X., Hu, W. P., Wang, Q. Y., Wang, C., Yang, G., & Zhu, Y. T. (2014). An Ideal Ultrafine-Grained Structure for High Strength and High Ductility. *Materials Research Letters*, *3*(2), 88–94.

[23] Le, G. M., Godfrey, a., & Hansen, N. (2013). Structure and strength of aluminum with sub-micrometer/micrometer grain size prepared by spark plasma sintering. *Materials & Design*, *49*, 360–367.

[24]Saha, R., Ueji, R., & Tsuji, N. (2013). Fully recrystallized nanostructure fabricated without severe plastic deformation in high-Mn austenitic steel. *Scripta Materialia*, *68*(10), 813–816.

[25] Huang, X., Hansen, N., & Tsuji, N. (2006). Hardening by annealing and softening by deformation in nanostructured metals. *Science (New York, N.Y.)*, *312*(5771), 249–51.

[26] Huang, X., Kamikawa, N., & Hansen, N. (2010). Strengthening mechanisms and optimization of structure and properties in a nanostructured IF steel. *Journal of Materials Science*, *45*(17), 4761–4769

[27] Yu, C. Y., Kao, P. W., & Chang, C. P. (2005). Transition of tensile deformation behaviors in ultrafine-grained aluminum. *Acta Materialia*, *53*(15), 4019–4028.

[28] Elliot, R. a, Orowan, E., Udoguchi, T., & Argon, A. S. (2004). Absence of yield points in iron on strain reversal after aging, and the Bauschinger overshoot. *Mechanics of Materials*, *36*(11), 1143–1153.

[29] Taupin, V., Varadhan, S., Fressengeas, C., & Beaudoin, a. J. (2008). Directionality of yield point in strain-aged steels: The role of polar dislocations. *Acta Materialia*, *56*(13), 3002–3010.

[30] Sinclair, C. W., Poole, W. J., & Bréchet, Y. (2006). A model for the grain size dependent work hardening of copper. *Scripta Materialia*, *55*(8), 739–742.

[31] Bouaziz, O., Aouafi, a., & Allain, S. (2008). Effect of Grain Refinement on the Mechanical Behaviour of Ferritic Steels: Evolution of Isotropic Hardening and Kinematic Hardening. *Materials Science Forum*, *584-586*, 605–609.

[32] Wu, X., Yang, M., Yuan, F., Wu, G., Wei, Y., Huang, X., & Zhu, Y. (2015). Heterogeneous lamella structure unites ultrafine-grain strength with coarse-grain ductility, 1–6.

Chapter 2 Effect of interstitial impurities on yielding behavior and Hall-Petch relation in high purity iron

2.1 Introduction

In polycrystalline metallic materials, the yield stress increases with decreasing the mean grain size, according to well-known Hall-Petch relationship [1, 2]

$$\sigma_y = \sigma_0 + k_y d^{-1/2} \tag{2.1}$$

where σ_y is the yield stress, σ_0 the friction stress, k_y the Hall-Petch slope, and d the mean grain size. Different models have been proposed to explain this empirical equation, but its precise physical meaning remains still unclear [3]. Based on the most frequently used pile-up model, the term k_y is usually considered as a constant showing the ability of grain boundary to resist the slip transmission from one grain to the neighbor (the grain boundary strength, in other words) [2].

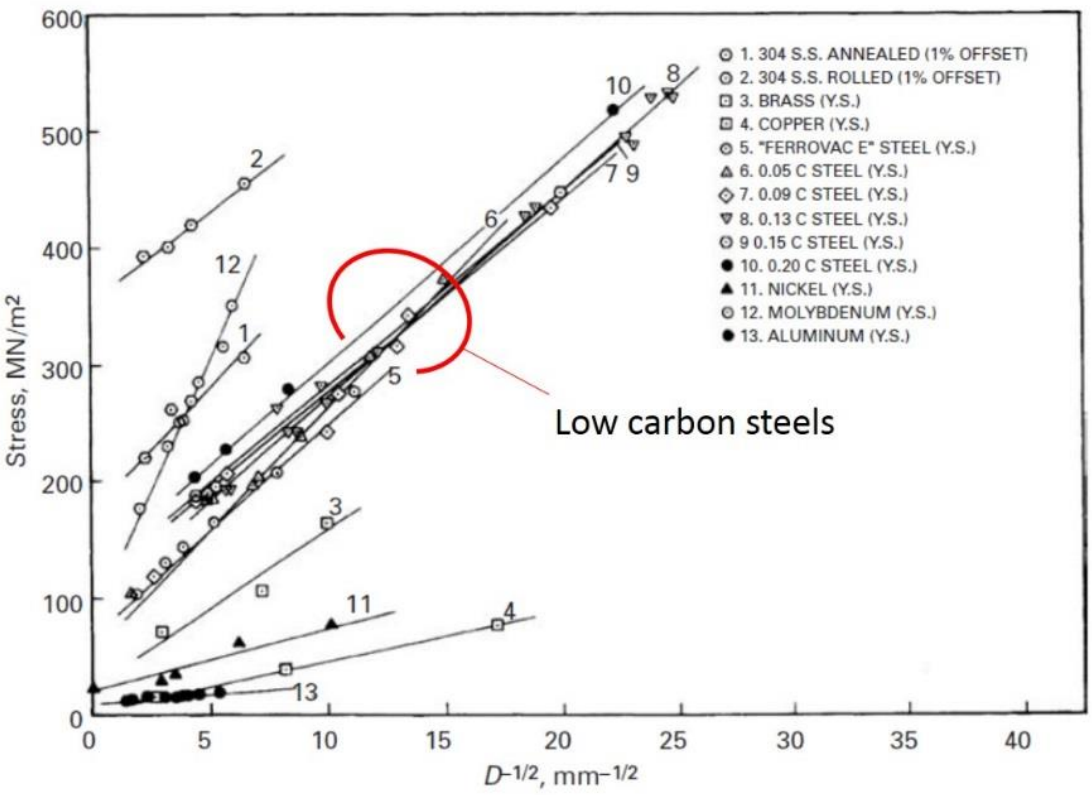

Figure 2.1 The Hall-Petch relationships for several common engineering materials [4].

The wide applicability of the Hall-Petch relation can be seen in **Figure 2.1** [4], in which Hall-Petch relationships of several engineering metallic materials are included. In commercial purity iron and low carbon steels, it has been reported that k_y shows nearly an identical value around 600 MPa·μm$^{-1/2}$ [5]. Although the low carbon steels had different carbon contents, they exhibited nearly the same k_y value, which is highlightened in **Figure 2.1**. In recent decades, with the development of the metallurgical technology, the ultra-low carbon interstitial free (IF) steels can be fabricated, in which the interstitial solute atoms such as N and C are substantially "killed" by fixing them as titanium/niobium nitrides and carbides (TiC, TiN, NbC, NbN). It is known that the IF steels exhibit continuous yielding and their k_y is very small, around 120MPa·μm$^{-1/2}$, compared with the

carbon steels [6]. On the other hand, recent studies revealed several times higher k_y in IF steel [6] and commercial purity Al [7] having UFG microstructures, compared with their coarse grain size counterparts. The UFG IF steel and UFG Al unexpectedly exhibited discontinuous yielding, while those materials with coarse grain sizes exhibited continuous yielding. Above results imply a certain correlation between Hall-Petch slope and yielding behaviors, in both conventional and ultra-fine grain size ranges. A study on the yielding theory and its relationship with the Hall-Petch relationship especially in a wide range of grain sizes including UFG regime is, thus, necessary to understand the fundamental plastic deformation and strength in metallic materials.

In this chapter, a high purity iron containing very small amount of interstitial carbon and nitrogen is used to study the relationship between the yielding behavior and the Hall-Petch relationship. It demonstrates that the identical material can exhibit different yielding behaviors depending on the heat treatment. In addition, a clear correlation between the yielding behavior and the value of the Hall-Petch slope, k_y is shown.

2.2 Experimental Procedure

2.2.1 Starting Material

The material used in this study is a high purity iron provided from Nippon Steel, Co.Ltd. The material was fabricated by vacuum melting and casting of electrodeposited iron under high vacuum and subsequent multiple-pass hot rolling. The chemical composition of the material was analyzed by optical emission spectrometry and shown in **Table 2.1**. The received material was a plate-shape with a thickness of 12 mm.

Table 2.1 Chemical composition of the high purity iron used in this study (mass ppm).

C	Si	Mn	P	S	Al	O	Ti	N	Fe
11	<30	<30	<20	<20	300	14	<20	8	Bal.

2.2.2 Mechanical and Thermal Treatment

2.2.2.1 Cold Rolling

The received plate was cut by a wire electrical discharge machine (HS-70A, Brother) into plates with thicknesses of 10 mm, 7 mm, 4 mm and 2 mm with the same normal direction (ND) as the received plate, and then cold rolled to a constant thickness of 1 mm. The corresponding cold rolling reduction was 90%, 85%, 75% and 50%, respectively. The

cold rolled sheets were then cut into rectangle-shaped specimens 50mm long and 20 mm wide, in order to perform subsequent annealing experiments.

2.2.2.2 Annealing

The annealing experiments were carried out in a tube-type vacuum furnace (TG22505, TOEI KAISHA, LTD.) under a vacuum of 5×10^{-3} Pa. The cold rolled sheets were annealed at various temperatures ranging from 650°C to 800°C for 30 minutes in order to achieve various mean grain sizes. After annealing, both of the cold rolled specimens were either water-cooled (WC) or air-cooled (AC) to room temperature. The detailed mechanical and thermal treatment for each specimen as well as the mean grain sizes, measured by the line interception method is listed in **Table 2.2**.

Table 2.2 Deformation and annealing conditions for the pure iron specimens together with the mean grain sizes. WC and AC mean water-cooling and air-cooling, respectively. Only the specimens having fully recrystallized microstructures are summarized in the table.

Cold-Rolling reduction	Annealing condition	Mean grain size	Cold-Rolling reduction	Annealing condition	Mean grain size
90 %	650°C×1.8ks+WC	15.2μm	90 %	650°C×1.8ks+AC	13.6 μm
	700°C×1.8ks+WC	16.2 μm		700°C×1.8ks+AC	13.8 μm
	750°C×1.8ks+WC	17.5 μm		750°C×1.8ks+AC	17.4 μm
85 %	700°C×1.8ks+WC	17.3 μm	85 %	700°C×1.8ks+AC	16.9 μm
	750°C×1.8ks+WC	21.8 μm		750°C×1.8ks+AC	22.8 μm
75 %	700°C×1.8ks+WC	25.4 μm	75 %	700°C×1.8ks+AC	23.5 μm
	750°C×1.8ks+WC	27.7 μm		750°C×1.8ks+AC	29.3 μm
	800°C×1.8ks+WC	36.7 μm		800°C×1.8ks+AC	38.4 μm
50 %	800°C×1.8ks+WC	45.1 μm	50 %	800°C×1.8ks+AC	41.8 μm

2.2.3 Optical Microscopy and EBSD Observations

Small piece specimens with a dimension of 10 mm in length × 2 mm in width × 1 mm thickness were cut off from the annealed sheets in order to perform microstructure observations. The longitudinal sections perpendicular to the transverse direction (TD) of the sheet specimens were mechanically polished by 2000 and 4000 grit sized fine sand papers and alumina suspensions to achieve a mirror-like surface. Etching was then carried out on those polished specimens in a Nital solution (3% HNO_3 and 97%C_2H_5OH) for 20

seconds to reveal ferrite grain boundaries. The microstructures were observed by an optical microscope (BX51M, OLYMPUS). The mean grain size was then measured by the interception method. For each specimen, at least 200 grains were countered in the measurement. To examine the distribution of grain boundary misorientation, some mechanically polished specimens were further electrically polished in a solution containing 10% $HClO_4$ and 90% CH_3COOH at 15V for 30 seconds at room temperature, and then provided to EBSD analysis. EBSD observations were then performed by using a SEM (XL30FEG-SEM, FEI Company) and EBSD system (TSL Data Collection ver. 5.0, TEX SEM Laboratory). The working distance and acceleration voltage of the SEM system was set to be 15 mm and 15kV, respectively. The results of the EBSD observations were analyzed by TSL OIM Analysis software ver. 5.0.

2.2.4 Tensile Test

Tensile test specimens were cut from the annealed sheets using an electrical discharge wire-cut machine. The sheet-type tensile test specimens with 10 mm in gauge length and 5 mm in gauge width were used, which had 1/5 miniaturized size of the JIS-5 standard specimen. Tensile test was performed on an universal test machine (AG-I, SHIMAZU Company) at room temperature and an initial strain rate of $8.3\times10^{-4}\ s^{-1}$. An extensometer (SG10-100AD, SHIMAZU Company) was attached on the specimens in the tensile test to measure the precise displacement.

The nominal stress (s), nominal strain (e), true stress (σ) and true strain (ε) were calculated by the following equation:

$$s = \frac{F}{A_0} \tag{2.2}$$

$$e = \frac{\Delta l}{L_0} \tag{2.3}$$

$$\sigma = s\,(1 + e) \tag{2.4}$$

$$\varepsilon = \ln\,(1 + e) \tag{2.5}$$

where F is the instant load, A_0 is the initial area of the cross section of the gauge, Δl is the displacement measured by the extensometer, and L_0 is the initial gauge length.

2.3 Results

2.3.1 Microstructure of annealed specimens

EBSD grain boundary maps of four kinds of cold-rolled specimens after annealing are selectively shown in **Figure 2.2.** The low angle grain boundaries ($2° \leqslant \theta \leqslant 15°$) and high angle grain boundaries ($\theta \geqslant 15°$) are indicated by red lines and green lines, respectively. These specimens display typical fully recrystallized microstructures characterized by nearly equiaxed grain shapes. The measured mean grain sizes were listed in **Table 2.2**. The range of the mean grain sizes after cold-rolling and annealing was from 10 μm to 50 μm. It should be noted that identical mean grain size were obtained from identical mechanical and heat treatments, which means that the cooling process, either water cooling or air cooling, did not have a significant effect on the final mean grain size.

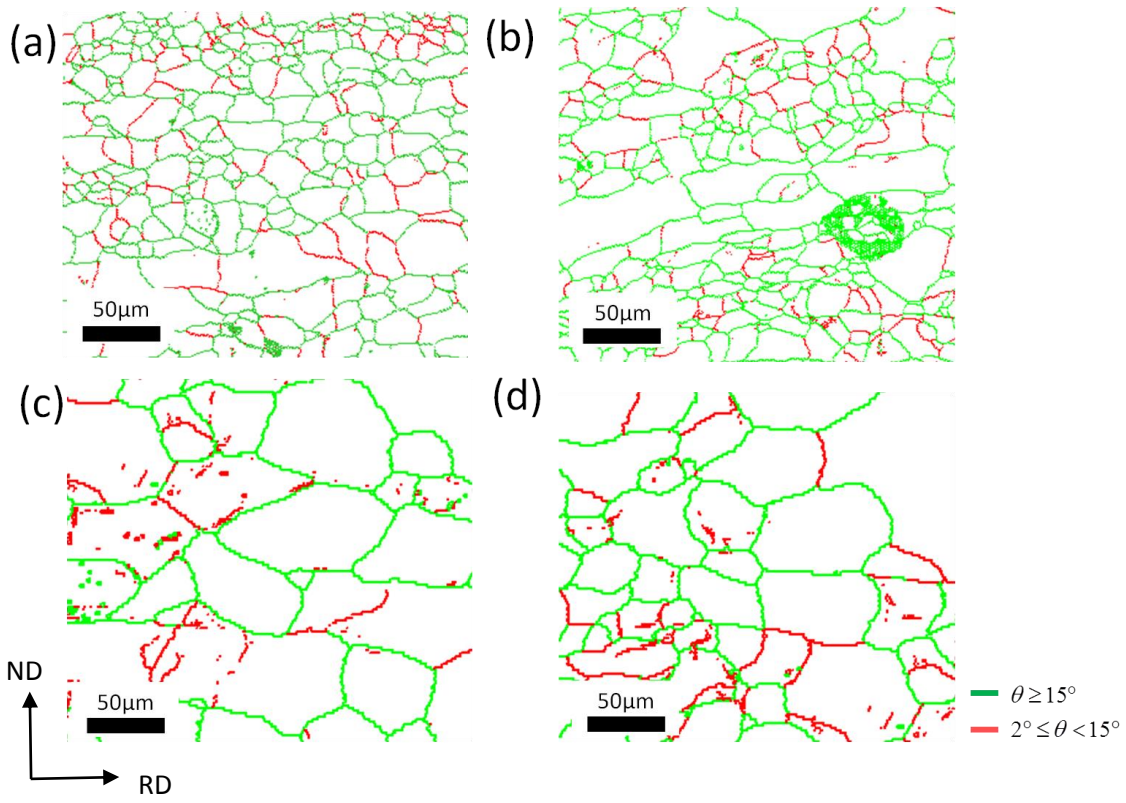

Figure 2.2 EBSD grain boundary maps of (a) 90% cold rolled + 650°C annealed + air-cooled (d=13.6μm), (b) 90% cold rolled + 650°C annealed + water-cooled (d=15.2μm), (c) 50% cold rolled + 800°C annealed + air-cooled (d=41.8μm) and (d) 50% cold rolled + 800°C annealed + water-cooled (d=45.1μm) specimens.

2.3.2 Nominal stress-strain curves of annealed specimens

Figure 2.3 (a) and **(b)** displays the representative nominal stress-strain curves selected from the water-cooled and air-cooled specimens respectively, with different mean grain sizes. The mean grain size of each specimen is also indicated in the figure. It can be seen that completely different yielding behaviors result from different cooling processes. The WC specimens exhibited continuous yielding, characterized by a gradual transition from elastic deformation to plastic deformation. On the other hand, the AC specimens exhibited

discontinuous yielding characterized by a distinct yield-drop and subsequent Lüders deformation. We believe that the different yielding behavior was attributed to the different distribution of interstitial atoms such as carbon and nitrogen. In the AC specimens, Cottrell atmosphere by interstitial atoms such as carbon and nitrogen formed to some extent during air-cooling and locked mobile dislocations or dislocation sources. Consequently discontinuous yielding occurred in the tensile test of the AC specimens. In the WC specimens, there was no enough time to form Cottrell atmosphere because of the rapid cooling process. Therefore the WC specimens exhibited continuous yielding.

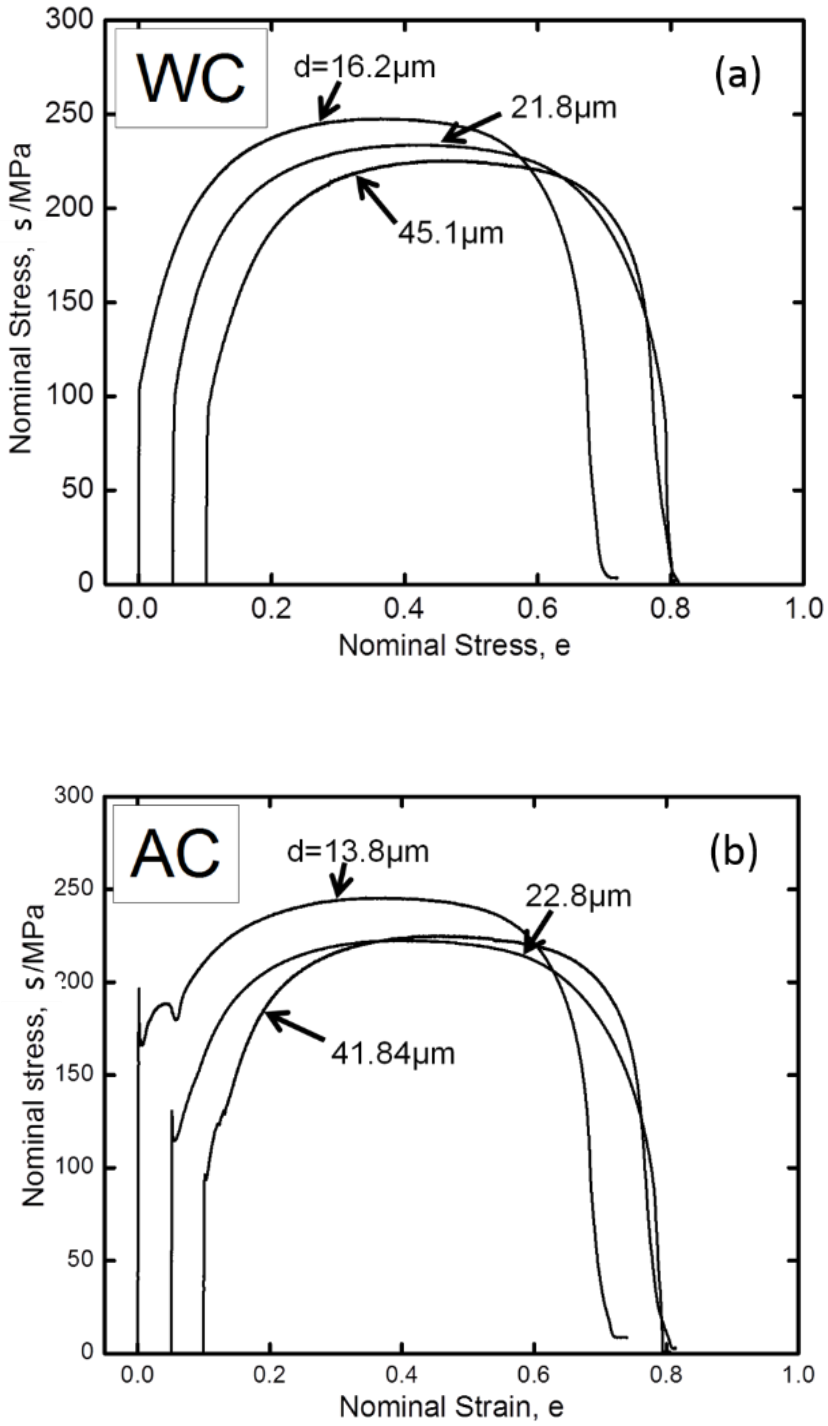

Figure 2.3 Selected nominal stress-strain curves of the water-cooled (WC) (a) and the air-cooled (AC) (b) specimens with different grain sizes.

2.3.3 Strain-ageing experiment

To confirm the occurrence of the dislocation locking by interstitials, the strain-ageing experiment was carried out on the AC specimens with the mean grain size of 13 μm. As shown in **Figure 2.4**, the 650°C annealed AC specimen having the mean grain size of 13 μm was pre-strained to 12.5% plastic strain, which is larger than the Lüders strain of this specimen, then unloaded and aged at 100°C for 2 hours in an oil bath. After the ageing treatment, the specimen was reloaded and it was found that the yield point phenomenon again occurred. Further ageing at 100°C for 12 hours and reloading again resulted in the occurrence of the yield point phenomenon.

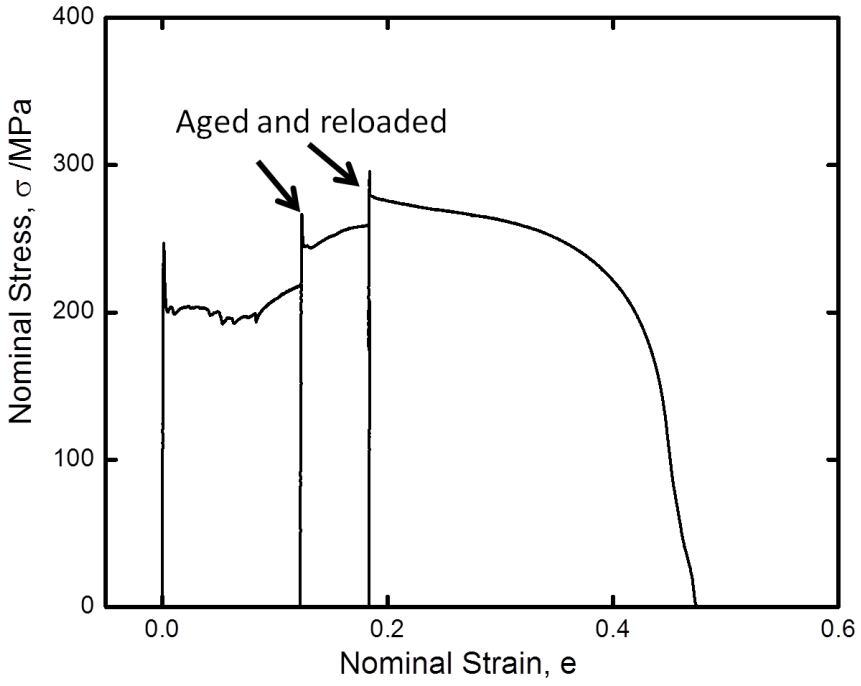

Figure 2.4 Nominal stress-strain curve obtained from the strain-ageing experiment. The specimen was cold-rolled by 90% and annealed at 650°C followed by air-cooling (AC). The reloading stress-strain curves after ageing treatments showed a clear discontinuous yielding.

It is considered that after the pre-strain, the mobile dislocations or dislocation sources were un-locked from interstitial atoms. If the tensile test were carried out immediately after the pre-strain, the yielding would be continuous. However, during the ageing treatment the segregation of interstitial atoms on dislocations was promoted and then mobile dislocations or dislocation sources were locked again by the Cottrell atmosphere. Therefore, yield point phenomenon repeatedly occurred in reloading. The strain-ageing experiment confirmed that the different yielding behaviors in the present study are related to interstitial atoms.

2.3.4 Effect of grain size on mechanical properties

Figure 2.5 shows the uniform elongation and total elongation plotted as a function of the mean grain size for the AC and WC specimens. It can be concluded that in the grain size range from 10 μm to 50 μm, the mean grain size did not have significant effect on the uniform elongation as well as total elongation.

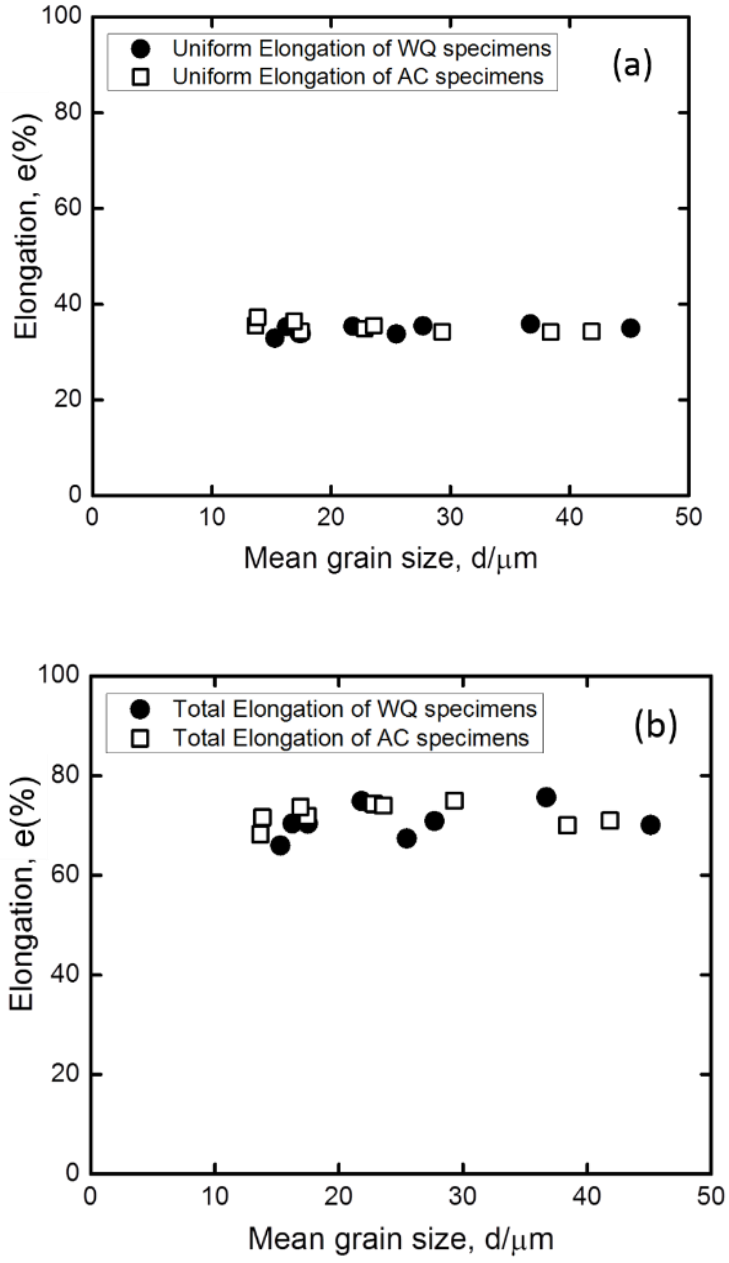

Figure 2.5 Uniform elongation (a) and total elongation (b) as a function of the mean grain size for the water-cooled and air-cooled specimens.

Figure 2.6 displays the ultimate tensile strength plotted as a function of the mean grain size for the AC and WC specimens. A slight increase in the tensile strength by decreasing

the mean grain size could be found for both AC and WC specimens. But there is little difference in the tensile strength between the AC and WC specimen having similar mean grain sizes.

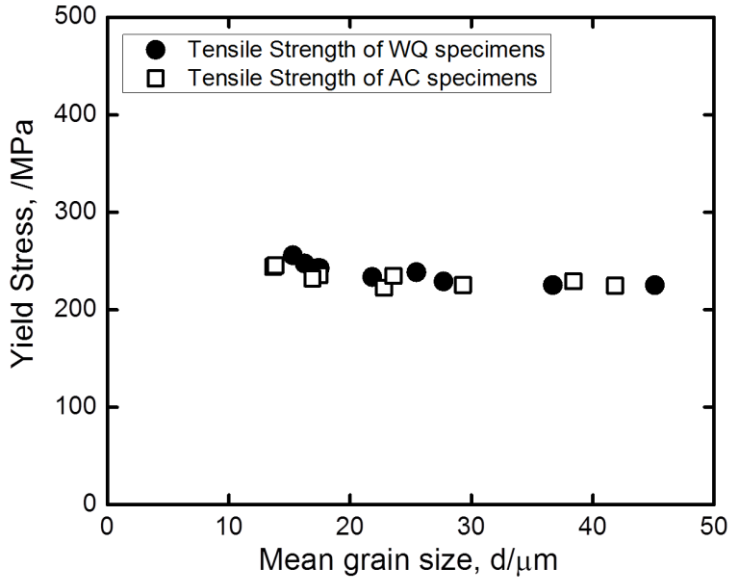

Figure 2.6 Tensile strength as a function of the mean grain size for the water-cooled and the air-cooled specimens.

2.3.5 Hall-Petch relationship of WC and AC specimens

In order to obtain the Hall-Petch relationship, the yield stress should be plotted against the inverse square root of the mean grain size. The determination of yield stress is different with respect to different yielding behaviors, as illustrated in **Figure 2.7**. For the WC specimens which exhibited a continuous elastic-plastic transition in the stress-strain curve, the point of yield is difficult to be determined precisely. Following to a conventional way, the 0.2% offset proof stress ($\sigma_{0.2\%}$) of the WC specimens was taken as the yield stress. For

the AC specimens which exhibited discontinuous yielding, yielding occurs by the yield drop followed by Lüders deformation, and a clear elastic-plastic transition point can be determined by the yield point. Therefore, the upper yield stress (σ_{UY}) and lower yield stress (σ_{LY}) were taken as the yield stress.

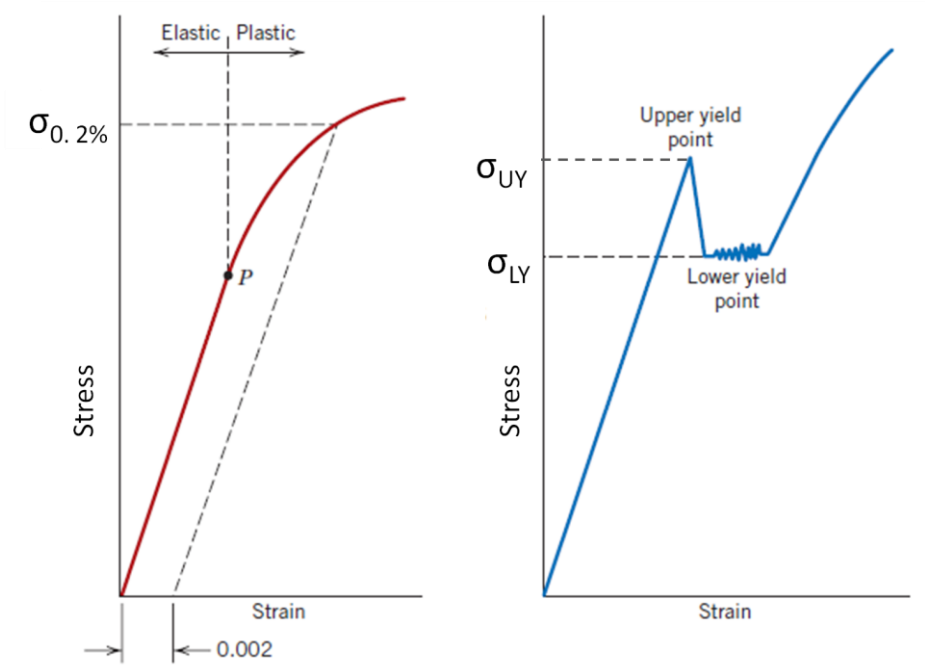

Figure 2.7 The different determination of the yield strength for (a) continuous yielding and (b) discontinuous yielding [8].

Figure 2.8 shows the Hall-Petch relationship of the WC and AC specimens. The Hall-Petch relationships were recognized by linear fitting, and represented by the straight broken lines in the figure. The slope of the straight line is the Hall-Petch slope and the interception with Y axis is σ_0. For the WC specimens, the $\sigma_{0.2\%}$ was plotted as a function of $d^{-1/2}$ and the k_y is linear fitted to be 168 MPa·μm$^{1/2}$, as illustrated in **Figure 2.8 (a)**. For the AC specimens, the σ_{UY} and σ_{LY} of the AC specimens were plotted as a function of $d^{-1/2}$ in **Figure 2.8 (b)**. It can be seen that the k_y is 650 MPa·μm$^{1/2}$ and 456 MPa·μm$^{1/2}$ for σ_{UY}

and σ_{LY} respectively, which is significantly higher than the k_y obtained from the WC specimens. Considering that the WC and AC specimens exhibit completely different yielding behaviors, these results indicate a strong correlation between the yielding behaviors and the value of k_y even in the same material.

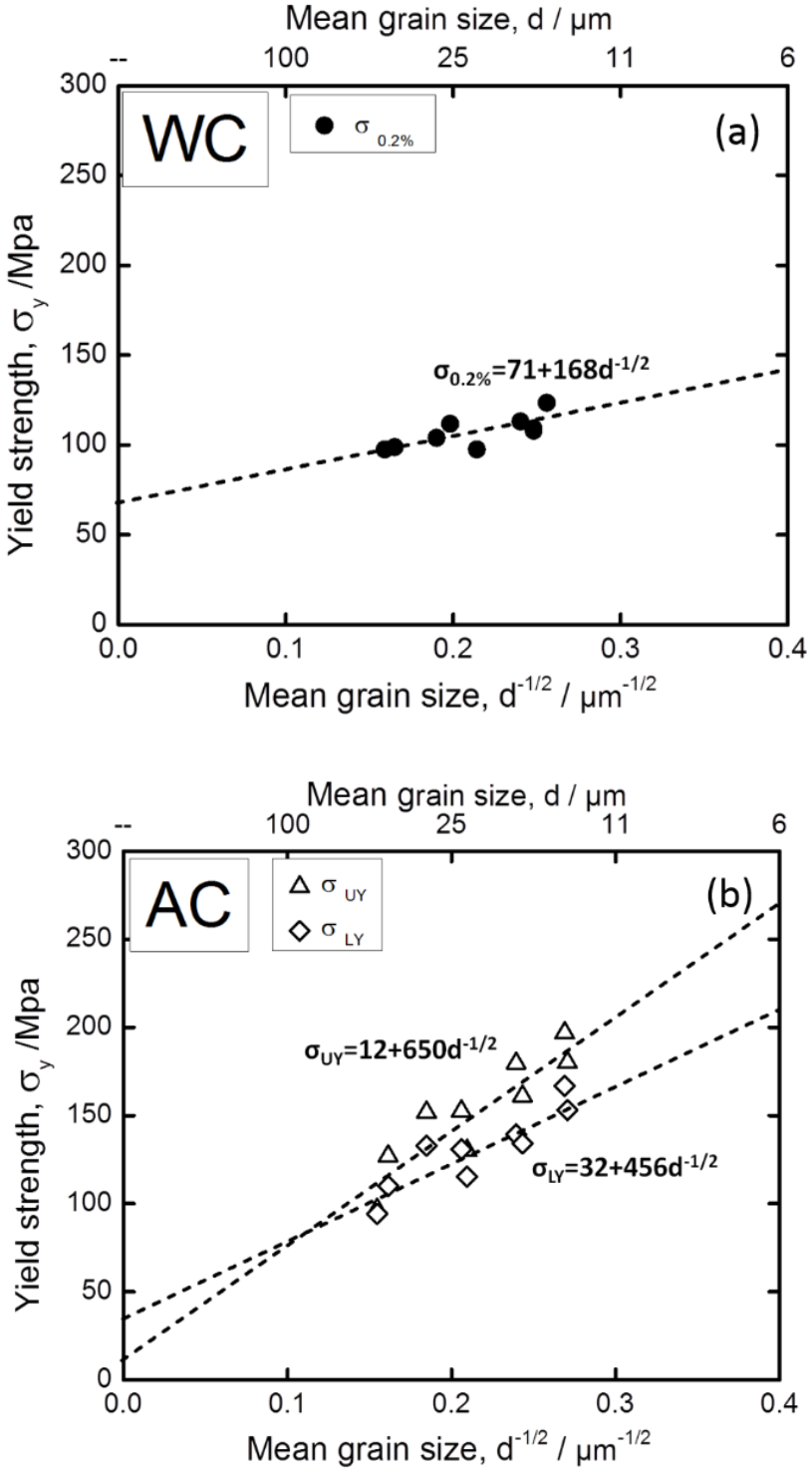

Figure 2.8 Hall-Petch relationships for the WC specimens (a) and for the AC specimens (b).

2.4 Discussion

2.4.1 Nature of discontinuous yielding

The discontinuous yielding was firstly found in a steel by Lüders [9] nearly 150 years ago. Intensive investigations on the yielding behaviors in various metals were conducted during 1960s. Cottrell and Bilby [10] proposed their famous dislocation locking theory in 1940s, in which the yield point behavior was attributed to the strong solution-dislocation interaction. Cottrell and Bilby showed that the interstitial solution atoms, such as carbon and nitrogen, would strongly interact with the strain field of dislocations. When the interstitial atoms move into such strain fields by diffusion, there would be an overall reduction of the strain energy. By this way, an atmosphere of interstitial atoms would form around the vicinity of dislocations. Consequently, the dislocations are locked by the atmosphere, which will increase the stress required to move dislocations. When the dislocations are unlocked from the atmosphere, yield drop occurs. On the other hand, Hahn [11] proposed another yield point model which related to the multiplication of mobile dislocations. Hahn suggested that the appearance of yield point should be attributed to the lack of initial mobile dislocations and stress-dependence of dislocation velocity. When there are few initial mobile dislocations, a high stress is required to rapidly multiply dislocations in order to accommodate the strain rate exerted by tensile testing. When enough mobile dislocations are multiplied, the yield stress will suddenly drop because less stress is required to move these mobile dislocations. In subsequent 40 years, the research intensity of yield point phenomenon has been decreased, but numbers of supplementary experiments and explanations have been carried out, by using advanced techniques such as

nanoindentation or FEM simulations [12, 13]. Although the precise physical meaning of discontinuous yielding is still unclear at present, for example, about the origin of the upper yield point and lower yield point, the mechanism of the Lüders band deformation, etc., it is generally agreed that the discontinuous yielding closely relates to the density of mobile dislocations. Actually, Hahn's dislocation density theory and Cottrell's dislocation locking theory are not exclusive to each other. For example, Cottrell atmosphere can lock the mobile dislocations or dislocation sources, thus the density of mobile dislocations or dislocation sources is decreased.

The mechanism of different yielding behaviors in the present material is illustrated in **Figure 2.9**. It is considered that carbon and nitrogen atoms have enough time to form atmosphere around dislocations during air-cooling so that the amount of mobile dislocations or free dislocation sources decreases. Consequently the AC specimens exhibit discontinuous yielding. In the water-cooled (WC) specimens, it is suggested that the interstitial atoms rarely segregate on mobile dislocations due to rapid cooling from annealing temperature and the atmosphere seldom forms or only a weak atmosphere forms. The number of mobile dislocations or free dislocation sources is much larger than that in the AC specimens. Therefore, relatively continuous yielding appears in the WC specimens during the tensile test. Previous research revealed that fully annealed and recrystallized low carbon ferritic steels, in which the carbon content is usually higher than several tens ppm, always exhibit discontinuous yielding either after water-cooling or air-cooling. Fully annealed IF steels, in which the solute carbon content is decreased to nearly zero, always exhibit continuous yielding. However, the present study demonstrates that when the carbon content is decreased to much lower than the level in the conventional low carbon

steels, the material could exhibit both kinds of yielding behaviors by different heat treatments. It indicates that yielding behaviors are affected not only by the total content of the interstitial elements in the material but also affected by the distribution of the interstitials controlled by heat treatments.

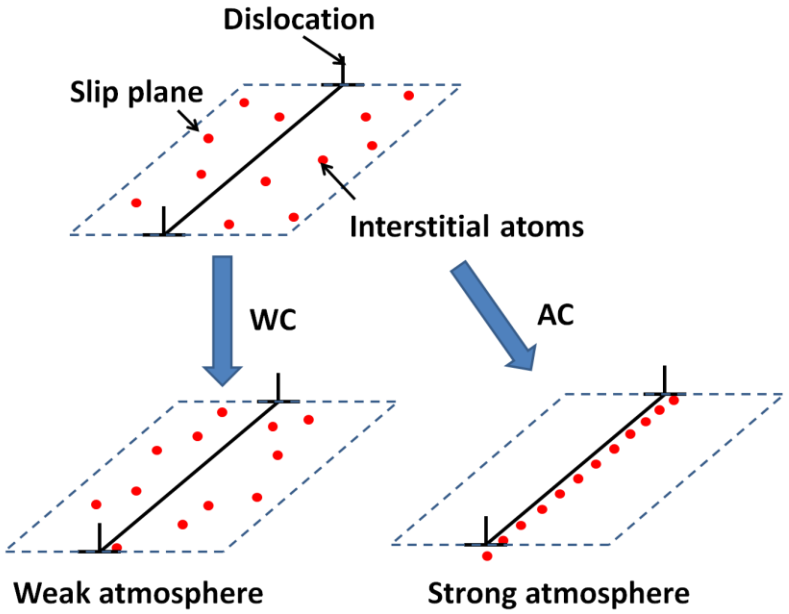

Figure 2.9. The mechanism of different yielding behaviors (or dislocation locking) is illustrated. At annealing temperature, the interstitial atoms are randomly distributed. By water-cooling or air-cooling to room temperature, Cottrell atmosphere forms to different degrees.

2.4.2 Relationship between yielding behaviors and Hall-Petch relationship

The Hall-Petch relationship was first proposed to describe the strength-grain size relationship in a mild steel and low carbon steels which exhibit discontinuous yielding.

There were several models proposed to explain this experimental result. Two of the widely accepted models are the dislocation pile-up model and grain boundary ledges model [14].

Many experiments revealed that in low carbon ferritic steels the Hall-Petch slope, k_y, is a constant around 600 MPa·μm$^{1/2}$ [8], while an extreme low k_y value around 100 MPa·μm$^{1/2}$ is also found in the IF steel by several researchers, as mentioned in the introduction of this chapter. Recently Takaki [15] found that the Hall-Petch slope continuously decreased with decreasing the carbon and nitrogen content in the range from 0 to 100 ppm, as shown in **Figure 2.10**.

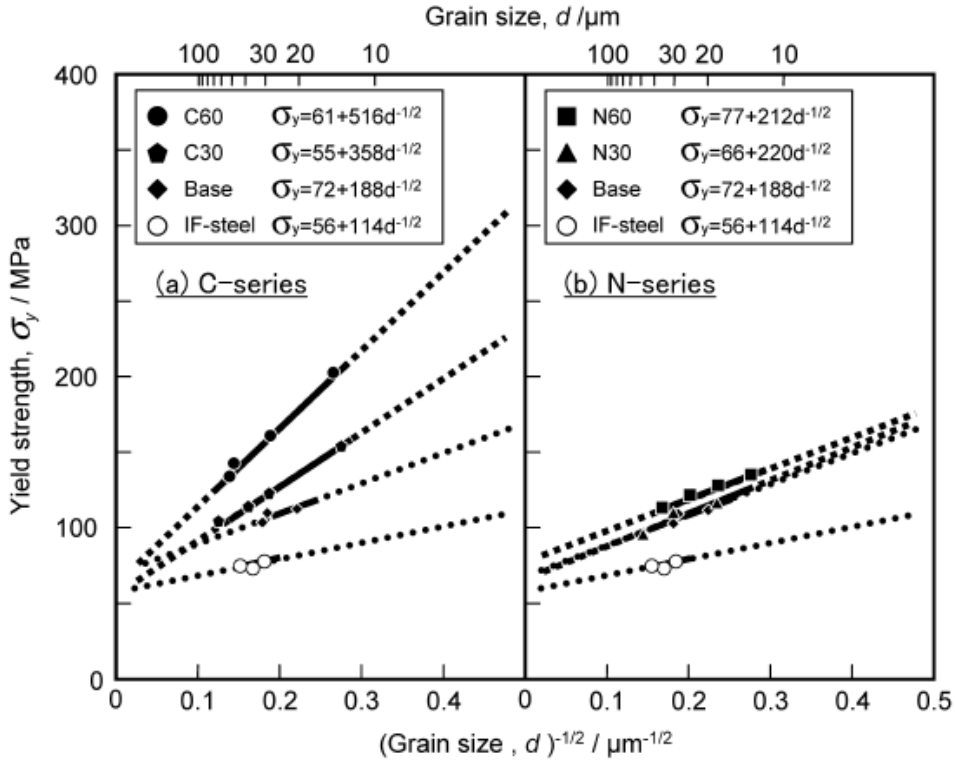

Figure 2.10 Hall-Petch slope, k_y, decreased with the decrease of carbon (left hand side) and nitrogen content (right hand side) [15].

Takaki [15] employed the grain boundary ledge model to explain the relationship between the amount of interstitial atoms and Hall-Petch slope. In this model the Hall-Petch

slope, k_y, is closely related to the critical stress to emit dislocations from grain boundary ledges. It is well-known that the interstitial atoms tend to segregate on grain boundaries in order to reduce the total strain energy. The grain boundary ledges, which act as dislocation sources, become energetically more stable by the segregation of those interstitial atoms. Therefore, by decreasing the total amount of interstitial atoms, the concentration of segregated interstitial atoms on the grain boundary decreases. Consequently, the grain boundary ledges become more unstable and the critical stress required to emit grain boundary dislocation become lower, leading to a smaller k_y.

Takaki's suggestions provide a reasonable explanation of the k_y changing with the amount of interstitial atoms, especially the different effects between carbon and nitrogen atoms. However, it has a critical drawback with respect to the mean grain size. It is obvious that with decreasing the mean grain size from coarse grain size range down to fine grain size smaller than 1μm, the grain boundary area per volume increases by tenfold. Assuming that the total amount of the interstitial atoms does not change, the concentration of interstitial atoms on the grain boundary will dramatically decrease with decreasing the mean grain size. According to Takaki's suggestion, a continuous decrease in k_y would be expected as the mean grain size decreases. However, such decrease in k_y has never been found in low carbon steels, even as the mean grain size is decreased to 1 μm, as shown in **Figure 2.11**. Therefore, Takaki's explanation is not consistent from the conventional grain size range (usually larger than 10 μm) to the ultra-fine grain size range (smaller than 1 μm).

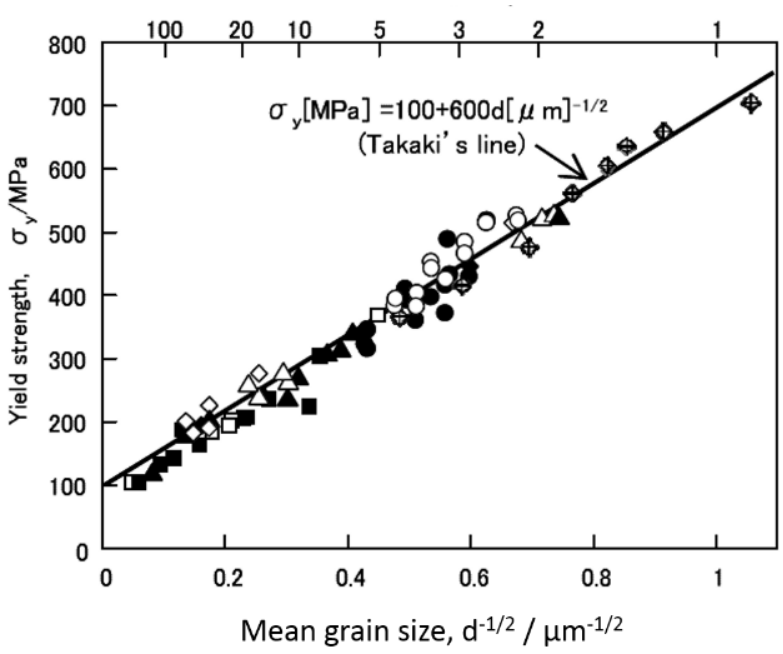

Figure 2.11 The Hall-Petch relationship for several low carbon steels [5].

It is reasonable to connect following two factors considering the experimental results: (1) IF steel is the only example exhibiting continuous yielding behavior in the family of low carbon ferritic steels. (2) IF steel has extremely low Hall-Petch slope, while the other low carbon ferritic steels have an identical k_y value around 600 MPa·μm$^{1/2}$. We demonstrated that a high purity iron containing small content of interstitial atoms (11 ppm carbon and 8ppm nitrogen) exhibited different yielding behaviors depending on the heat treatment. Once the material exhibits discontinuous yielding, high value of k_y is obtained from upper yield point or lower yield point of the stress-strain curves. When the material exhibits continuous yielding, an extremely low k_y is obtained. It should be noted that in the present study the k_y value obtained from the upper yield point (650 MPa·μm$^{1/2}$) is very close to the k_y summarized by Takaki for various kinds of low carbon ferritic steels (600 MPa·μm$^{1/2}$), and the k_y evaluated from continuous yielding, 168 MPa·μm$^{1/2}$, is comparable

to the k_y of IF steel (120 MPa·μm$^{1/2}$). These results suggest that the value of k_y in iron and low carbon ferritic steels strongly depends on the yielding behaviors.

Commercial low or ultra-low carbon ferritic steels, with fully annealed microstructures, can only exhibit discontinuous yielding probably because of enough amounts of interstitial carbon and nitrogen atoms. Thus an identical k_y value could result from discontinuous yielding. The IF steel, in which the amount of interstitial atoms is none, can only exhibit continuous yielding. Thus an extremely low k_y value can be obtained from the IF steel. However, the high purity iron, in which the amount of interstitial atoms is between commercial ultra-low carbon steels and the IF steel, can exhibit both continuous yielding and discontinuous yielding by controlling the heat treatment. Consequently, the k_y value obtained from the high purity iron was either close to low carbon steels or to IF steel. We suspect that in Takaki's work the yielding behavior transferred from continuous yielding to discontinuous yielding with increasing the carbon content or nitrogen in the specimens; consequently, a continuous increase in k_y was obtained. Our consideration would be reasonable because it was mentioned in his paper that both kinds of yielding behaviors occurred in the tensile tests, although the actual stress-strain curves are not presented in the paper [15].

2.4.3 Hall-Petch slope and grain boundary strength

Since the explanation by the grain boundary ledge model seems not appropriate to the present result, the author believes that the dislocation pile-up model is still valid, at least in the conventional grain size range. According to the dislocation pile-up model, the term k_y

represents the intrinsic resistance of the grain boundary to the plastic deformation from one grain to another (in other word, the intrinsic grain boundary strength).

Then the questions arise: in the present study, do different yielding behaviors represent different intrinsic grain boundary strength? If not, then which k_y value does represents the essential intrinsic grain boundary strength of the material?

To answer to above questions, the author conducted the extrapolation analysis on the true stress-strain curves [16]. The extrapolation technique was conducted using the Hollomon equation:

$$\sigma = K\varepsilon^n \tag{2.6}$$

where σ is the flow stress, K is strength index, ε is the true strain and n is strain hardening exponent. The extrapolation process on an AC specimen was illustrated in **Figure 2.12**. The work hardening region of the true stress-strain curve was fitted with the Hollomon equation and extrapolated back to the elastic deformation region. The fitted and extrapolated curves exhibit perfectly continuous yielding from which the $\sigma_{0.2\%}$ could be determined even in the specimens showing discontinuous yielding. The Hall-Petch analysis shown in **Figure 2.13** revealed that the k_y obtained from the $\sigma_{0.2\%}$ of the AC specimen is only 170 MPa·$\mu m^{1/2}$, which is significantly lower than the k_y obtained from σ_{UP} (650 MPa·$\mu m^{1/2}$) and σ_{LYP} (456 MPa·$\mu m^{1/2}$) and very close to the k_y (120 MPa·$\mu m^{1/2}$) of IF steel. This result implies that the great difference in the k_y value between the low carbon steels and IF steel should be attributed to the different yielding behaviors in the two kinds of materials.

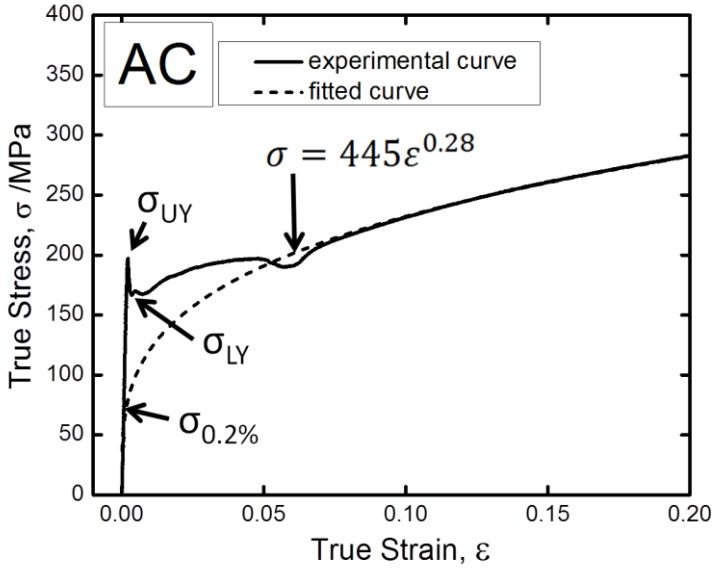

Figure 2.12 The extrapolation process on an AC specimen is shown. Dashed line represents the extrapolated stress-strain curve according to Hollomon's formula, from which the $\sigma_{0.2\%}$ can be determined.

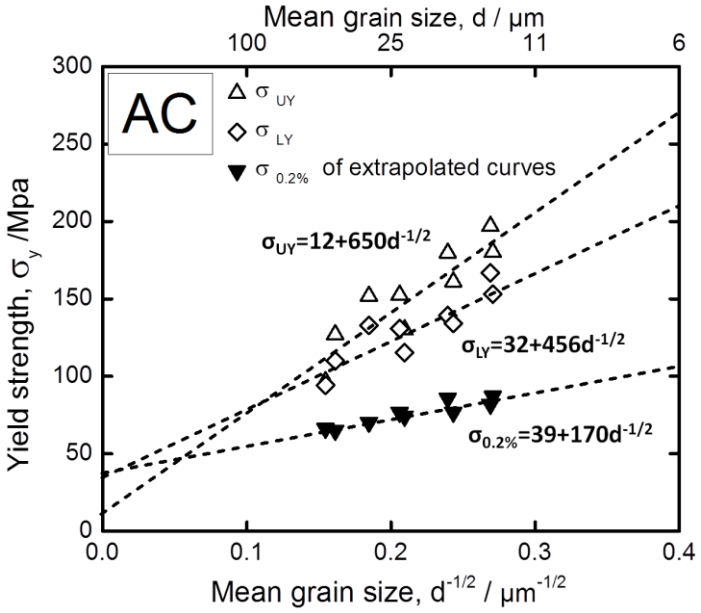

Figure 2.13 The σ_{UY}, σ_{LY} and $\sigma_{0.2\%}$ measured from the stress-strain curves of the AC specimens were plotted against $d^{-1/2}$. The Hall-Petch relationship of each kind of yield stress is also given.

The extrapolation technique was also carried out for the water-cooled specimens and the $\sigma_{0.2\%}$ were measured from the extrapolated curves, as shown in **Figure 2.14**. The k_y obtained from the extrapolated method is measured to be 127 MPa·μm$^{1/2}$ and shown in **Figure 2.15**. This value is again very close to the k_y of IF steels (120 MPa·μm$^{1/2}$). It should be noted that although the water-cooled specimens exhibited continuous yielding, the transition from elastic deformation to plastic deformation was still somehow discontinuous, by comparing the original stress-strain curve with the extrapolated stress-strain curve showing a perfectly continuous yielding character. We consider that a weak Cottrell atmosphere by interstitial atoms is formed even at annealing temperature as well as during water-cooling. As a result, the mobile dislocations or dislocation sources are locked by the weak Cottrell atmosphere and the water-cooled specimens exhibit slightly abrupt yielding behaviors instead of perfectly continuous yielding.

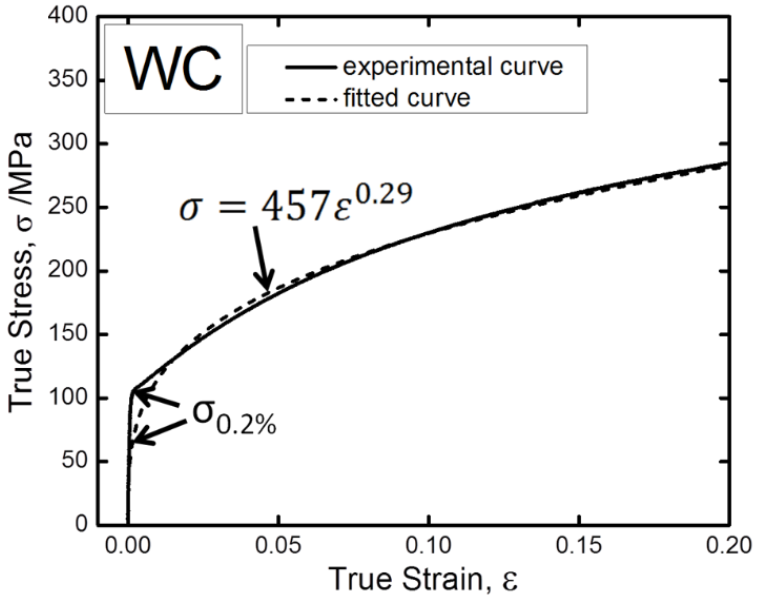

Figure 2.14 The extrapolation process on a WC specimen is shown. Note that the yielding behavior of the WC specimen is somewhat discontinuous compared with the extrapolated curve.

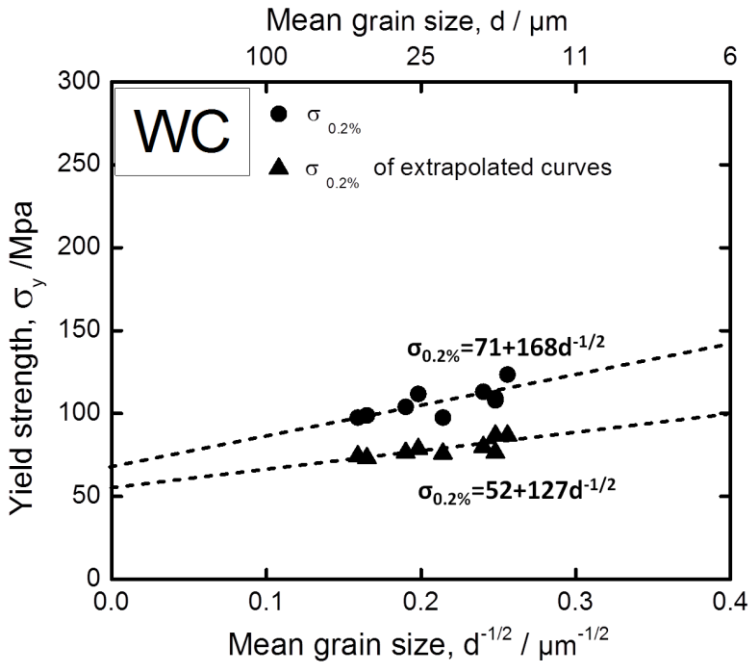

Figure 2.15 The $\sigma_{0.2\%}$ measured from the stress-strain curves of the WC specimens are plotted against $d^{-1/2}$. The Hall-Petch relationship is also given.

So far, we obtained nearly identical and extremely low k_y value of 100 ~ 200 MPa·$\mu m^{1/2}$ from the original stress-strain curve of the WC specimens, and the extrapolated stress-strain curves of the AC specimens and the WC specimens. The yielding behavior of these stress-strain curves are continuous yielding in common. A clear relationship between the yielding behavior and Hall-Petch relationship are summarized in **Figure 2.16**.

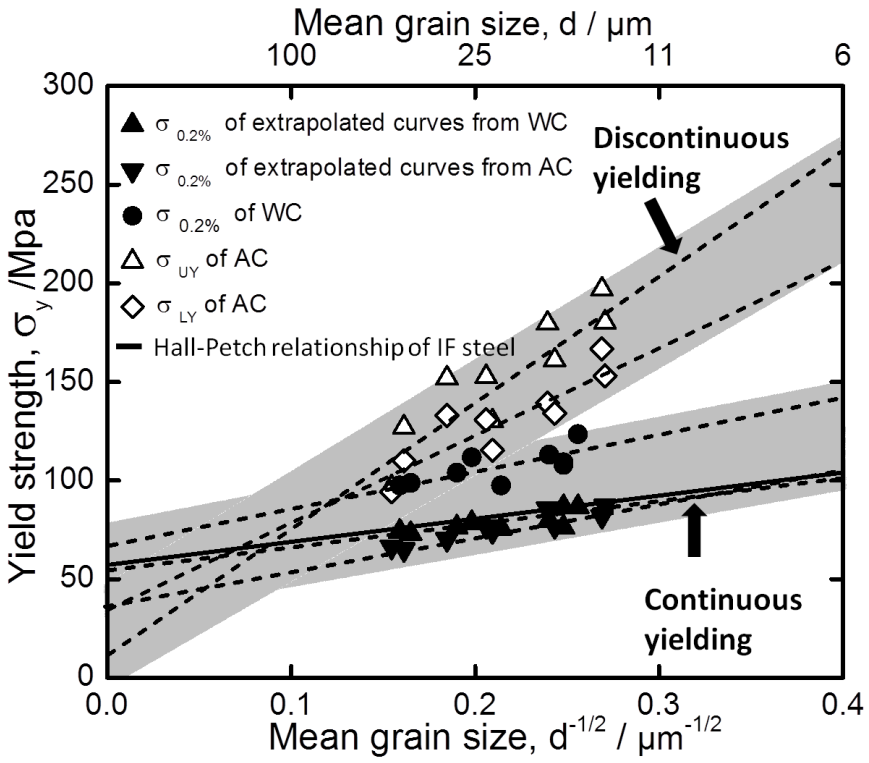

Figure 2.16 The dependence of Hall-Petch relationships on different yielding behaviors is summarized in this figure.

Therefore, the author believes that there exists an intrinsic k_y value in the high purity iron, k_y=100 ~ 200 MPa·μm$^{1/2}$. The intrinsic k_y value represents the essential grain boundary strength of the high purity iron, no matter the specimen exhibit continuous yielding or not (although the intrinsic k_y value can be revealed only from the stress-strain curves exhibiting continuous yielding).

Another question then arises: how can we explain the high k_y value obtained from discontinuous yielding?

According to Cottrell's early theory, the upper yield stress, which represents the depinning stress of dislocations from the Cottrell atmosphere, must be independent of the grain size. It was obviously contrary to the numerous experimental results. Cottrell [17] then developed the pile-up theory in the late 1950s. By using the pile-up model, Cottrell proposed that the stress concentration at the grain boundary initiates Frank-Read sources near the grain boundary in the neighboring grains. Then, the Hall-Petch slope, k_y, is determined as the critical stress to activate the Frank-Read source near the grain boundary. When the Frank-Read source is locked by interstitial atoms, higher critical stress is required in order to unlock the Frank-Read source, corresponding to the occurrence of yield point phenomenon. Consequently, a high k_y is obtained from discontinuous yielding. When the Frank-Read source is not locked, continuous yielding occurs and the low critical stress results a low k_y. According to his explanation, the critical stress should be sensitive to temperature, strain rate and even dislocation density. However, it is not consistent with the experimental results: the k_y obtained from discontinuous yielding did not change with temperature and strain rate [18].

Another explanation on the grain size dependence of discontinuous yielding was proposed by Petch [19] in 1962. Petch considered the fact that before macroscopic yielding, micro-yielding have already occurred within some grains. The micro-yielded grains are the ones which are favorably suited and oriented for the deformation, so that their number is quite small compared with the overall number of the grains. The plastic deformation during discontinuous yielding is localized in on these micro-yielded grains in the polycrystal; thus the local strain rate would be much higher in these grains than the macroscopic-strain rate exerted by the tensile test machine. For a strain rate sensitive

material, the higher local strain rate will result in an increase of the yield stress. The decrease of the mean grain size will result in an increase in the local strain rate; consequently, the yield stress will increase. This is the reason why the discontinuous yielding exhibits grain size dependence. Petch's explanation connected the micro-yielding with macroscopic yielding. However, he did not mention the role of carbon in his discontinuous yielding theory.

It is difficult to explain the grain size dependence of discontinuous yielding at present. The difficulty comes from both sides: the origin of Hall-Petch relationship and yielding behaviors. Recent study on ultra-fine grained materials revealed that discontinuous yielding occurs in most of the UFG materials while their coarse grain sized counterparts exhibit continuous yielding. Those results even imply a grain size dependence of yielding behavior itself. The grain size effect on the yielding behavior will be studied in the next chapter.

2.5 Conclusion

1. It was clearly demonstrated that an identical high-purity iron exhibited different yielding behaviors. It was confirmed that the discontinuous yielding was related to the dislocation locking by the interstitial atoms in the material. The changing of yielding behaviors is attributed to the difference in the distribution state of the interstitial atoms caused by different cooling processes.
2. The Hall-Petch slope for the yield stress, k_y, showed a strong correlation with the yielding behavior. A much higher k_y value was obtained in the specimens showing discontinuous yielding than that in the specimens showing continuous yielding.
3. By the extrapolation method, it was revealed that an identical k_y value existed in the high purity iron, which was not affected by different yielding behaviors. The author believes that this k_y value relates to the essential grain boundary strength of the high purity iron.

References

[1] EO. Hall, The Deformation and Ageing of Mild Steel, *Proceedings of the Physical Society. Section B*, 64(1951), pp.747-753.

[2] NJ. Petch, The cleavage strength of polycrystals, *Journal of the Iron and Steel Institute*, 174(1953), pp. 25-28.

[3] JW. Morris, The influence of grain size on the mechanical properties of steel http://escholarship.org/uc/item/88g8n6f8.pdf .

[4] M. Mayers, Mechanical behavior of materials, Cambridge University Press, 2009.

[5] S.Takaki, Review on the Hall-Petch Relation in Ferritic Steel, *Materials Science Forum*, 654-656(2010), 11–16.

[6] N. Tsuji, Y. Ito, Y. Saito, Y. Minamino, *Scripta Materialia*, 47 (2002), 893-899.

[7] N.Kamikawa , X. Huang., N. Tsuji, N. Hansen.. *Acta Materialia*, *57* (2009), 4198–4208.

[8] William D. Callister, Materials science and engineering: an introduction. John Wiley & Sons, Inc. 2007

[9] W.Lüders Dinglers, *Polytech J*, (1860), 155:18.

[10] A. Cottrell, B. Bilby, Dislocation theory of yielding and strain ageing of iron, *Proc.Phys. Soc. A*, 49 (1949), 49-62.

[11] G.Hahn, A model for yielding with special reference to the yield-point phenomena of iron and related bcc metals, Acta metallurgica, 10(1962), 727.

[12] K.Sekido , T.Ohmura, , L.Zhang, , T.Hara, , K.Tsuzaki, The effect of interstitial carbon on the initiation of plastic deformation of steels, *Materials Science and Engineering: A*, 530 (2011), 396–401.

[13] F.Yoshida , Y.Kaneda, S. Yamamoto. A plasticity model describing yield-point phenomena of steels and its application to FE simulation of temper rolling, *International Journal of Plasticity*, 24(2008), 1792–1818.

[14] J. C. M. Li, Petch relation and grain boundary sources, Trans. TMS-AIME, 227 (1963), 239.

[15] K.Takeda , N.Nakada , T.Tsuchiyama, S.Takaki , Effect of Interstitial Elements on Hall-Petch Coefficient of Ferritic Iron, *ISIJ international*, 48 (2008), 1122–1125.

[16] W. Phillips, RW. Armstrong, The strain dependence of the flow stress-grain size relation for 70: 30 brass, *Metallurgical and Materials Transactions B*, 3 (1972) , 2571-2577.

[17] A. H. Cottrell, Trans. Theory of brittle fracture in steel and similar metals, TMS-AIME, 212 (1958), 192.

[18] M. Hutchinson. *Philos Mag* 1963;8:121.

[19] N.Petch, The upper yield stress of polycrystalline iron, *Acta Metallurgica*,12 (1964),59.

Chapter 3 Grain size effect on yielding behavior in ultra-fine grained ultra-low carbon IF steel

3.1 Introduction

According to the well-known Hall-Petch relationship, the yield stress of polycrystalline materials increases with decreasing the average grain size [1,2]:

$$\sigma_y = \sigma_0 + k_y d^{-1/2} \quad (3.1)$$

where σ_y is the yield stress, σ_0 the friction stress, k_y a constant (Hall-Petch slope), and d the mean grain size. According to the Hall-Petch relationship, superior yield strength is expected if the mean grain size of the materials can be refined to be smaller than 1 μm. Nowadays significant grain size refinement, which is even smaller than 1 μm, could be achieved by using severe plastic deformation (SPD) processes during which very high plastic strains are applied to the material. The SPD processed materials usually exhibit a very high strength as well as a good toughness, but a very limited tensile ductility [3].

Other unique mechanical properties have been found in those nanostructured metals fabricated by SPD processes. Huang et al. [4,5] found that in Al and interstitial free (IF) steel processed by accumulative roll-bonding (ARB), the strength decreased by deformation while it increased by annealing. This interesting behavior, so called 'hardening by annealing and softening by deformation', is totally opposite to the commonsense in conventional metals which usually exhibit hardening by deformation (strain hardening) and softening by annealing. The elongation of the materials was also found to be closely related to the hardening and softening phenomena: the nanostructured

material hardened by annealing exhibited a reduction in elongation while the materials softened by deformation showed an increased elongation. Huang et al. systematically investigated the effect of subsequent cold deformation and annealing on the elongation of the ARB processed Al alloys and IF steel [4, 5, 6], and concluded that the dislocation density was the critical parameter for this unique behavior: the deformation becomes more homogeneous by introducing mobile dislocations while it becomes more inhomogeneous by decreasing free dislocations.

On the other hand, the yield point phenomenon (or discontinuous yielding) has been found in many nanostructured metals such as Cu [7], Al [3, 8] and Ti [9], although it is well-known that those materials exhibit continuous yielding behavior in their coarse grained states. Yield point phenomenon was firstly found in low carbon steels, which is characterized by a distinct yield drop and subsequent Lüders-band type deformation. It is generally believed that the yield point phenomenon in the conventional grain sized materials is attributed to the lack of initial mobile dislocations caused by the dislocation locking mechanism by impurity atoms [8]. However, it is also obvious that in the IF steel, or commercial purity Al and Cu with UFG microstructures, the amount of impurity atoms is not sufficient to cause the yield point phenomena. Therefore, it is supposed that the yield point phenomenon in the UFG materials is due to the fine grain size.

The 'hardening by annealing and softening by deformation' in nanostructured metals might be explained from a viewpoint of yielding behavior. In this chapter, the IF steel specimens with different grain sizes were fabricated by the ARB process and subsequent annealing. It is firstly demonstrated that the dramatic loss in the uniform elongation of the fine grain specimens is attributed to the appearance of the yield point phenomenon by using

the Hall-Petch analysis for the yield and flow stresses. Then, it is shown that the enhancement and reduction in the uniform elongation could be achieved by altering the yielding behavior of the fine grained IF steel specimen.

3.2 Grain size effect and yielding behavior of IF steel having various mean grain sizes

3.2.1 Experimental procedure

3.2.1.1 Starting material and ARB process

The chemical composition of the IF steel used in this study is given in **Table 3.1**. The starting material has a fully recrystallized microstructure with an average grain size of around 30 μm. Accumulative roll-bonding (ARB) process was applied on the material in order to refine the microstructures.

Table 3.1 Chemical composition of the IF steel used in this study (mass %).

C	N	Si	Mn	P	S	Al	Ti	Fe
0.002	0.0027	0.01	0.10	0.005	0.006	0.032	0.039	Bal.

The starting sheet having 2 mm in thickness, 50 mm in width and 300 mm in length was rolled at 500°C by 50 % reduction in one pass, without lubrication. Then the sheet having 1 mm thickness was cut, stacked, and roll-bonded at 500°C by a 50% reduction without lubrication again, which is illustrated in **Figure 3.1**.

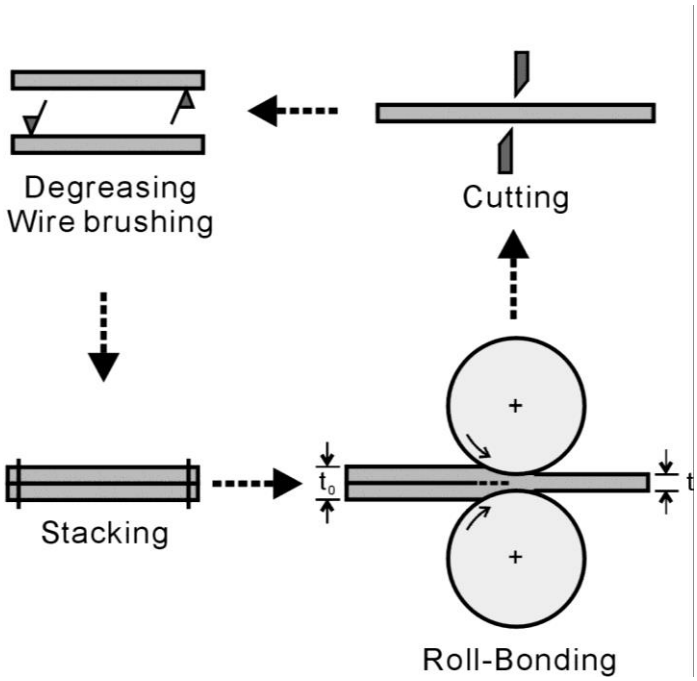

Figure 3.1 Illustration of the accumulative roll-bonding (ARB) process.

Up to 5 cycles of the ARB process was repeatedly carried out on the specimen up to 5 cycles after the first 50% rolling. After the first 50% rolling and subsequent 5 cycles of the ARB process, the total reduction in thickness imposed was 98.4% and the total equivalent strain was 4.8. The ARB processed specimens (hereafter refer to as as-ARB specimen) were annealed in a salt bath at different temperatures ranging from 500°C to 800°C for 30 minutes in order to obtain different average grain sizes, and then quenched into water. Small piece specimens with a dimension of 10 mm in length × 2 mm in width × 1 mm thickness were cut off from the annealed sheets and then electrically polished in a solution containing 10% $HClO_4$ and 90% CH_3COOH at 15V for 30 seconds at room temperature in order to observe the microstructure. EBSD observations were performed by using a SEM (XL30FEG-SEM, FEI Company) and EBSD system (TSL Data Collection ver. 5.0, TEX SEM Laboratory). The observations were carried out on longitudinal

sections perpendicular to the transverse direction (TD) of the sheets. Average grain sizes of the specimens were determined by the linear interception method using EBSD grain boundary maps.

3.2.1.2 Tensile test

Mechanical properties were evaluated by tensile test at ambient temperature with an initial strain rate of 8.3×10^{-4} s^{-1}. Tensile test specimens with 10 mm in gauge length and 5mm in gauge width were cut from the ARB processed and annealed sheets, so as to make the tensile axis parallel to RD. A digital CCD camera was used in the tensile tests in order to capture the surface morphology of the specimens during tensile deformation. The precise elongation of the specimen's gauge length was measured by the digital image correlation (DIC) software, which will be described in details in section 3.3.

3.2.2 Results

3.2.2.1 Microstructure observation

EBSD grain boundary maps of four different specimens are selected to demonstrate the typical microstructures of the deformed and annealed specimens, as shown in **Figure 3.2**.

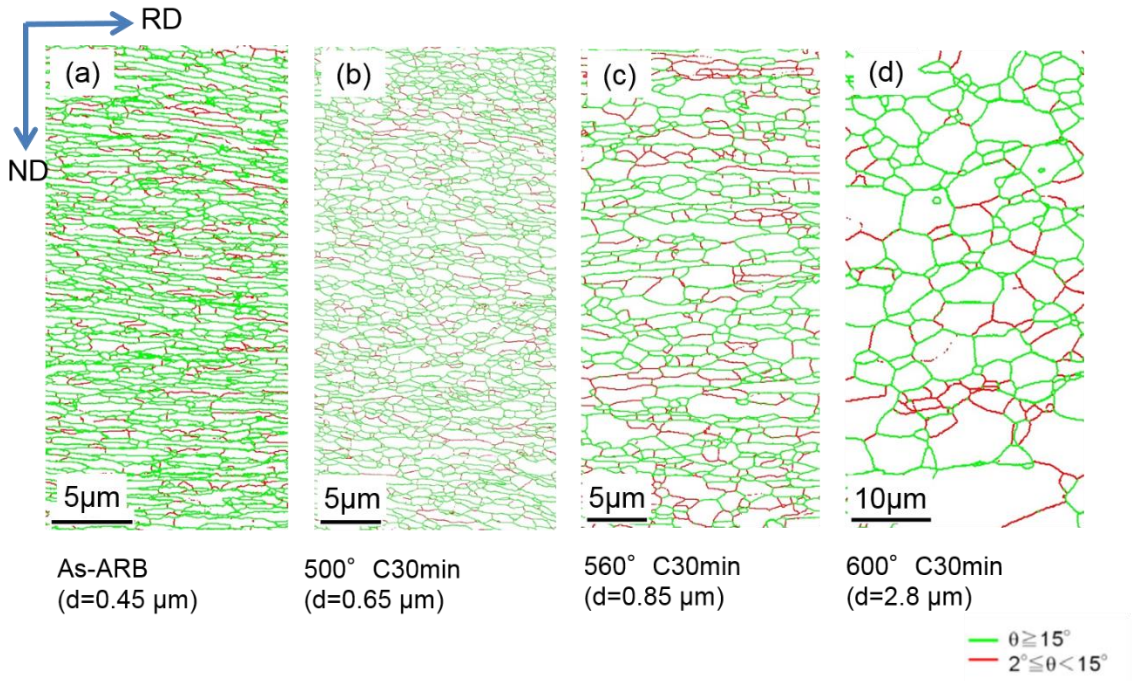

Figure 3.2 EBSD boundary maps of the IF steel specimens ARB processed to an equivalent strain of 4.8 and subsequently annealed at various temperatures for 1.8 ks. (a) As ARB processed. (b) Annealed at 500°C. (c) Annealed at 560°C. (d) Annealed at 600°C.

In the figure, low angle boundaries with misorientation between 2° and 15°, and high angle boundaries with misorientation larger than 15° are drawn in red and green lines, respectively. The as-ARB processed specimen shows elongated ultrafine grains surrounded mostly by high angle grain boundaries, with a mean grain size (thickness) of 0.3 μm (**Figure 3.2 (a)**), which is a typical UFG microstructure after the ARB process [10]. After annealing at 500°C for 30 minutes, coarsening of the microstructure is recognized in **Figure 3.2 (b)**. With further increasing the annealing temperature to 560°C, the majority of the structures shows an almost equiaxed morphology as shown in **Figure 3.2 (c)**. A complete equiaxed microstructure was obtained in the specimen annealed at higher temperatures, for example at 600°C, as shown in **Figure 3.2 (d)**. The average grain sizes of the four specimens shown in **Figure 3.2** are 0.45 μm, 0.65 μm, 0.85 μm, and 2.8 μm,

respectively. Larger grain sizes with equiaxed morphologies were obtained at higher annealing temperatures above 600°C.

3.2.2.2 Mechanical property

Nominal stress strain curves of the as-ARB specimens and annealed specimens are shown in **Figure 3.3**. Their average grain sizes are indicated in the figure.

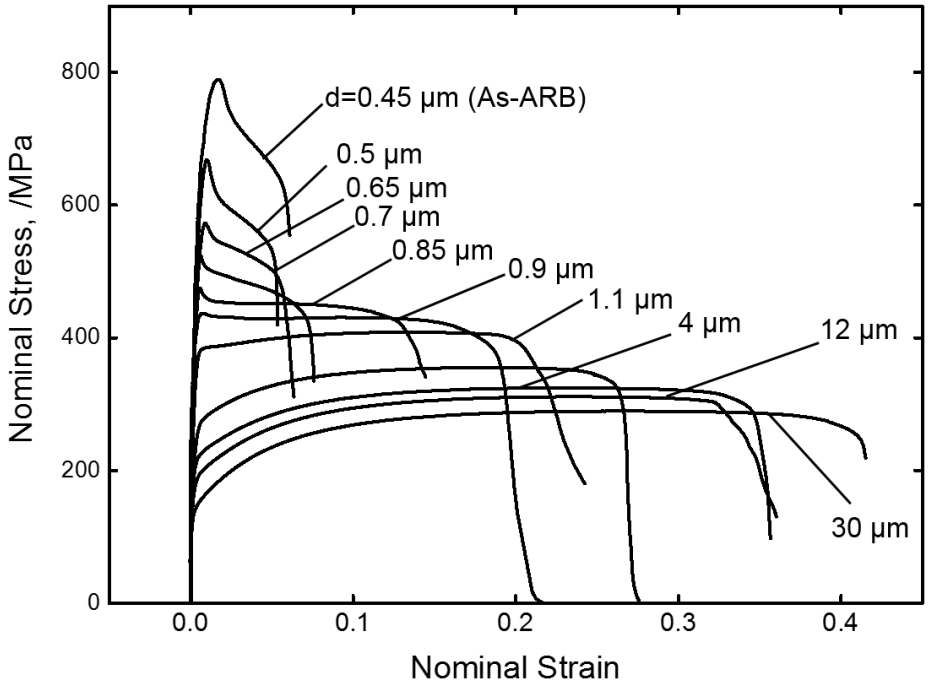

Figure 3.3 Nominal stress-strain curves of the ARB processed and annealed IF steel with various mean grain sizes ranging from 30 μm to 0.45 μm.

The as-ARB processed specimen with the mean grain size of 0.45 μm shows very high yield strength (790 MPa) and quite limited uniform and total elongation (1.6 % and 6.5 %, respectively). With increasing the mean grain size by rising the annealing temperature, the strength decreases while elongation increases, as generally observed in the ARB processed

and subsequently annealed materials [10]. It is noteworthy that the specimens with ultrafine grain sizes (d = 0.45 μm ~ 1.1 μm) exhibit discontinuous yielding characterized by a clear yield point phenomenon, while the coarser grain sized specimens (d > 1.5 μm) exhibit continuous yielding. Macroscopically homogeneous deformation occurs in those coarse grain-sized specimens exhibiting continuous yielding. When the discontinuous yielding occurred in the specimens with fine grain sizes, Lüders deformation was observed. In the specimens whose grain sizes were smaller than 0.9 μm, macroscopic necking immediately occurred after the yield point and localized shear bands were observed on the surface of the tensile specimens.

Yield stress obtained from the tensile test is plotted as a function of $d^{-1/2}$ in **Figure 3.4** (Hall-Petch plot). The upper yield stress (yield point stress) was taken as the yield stress for the specimens exhibiting clear yield point phenomenon, while the 0.2 % offset proof stress was taken as the yield stress for the specimens exhibiting continuous yielding. It is seen that two distinct Hall-Petch relations are obtained depending on the average grain size range, with the different values of k_y and σ_0 given in the figure. In the larger grain size range (d = 1.5 ~ 30 μm), a low k_y value (270MPa·μm$^{1/2}$) is obtained by linear fitting, which is comparable with previous results from conventionally coarse grained specimens [11]. While in the fine grain size range (d = 0.45 ~ 0.9 μm), a very high k_y value (811MPa·μm$^{1/2}$) and a negative σ_0 (-750MPa) are obtained. The deviation of the yield stress from the Hall-Petch relation extrapolated from the conventional grain size range is refer to as "extra-hardening", as previously reported in IF steel and Al having fine grain sizes [3].

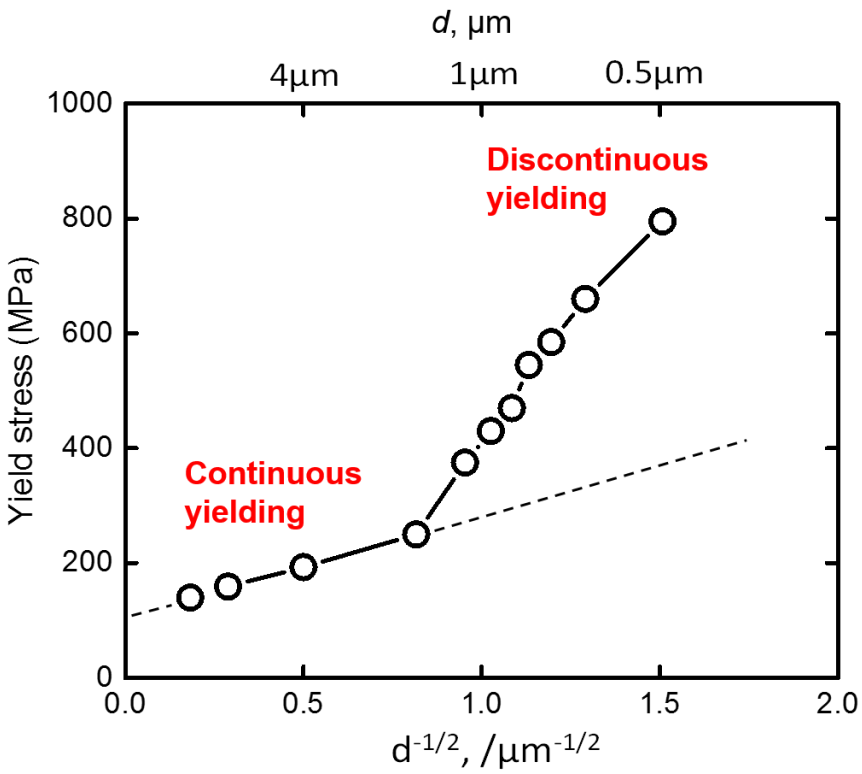

Figure 3.4 Yield stress of the IF steel specimens plotted as a function of inverse square root of the mean grain size (Hall-Petch plot).

The uniform elongation values of the IF steel specimens are plotted as a function of $d^{-1/2}$ in **Figure 3.5**. It is seen that the uniform elongation slightly increases and then continuously decreases with decreasing the mean grain size (d) from 30 μm to 1.5 μm. A dramatic drop in the uniform elongation is observed as the grain size becomes smaller than 1.5 μm. When the grain size is smaller than 0.9 μm, the uniform elongation becomes very low, smaller than 1.5 %.

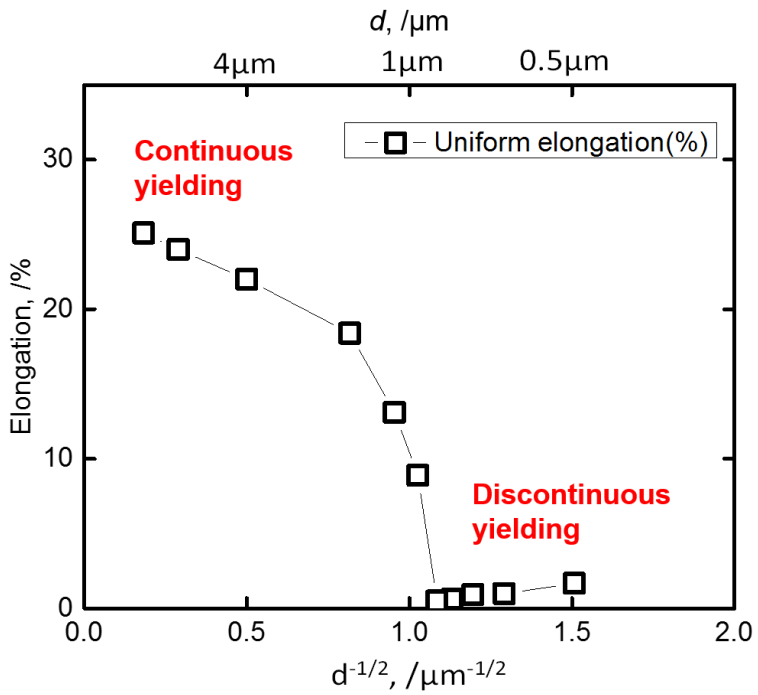

Figure 3.5 Uniform elongation of the IF steel specimens plotted as a function of inverse square root of the mean grain size. A dramatic drop in the uniform elongation occurs in the range 0.45 μm < d < 0.9 μm.

3.2.3 Discussion

3.2.3.1 Yield point phenomenon

Yield point phenomenon often occurs in the materials having a strong dislocation-impurity interaction, such as iron with interstitial carbon and nitrogen, as shown in Chapter 1. According to Cottrell and Bilby theory proposed in 1950s [12], the yield point is attributed to the dislocation locking by impurity atoms. Stress drop corresponds to the

event making dislocations free from the atmosphere of impurity atoms. Later, Hahn [13] proposed the mobile dislocation density model by considering the relationship between the dislocation velocity and the mobile dislocation density, and attributed yield point phenomenon to the lack of initial mobile dislocation density and sudden multiplication of mobile dislocations. It is obvious that the dislocation locking mechanism cannot explain the yield point phenomenon in the present study because interstitial carbon and nitrogen atoms are fixed by titanium to form carbide and nitride in the present IF steel. In recent years, the yield point phenomenon has been more and more found to occur in fine grained materials such as pure Cu [7], Al [3], Ti and their alloys [9, 7, 14] and austenitic steels [15], all of which do not exhibit yield point in the coarse grained microstructures. It is generally accepted that Hahn's model is applied to explain the yield point phenomenon in the fine grained materials. Since the mobile dislocation density required to initiate plastic deformation increases with decreasing the average grain size, it is generally believed that the initial mobile dislocation density (or dislocation source density) is inherently insufficient in these fine grain sized materials with limited volumes (especially after annealing) [8]. As a result, the yield point phenomenon occurs in such fine grained materials.

3.2.3.2 Hall-Petch relationship in fine grained IF steel

As shown in **Figure 3.4**, positive deviation of the yield stress from the Hall-Petch relationship of the yield stress was found to occur when the grain size was smaller than 1.5 μm, which exactly coincided with the grain size below which the specimen started to

exhibit the yield point phenomenon. As the mean grain size further decreased, the yield point phenomenon became more prominent and the deviation from the Hall-Petch relationship for coarse-grained specimens also increased. It has been demonstrated in the previous chapter that a higher Hall-Petch slope can be obtained in the specimens exhibiting the yield point phenomenon in the ultra-low carbon steel. These results strongly suggest that the deviation of the yield stress from the Hall-Petch relation extrapolated from the coarse grain size range is caused by the yield point phenomenon. It is interesting that even the deviated yield stresses in the fine grain sized range follow another good linear relationship with the inverse square root of the mean grain size. This result seems to imply that two different Hall-Petch relationships can be obtained in the identical material by only refining the grain size.

The yield stress deviation from the Hall-Petch relationships in the conventional grain size range had been reported in nanocrystalline materials previously [10]. However, in those cases the deviation was negative, and the Hall-Petch slope was even a negative value, which was so called "inverse Hall-Petch relationship" [16]. The inverse Hall-Petch relation was often observed in the materials having the nano-sized grain, which is in the range from 1 nm to 100 nm. It was widely accepted that in the nano-sized range, the plastic deformation is dominated by the excessive grain boundaries and the inverse Hall-Petch relationship is triggered by the grain boundary creep mechanism. It is obviously not the case in the present study because the mean grain size is much larger than the nano regime.

Based on the physical model of the Hall-Petch relationship, the Hall-Petch slope is closely related to the strength of the dislocation sources in the material. The present results seem to imply that the strength of the dislocation sources in the materials becomes higher

in the fine grain size. Some molecular dynamics simulation studies showed that as the mean grain size was decreased to some critical value, grain boundaries became the main dislocation sources in the material instead of the in-grain sources such as low angle grain boundaries, dislocation cells and dislocation tangles [17]. The yield point phenomena in the stress-strain curve was often seen in those simulated works, which usually corresponded to the nucleation of dislocations from grain boundary dislocation sources. However, the grain size adopted in the molecular dynamics simulation works was still too small (usually smaller than 100 nm) compared with the present study (from 0.5 μm to 2 μm). Secondly, in the molecular simulation works the temperature was often set to be extremely low and the strain rate was very high, which is far from the real experimental conditions. The positive deviation from the conventional Hall-Petch relation was also hardly seen in those simulation works.

Nevertheless, it can be seen from the present results that the extra-hardening is closely related to the appearance of the yield point phenomena in the fine grain sized material. The mechanism of the extra-hardening will be further discussed in Chapter 4.

3.2.3.3 Dramatic drop in uniform elongation

It is noteworthy that the uniform elongation dramatically drops to less than 1.5 % as the average grain size decreases down to values smaller than 0.95 μm, as shown in **Figure 3.5**. This sudden drop in uniform elongation can be also explained by the Hall-Petch analysis for the yield stress and flow stresses. In **Figure 3.6**, the yield stress and flow stresses at different true strains of 0.05, 0.1, 0.15 and 0.2, which are obtained from true

stress strain curves of the coarse grain-sized specimens, are plotted as a function of $d^{-1/2}$.

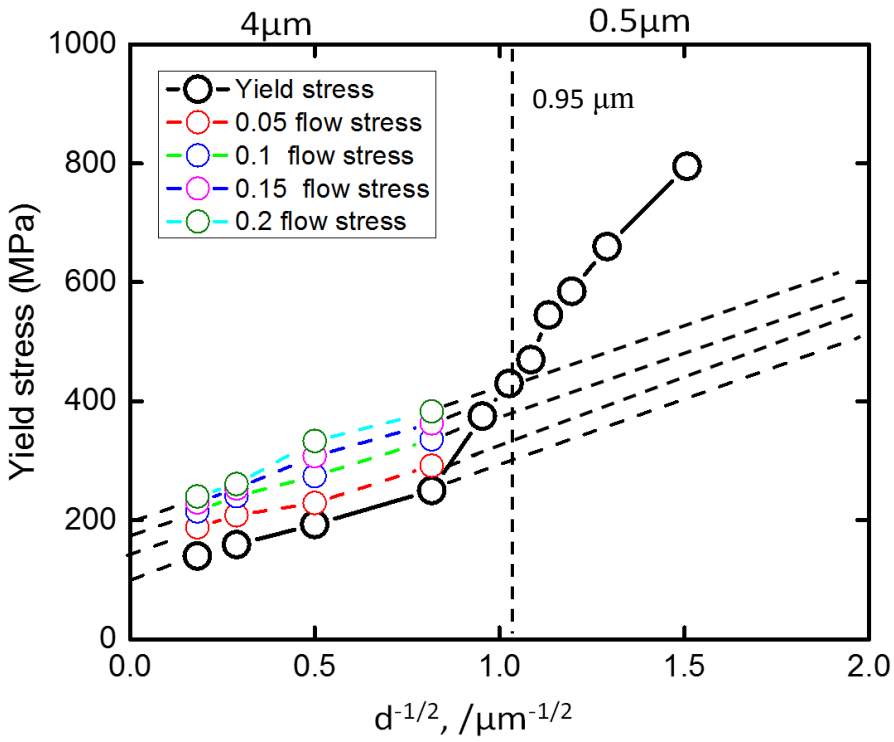

Figure 3.6 Flow stresses at different true strains of 0.05, 0.1, 0.15, and 0.2 plotted against the inverse square root of the mean grain size. The Hall-Petch slopes for the flow stresses at given strains show similar values of around 250 MPa·μm$^{1/2}$.

For the fine grain-sized specimens, the uniform elongation is too small to measure the flow stress from the true stress strain curves. It is known that the Hall-Petch relationship can be applied not only for the yield stress but also for the flow stress at a given strain [18]:

$$\sigma_\varepsilon = \sigma_{\varepsilon 0} + k_\varepsilon d^{-1/2} \qquad (3.2)$$

where σ_ε , $\sigma_{\varepsilon 0}$ and k_ε are the flow stress, friction stress and Hall-Petch slope at a given strain, respectively. It is found in **Figure 3.6** that the flow stresses at given true strains also follow Hall-Petch relationship with a slope similar to that for the yield stress in the coarse grain size range (250MPa· μm$^{1/2}$). However, because of the higher Hall-Petch slope for the yield stress in the fine grain size range, the yield stress increases more rapidly than the flow

stress with decreasing the grain size. When the mean grain size becomes smaller than 0.95 μm, the yield stress eventually intersects with and soon exceeds the flow stresses in the Hall-Petch plot in **Figure 3.6**. When the yield stress exceeds the extrapolated flow stress, a strain localization occurs at the onset of yielding, which corresponds to the yield point phenomenon (or discontinuous yielding) in the present study. At medium grain sizes, for example 0.95 μm, the yield stress is between the flow stresses at strains of 0.05 and 0.1, which indicates that the strain localization in this specimen must not be significant. This can be confirmed by the stress strain curve of this specimen, which still shows an uniform strain hardening part after the yield point and Lüders deformation as shown **in Figure 3.3**. As the grain size becomes smaller than 0.95 μm, the yield stress already reaches or even exceeds the flow stress at a strain of 0.2, indicating significant strain localization should happen at the onset of yielding. This leads to the macroscopic necking immediately after yielding, as shown in the form of the highly localized shear bands and by the stress strain curves shown in **Figure 3.2**. It should be noted that overtaking of the yield stress against the flow stresses occurs in a very narrow grain size range (from d = 1.5 μm to 0.85 μm, indicated in red range in **Figure 3.7**) which coincides well with the same grain size range (indicated in the red color in **Figure 3.7**) where the uniform elongation suddenly drops to less than 2 %. This means that the abrupt drop in the uniform elongation in the fine grain size range results from the appearance of the discontinuous yielding behavior (accompanying with strain localization).

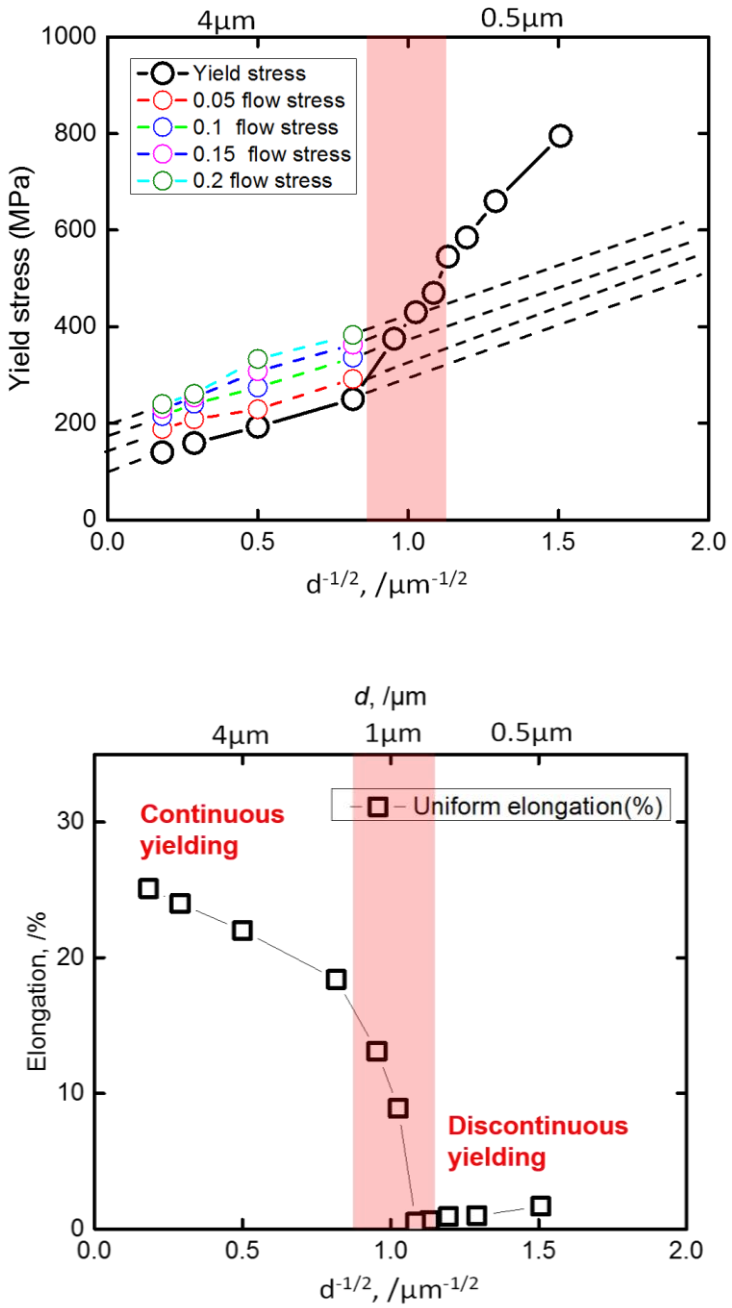

Figure 3.7 Yield stress, flow stresses at different true strains of 0.05, 0.1, 0.15, and 0.2 and the uniform elongation plotted against the inverse square root of the mean grain size. The region colored in red is the range where the yield stress overtakes the flow stress and the dramatic drop in the uniform elongation occurrs.

3.3 Strain localization in IF steel with different grain sizes

It was demonstrated in the previous part that the dramatic drop in the uniform elongation in the fine grained IF steel was attributed to the early plastic instability associated with the occurrence of discontinuous yielding behavior accompanying strain localization (or Lüders band) in the fine grained specimens, which could be explained by using the Hall-Petch analysis for the yield and flow stresses. In this part, the strain localization associated with the yield point phenomena is characterized by the digital image correlation (DIC) technique to confirm the relation between the yield point phenomenon and uniform elongation in the fine grained IF steel.

3.3.1 Experimental procedure

3.3.1.1 The digital image correlation

Digital Image Correlation (DIC) is a computer-aided measurement technique to trace the changes of identical points in the digital images. The DIC system consists of two parts: the recording system and measurement system. During the tensile test, the recording system captures the images of the deforming specimen, and then the measurement system can calculate the local strain distribution and evolution on the specimen surface by comparing the difference between every sequential two images. The surface of the specimen is usually painted by matt white in order to avoid the light reflection and then covered by a stochastic dot pattern, as shown in **Figure 3.8**.

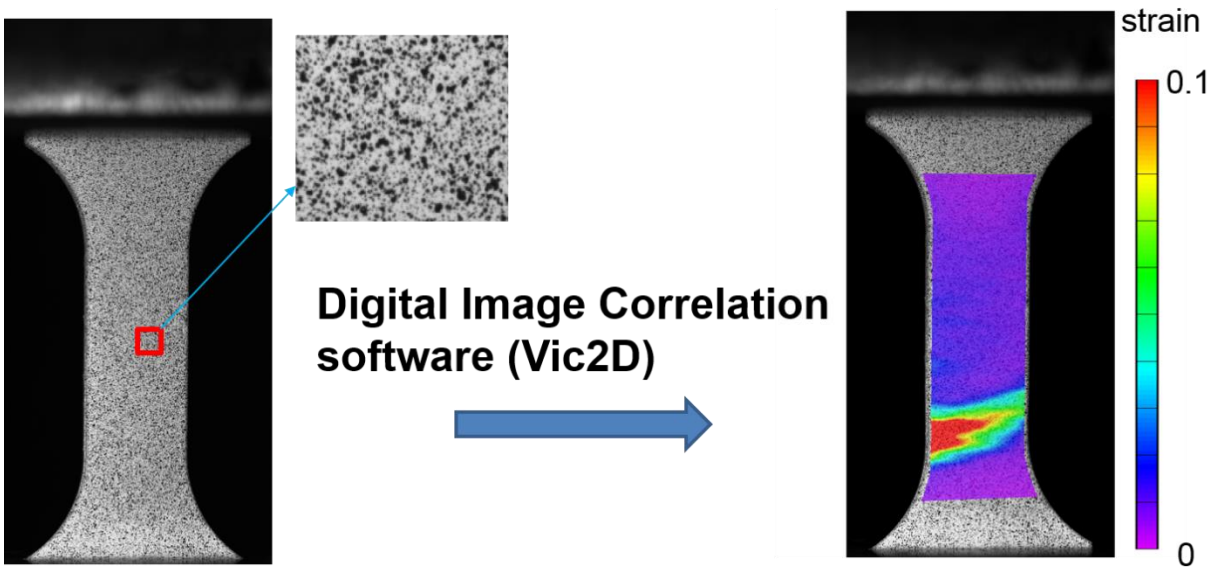

Figure 3.8 A digital image taken by the CCD camera during a tensile test (left hand side) and the strain contour calculated by the DIC software (right hand side).

The measurement system will divide the image into small squares, called facets, and each facets have its identical dot pattern. The identical dot pattern is confirmed by comparing the contrast/brightness patterns in the digital images. By comparing the distortion of the facets, the 2-dimensional strain tensor at a local position on the surface can be then calculated.

In the present study a high resolution CCD camera was used for recording the image. The resolution of the camera is 2048×1024 pixels and each pixel corresponds to a length of 10.9 μm. 10 frames were taken in every seconds during the tensile test. The commercial software VIC-2D was used as the measurement system. The facet size was set to be 25 pixels and the step size was 3 pixels for the strain measurement and the strain tensor in two dimensions was calculated. The precise elongation of the gauge length of the specimen during the tensile test can be also calculated in the VIC-2D system. By combining the stress

measured from the tensile test machine and the elongation calculated by VIC-2D, the stress-strain curve can be precisely obtained as well.

The DIC measurements were carried out on the specimens having different grain sizes, which was shown in the previous section, in order to capture the features of the strain localization depending on the grain size.

3.3.1.2 Results

The strain distribution on the gauge part of the specimen can be visualized by the strain contour maps, as illustrated in **Figure 3.8**. The gradient distribution of the color represents different level of the von Mises equivalent strain. One can easily realize the strain distribution at any strain stage in the tensile deformation from the contour map.

By using the inspection line drawn on **Figure 3.9 (a)**, the strain distribution along a line on the gauge part can be measured and plotted as a function of the pixels. Figures like Figure 3.9 (a) are referred to as strain distribution plot hereafter. The X axis (pixel) represents the relevant position along the gauge length.

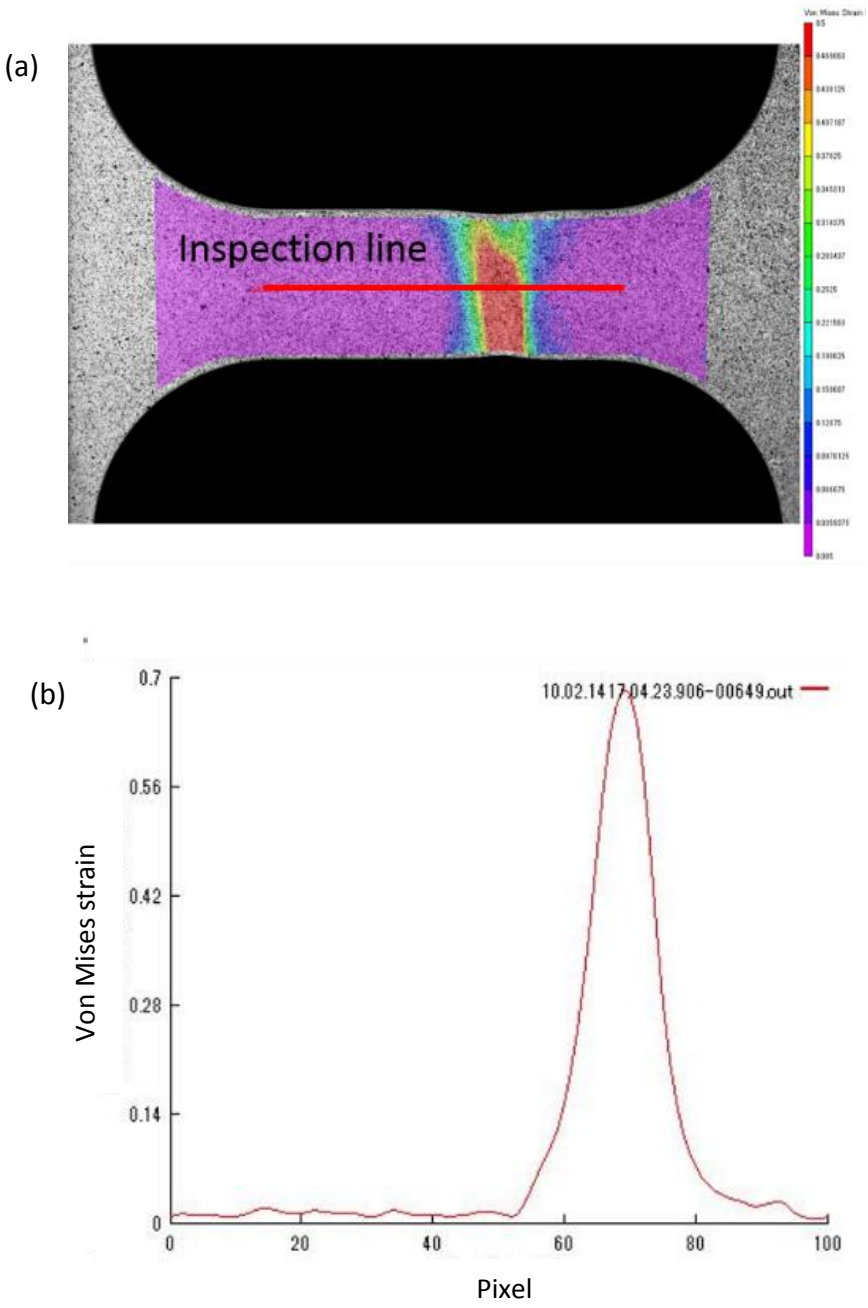

Figure 3.9 (a)A strain contour map obtained from the DIC analysis, and (b) equivalent strain distribution along the inspection line on the gauge part shown in (a).

The DIC measurements were conducted on all of the specimens shown in section 3.1. For the convenience, the strain distribution plot of three representative specimens are chosen to show in **Figure 3.10**. Their stress-strain curves are shown in **Figure 3.10 (a)**.

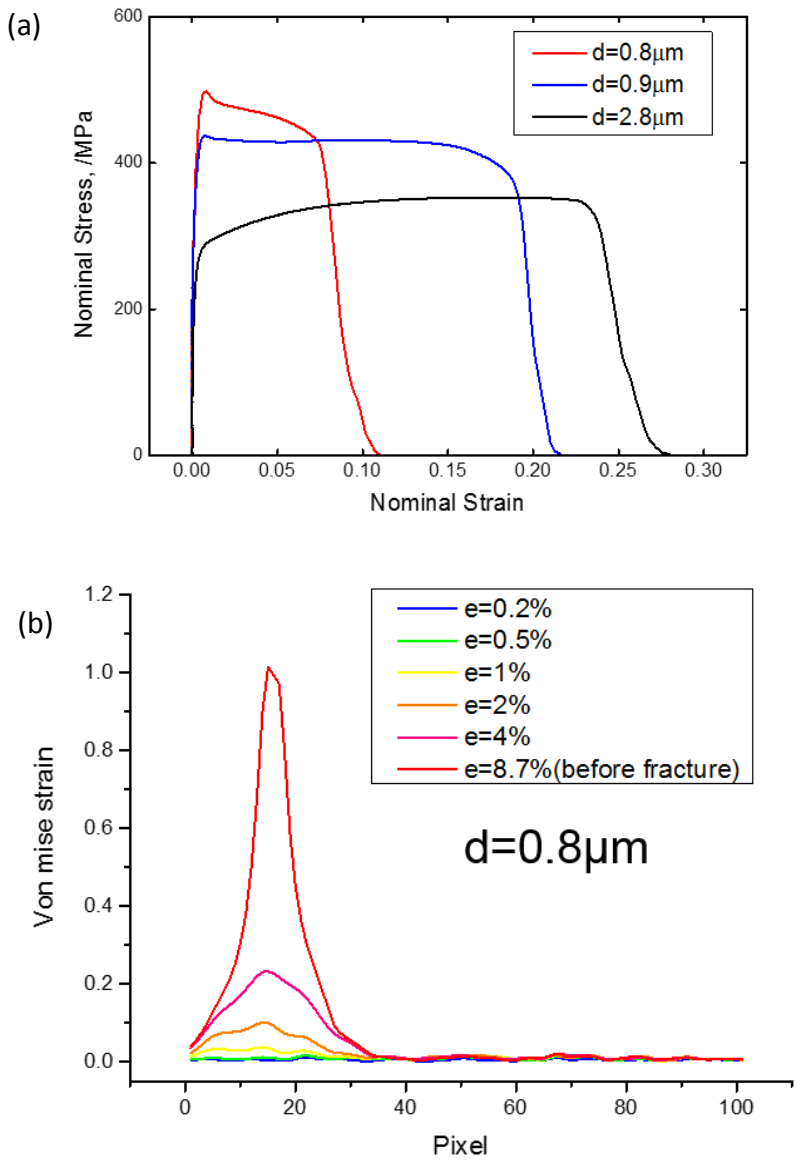

Figure 3.10 (a) Representative stress-strain curves of the specimens having different mean grain sizes. (b~d) The strain distribution plots during tensile test of the specimens having (b) d=0.8 μm (c) d=0.9 μm and (d) d=0.8 μm.

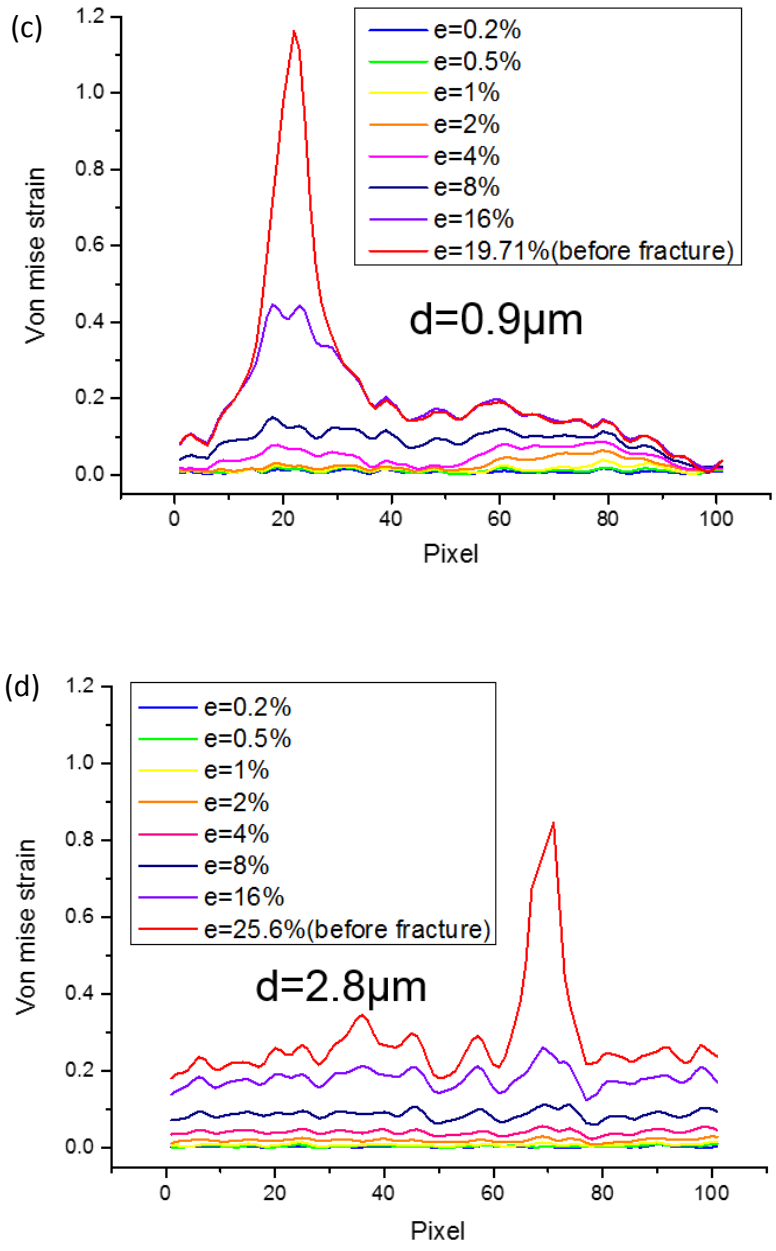

Figure 3.10 (Continued) (a) Representative stress-strain curves of the specimens having different mean grain sizes. (b~d) The strain distribution plots during tensile test of the specimens having (b) d=0.8 μm (c) d=0.9 μm and (d) d=0.8 μm.

The specimen with a grain size d=0.8 μm exhibits yield drop and immediate necking. The specimen with d=0.9 μm exhibits yield drop and plateau, followed by a small portion

of uniform elongation. The specimen with d=2.8 μm exhibit a continuous yielding followed by a normal strain hardening and final necking. In Figure 3.10 (b) – (d), the strain distributions along the gage length at different tensile strain stages from e=0.2% until failure are plotted. Firstly, it is seen that the strain distribution is always not uniform along the gauge length at any elongation stages. It is more or less inhomogeneous. Despite of that, it can be seen that the strain localization is more severe as the mean grain size is decreased, especially when the elongation stage is larger than 2%. For example, at e=4% (the pink color curves in the three figures), the maximum von Mises strain on the gauge part is 0.045, 0.09, 0.25 with decreasing the mean grain size from 2.8 μm to 0.8 μm. It should be noted that the Lüders band deformation is well captured in the specimen with d=0.9 μm by the DIC analysis, as can be seen in **Figure 3.11**. In **Figure 3.11** two clear bands were nucleated on the gauge of the specimen at the beginning of the tensile test, then propagated and finally emerged to one band at the gauge center. The propagation of the Lüders band can be realized in the strain distribution plot. As the mean grain size is smaller than 0.9 μm, the necking immediately occurred with the initial strain localization, so that it was difficult to distinguish the yield point from macroscopic necking by the strain distribution plot.

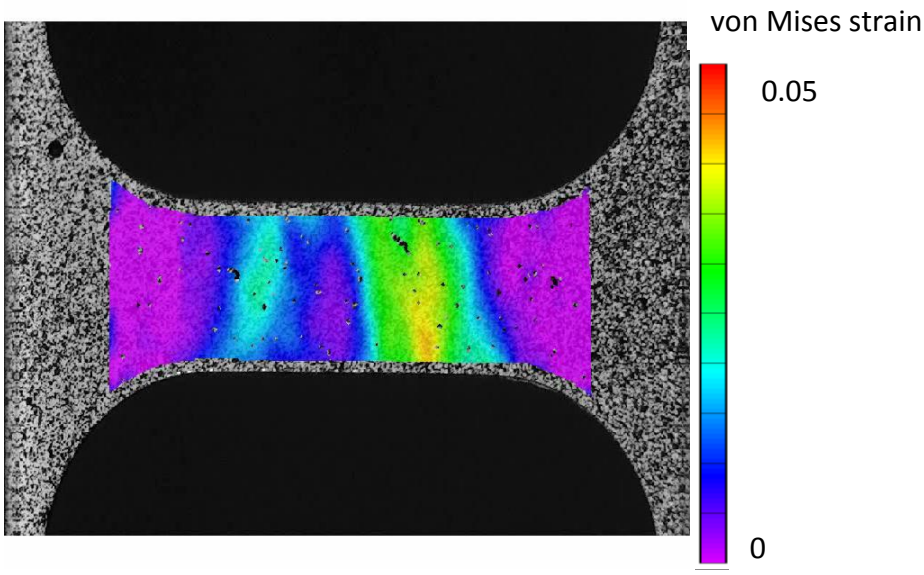

Figure 3.11 Two Lüders bands propagation captured by the CCD camera for the specimen having d=0.9 μm at the tensile strain of 0.02.

3.3.1.3 Discussion

In section 3.2, it was considered that the dramatic loss in the uniform elongation was due to the strain localization associated with the yield point. The degree of the strain localization became higher as the difference between the yield stress and flow stress increased.

The degree of the strain localization at the beginning of the tensile test can be also realized by using the strain distribution plot. The maximum local strain within the gauge length obtained from the DIC analysis at 2% tensile elongation was measured for the specimens having different grain sizes. Then the maximum local strains are plotted as a function of $d^{-1/2}$ in **Figure 3.12**. The true strains corresponding to the uniform elongation of the specimens having different grain sizes are also plotted in the figure. It is seen that the maximum local strain slightly increased when the grain size decreased, but dramatically

increased as the mean grain size became smaller than 2 μm. At the grain size around 1 μm, the local maximum strain becomes nearly the same as uniform elongation. It can be expected that the local maximum strain will continues to increase when the grain size becomes smaller than 1 μm and finally become higher than the uniform elongation, leading to a dramatic drop in the uniform elongation, as shown in the dashed line in the figure. Therefore, the dramatic drop in the uniform elongation in the IF steel is due to the rapidly increased localized strain (Lüders strain), which is caused by the yield point, eventually became larger than the uniform elongation as the mean grain size is smaller than 1 μm.

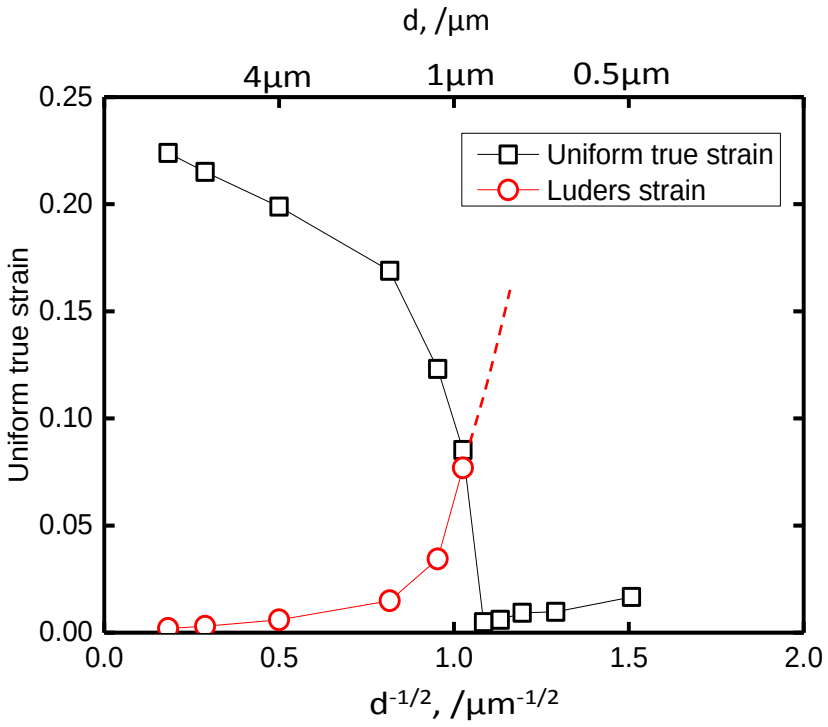

Figure 3.12 True strain corresponding to the uniform elongation and the maximum local strain obtained from the DIC analysis at 2% plastic tensile strain of the specimens having different grain sizes are plotted against $d^{-1/2}$. The dramatic increasing of the local strain in the fine grain size range can be seen.

3.4 Effect of post-annealing cold rolling on elongation of fine grained specimen

3.4.1 Experimental procedure

In order to investigate the effect of the post-annealing cold rolling on the elongation of the fine grained material, cold rolling by 5%, 10%, 20% reduction was applied on the as-ARB specimen and the annealed specimen having the grain size d=0.8 μm. Before cold rolling, the surface of the sheet specimen was carefully polished by grind paper and OPS (oxidized silicon particles) solution to get a mirror-like surface. Multiple-pass rolling was applied on the specimen in order to obtain the precise reduction. The reduction for each pass was carefully controled to maintain the ratio of the contact length to the sample thickness in the range of 1.5–3.0, in order to avoid redundant shear deformation during rolling. Then, tensile test specimens were cut out from these cold rolled sheets, and the tensile test and DIC analysis were carried out on those specimens.

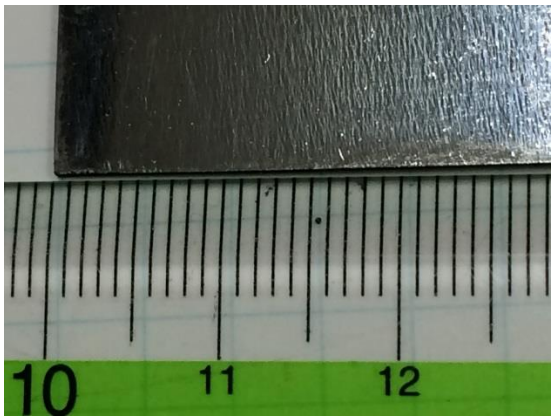

Figure 3.13 Surface morphology of the ARB processed and 540°C annealed specimen with a grain size d=0.8 μm after 5% post-annealing cold rolling.

3.4.2 Result and discussion

The surface appearance of the specimen with d= 0.8 μm after 5% cold rolling is seen in **Figure 3.13**. Numerous number of small localized deformation marks can be observed even by naked eyes. These deformation marks were observed on both specimens. The dark field image of the surface taken from the optical microscope of the as-ARB specimen after various reduction of cold rolling are shown in **Figure 3.14** and **3.15**. It is seen that with only 5% cold rolling, clear deformation zone can be recognized (the bright region) having widths from 0.05 mm to 0.1 mm in both specimens. With increasing the cold rolling reduction, the deformation zone seems broadened to the un-deformed zone (dark area). By 20% cold rolling, most of the surface area were occupied by the bright region. This result indicate that the plastic deformation of the sheets started by inhomogeneous deformation even in rolling process. By applying a small amount of rolling reduction, the numerous plastic zones (deformation bands) nucleated on the specimen inhomogeneously, and then propagated or broadened toward the un-deformed region.

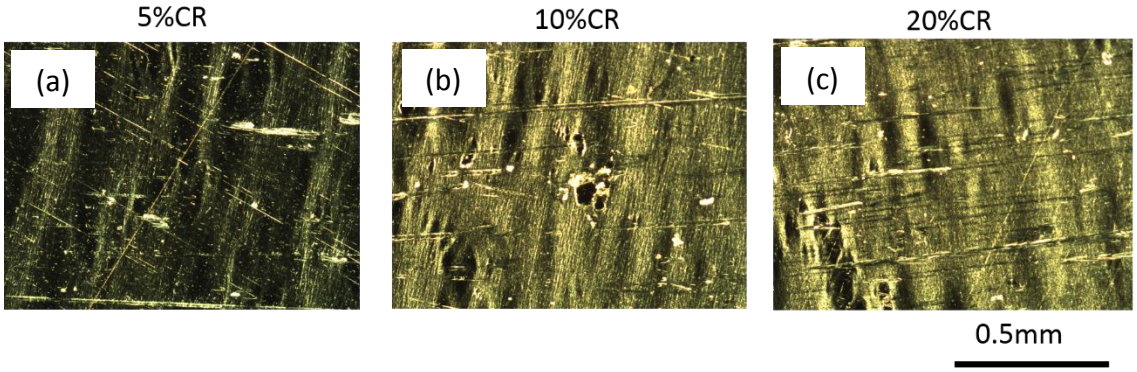

Figure 3.14 Optical micrographs showing the surface morphologies of the as-ARB specimen after cold rolling by (a) 5%, (b) 10% and (c) 20%.

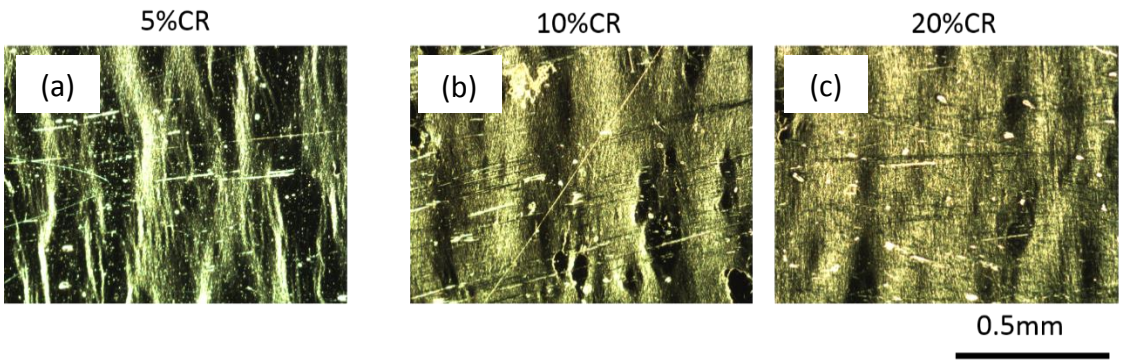

Figure 3.15 Optical micrographs showing the surface morphologies of the ARB+540°C annealed specimen with d=0.8 μm after post-annealing cold rolling by (a) 5%, (b) 10% and (c) 20%..

The stress-strain curves of the as-ARB processed specimen and the ARB processed and then cold-rolled specimens are shown in **Figure 3.16**. It is seen that by applying cold rolling, the yielding behavior becomes more continuous, i.e., the stress peak becomes more round. The yield stress and ultimate tensile strength (UTS) are plotted as a function of the cold rolling reduction in **Figure 3.17** (a), and the uniform elongation, and total elongation are also plotted in **Figure 3.17** (b) for the as-ARB processed specimen and the specimens ARB processed and then cold-rolled.

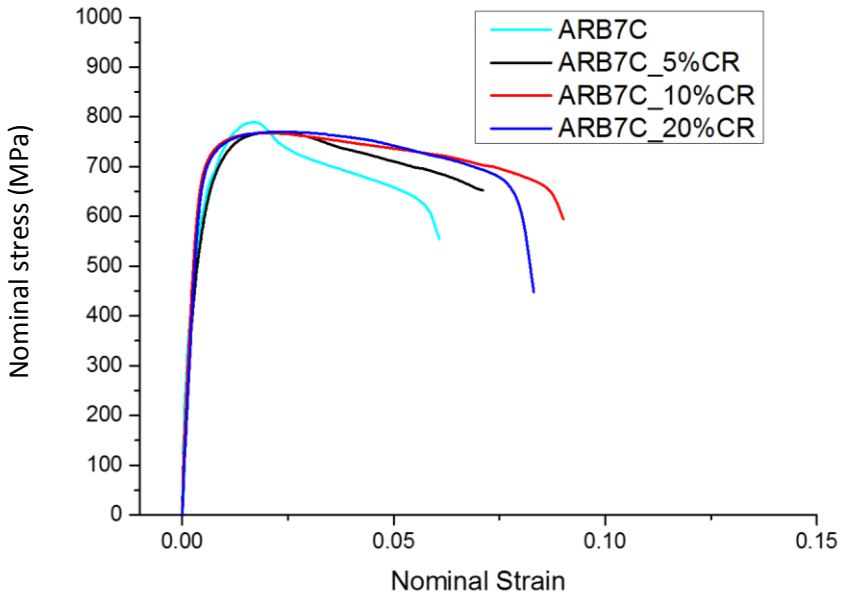

Figure 3.16 Stress-strain curves of the as-ARB processed specimen and ARB processed and cold-rolled specimen.

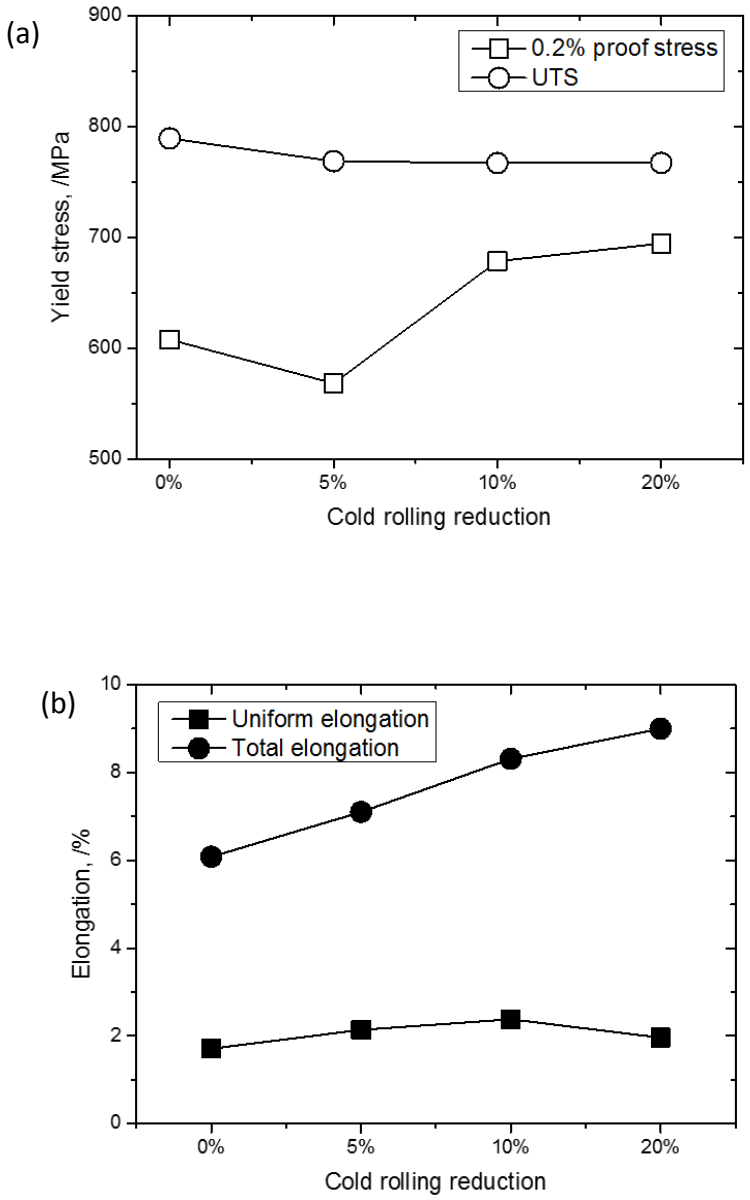

Figure 3.17 The yield stress and UTS (a), uniform elongation and total elongation (b) are plotted as the function of the cold rolling reduction of the as-ARB processed specimen and ARB processed and cold-rolled specimen.

It could be seen that the yield stress showed a softening by 5% cold rolling reduction, which corresponded to the "softening by deformation" behavior. By increasing the cold

rolling reduction, the yield stress increased to around 700MPa. The UTS slightly decreased by the first 5% cold rolling and then saturated. The results indicate that the cold rolling has more effect on the yield stress rather than the UTS. Moreover, the saturation of the UTS indicates that the "softening by deformation" still occurs by applying large amounts of cold rolling reduction even up to 20%. On the other hand, the uniform elongation merely changed while the total elongation monotonically increased with increasing the rolling reduction. The strain distribution map of of the as-ARB processed specimen and the ARB processed and then cold-rolled specimens are shown in **Figure 3.18**. It could be seen that by increasing the cold rolling reduction, local strains became uniformly distributed along the gauge part until the necking occurred, which corresponded to the increase of the total elongation.

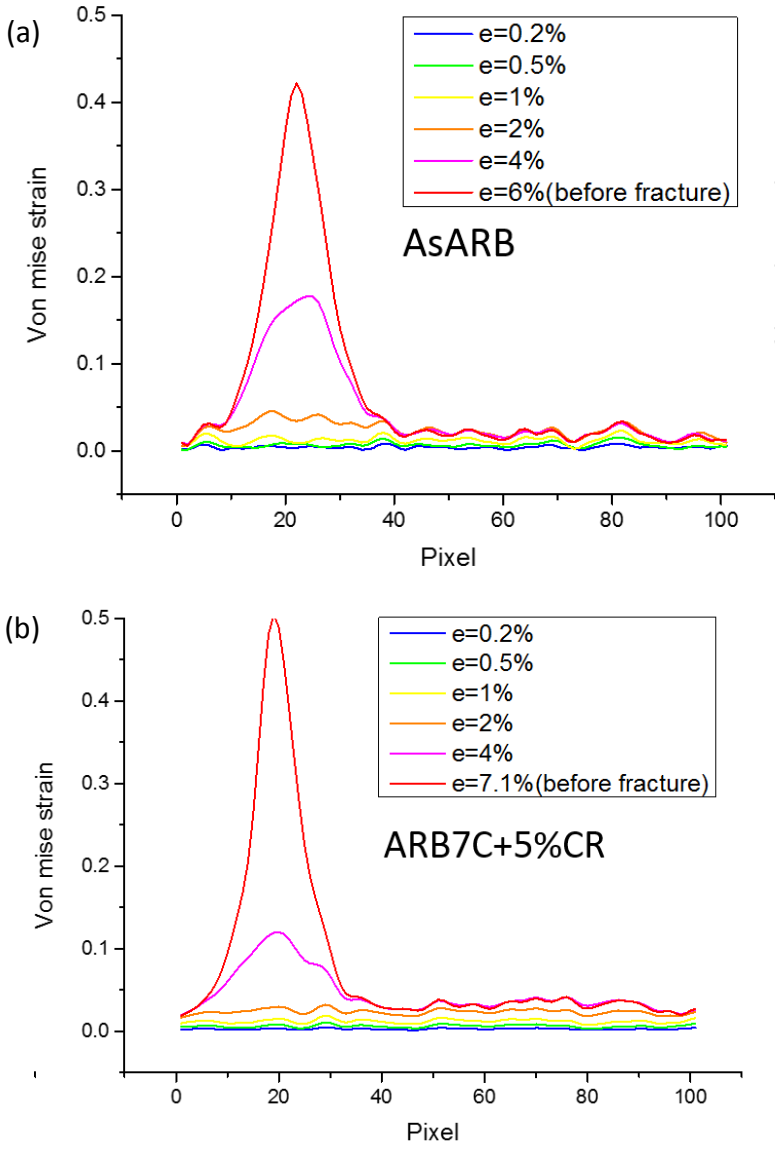

Figure 3.18 Strain distribution maps of the (a) as-ARB specimen and the ARB processed specimen cold-rolled by (b) 5%, (c) 10% and (d) 20%

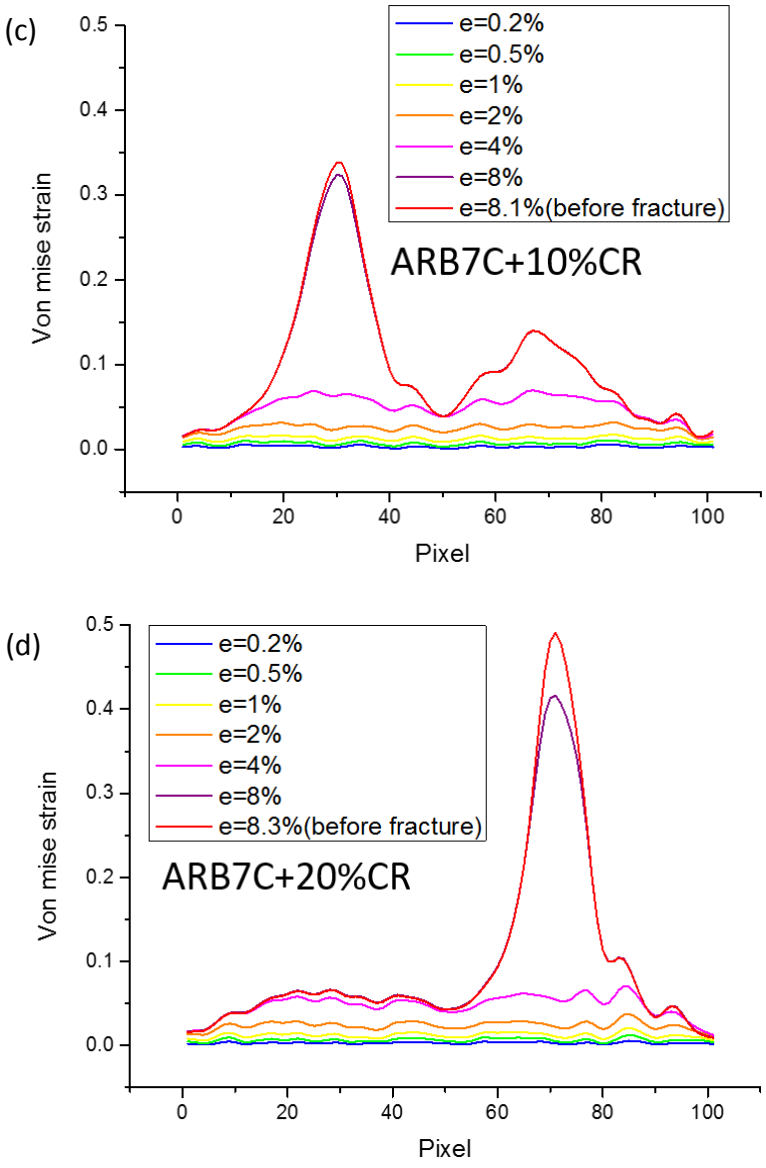

Figure 3.18 (Continued) Strain distribution maps of the (a) as-ARB specimen and the ARB processed specimen cold-rolled by (b) 5%, (c) 10% and (d) 20%

For the specimen having d=0.8 μm, the stress-strain curve showed a sharp yield point phenomenon before cold rolling, as shown in **Figure 3.19**. By applying cold rolling, the sharp yield point disappeared in the subsequent tensile test. At the same time, the elongation of the material increased. The result indicates that the "softening by deformation" behavior of the UFG material is closely related to the yield point phenomena. The yield

stress and UTS both decreased by applying 5% cold rolling reduction, and then monotonically increased by increasing the cold rolling reduction, as shown in **Figure 3.20 (a)**. This means that the "softening by deformation" behavior only occurs by the 5% cold rolling. After that, normal strain hardening begins by increasing the cold rolling reduction furthermore. The uniform elongation and total elongation also increased by 5% cold rolling and then decreased by applying more cold rolling reductions, as shown in **Figure 3.20 (b)**.

The strain distribution map is shown in **Figure 3.21**. The local strain distribution along the gage length became more homogeneous by the first 5% cold rolling, and then the strain distribution became more concentrated by increasing the cold rolling reduction.

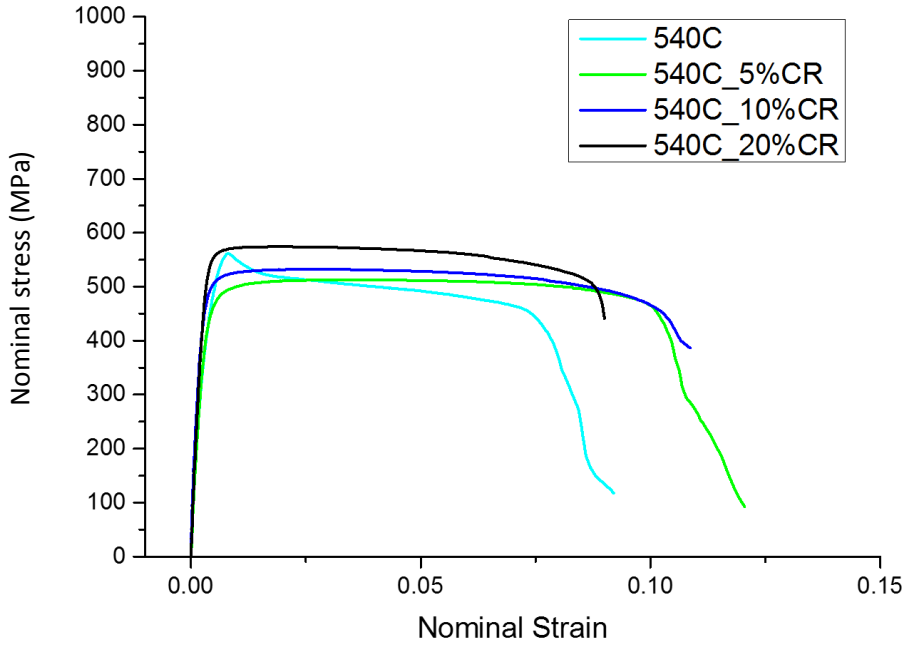

Figure 3.19 Stress-strain curves of the specimen with d=0.8 μm, after post-annealing cold rolling by different reductions.

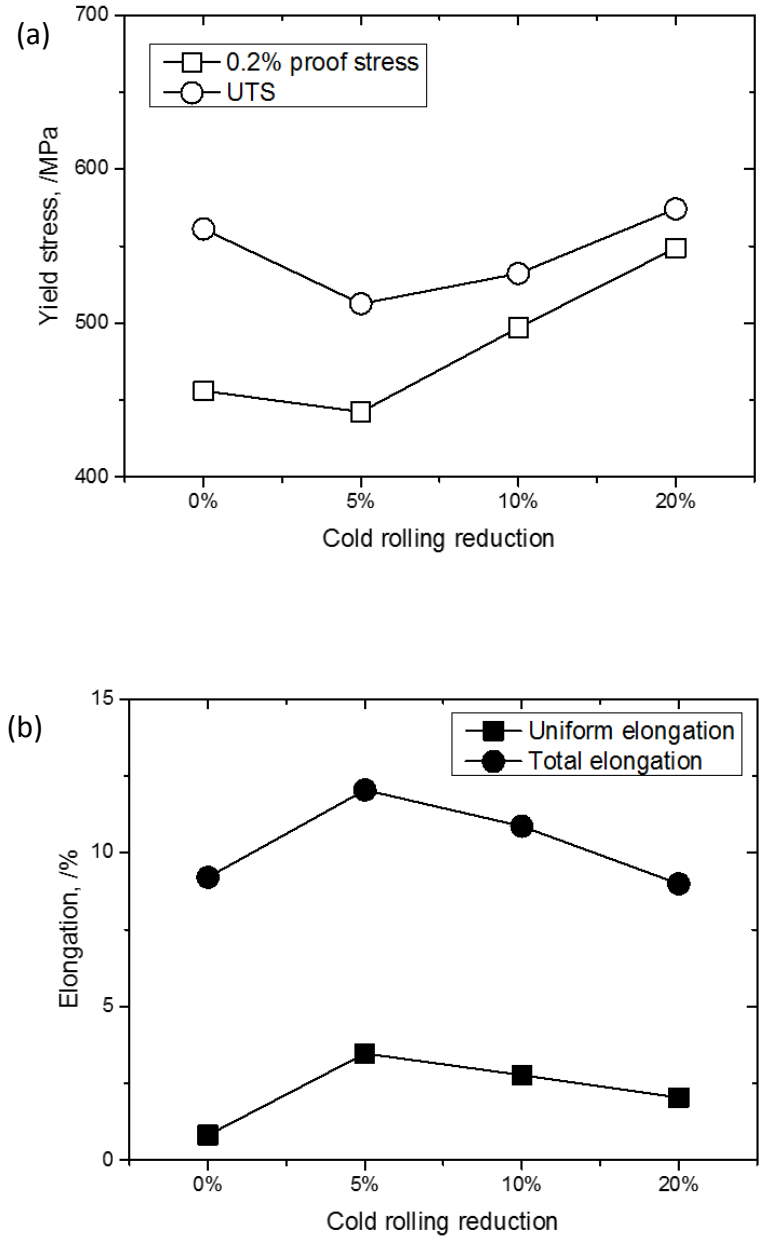

Figure 3.20 The yield stress and UTS (a), uniform elongation and total elongation (b) of the specimen having d=0.8 μm are plotted as the function of the cold rolling reduction.

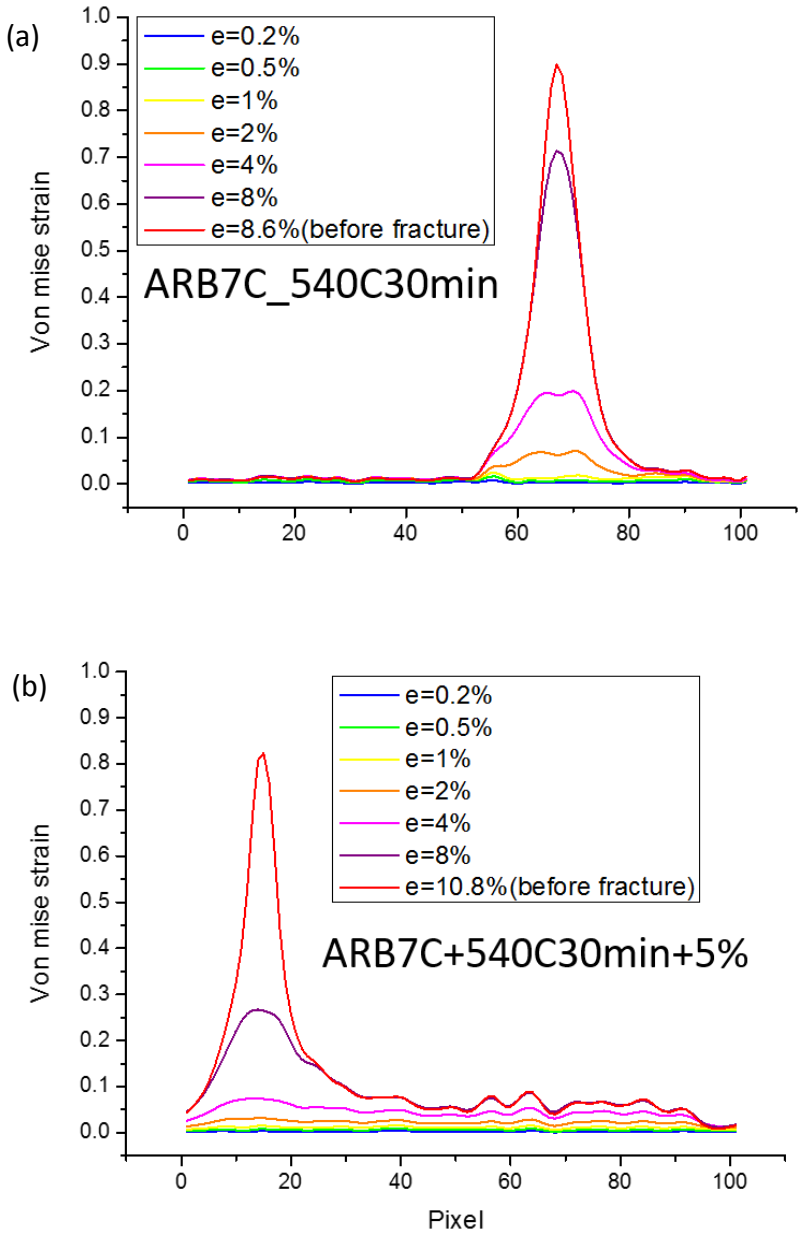

Figure 3.21 Strain distribution maps of the specimen having d=0.8 μm and cold-rolled by (a) 0% (b) 5%, (c) 10% and (d) 20%.

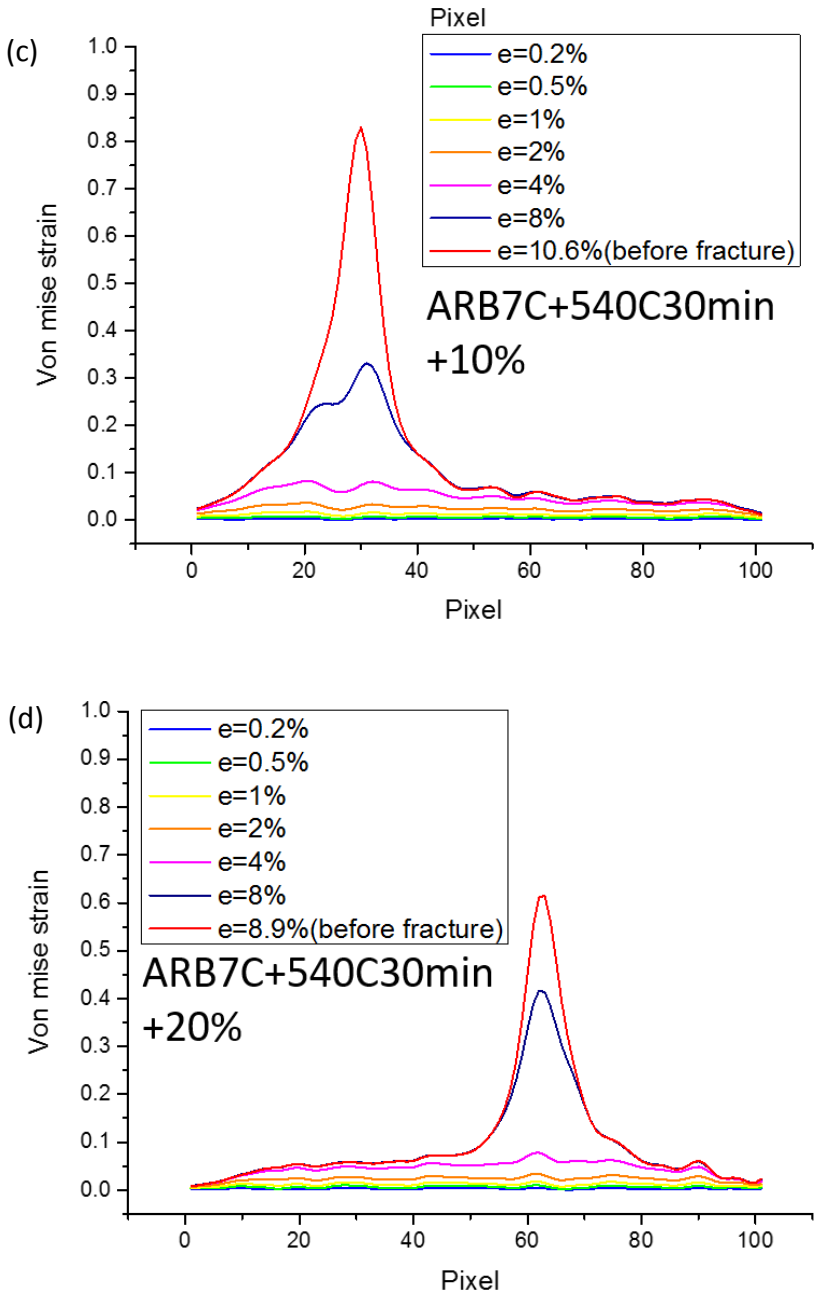

Figure 3.21 (Continued) Strain distribution maps of the specimen having d=0.8 µm and cold-rolled by (a) 0% (b) 5%, (c) 10% and (d) 20%.

The above mentioned results indicates that the both of the grain size and initial dislocation density have a significant effect on whether the material exhibits the "softening

by deformation" behavior or not. This unique behavior seems more sensitive to the grain size rather than to the dislocation density, because the as-ARB processed specimen having finer grain size exhibits the stronger "softening by deformation" behavior, although it contains higher dislocation density.

3.5 Conclusion

In this chapter, IF steel specimens with different grain sizes ranging from 30 μm to 0.45 μm were fabricated by ARB process and subsequent annealing. Tensile tests at room temperature revealed a transition from continuous yielding to discontinuous yielding behaviors with decreasing the mean grain size down to an ultra-fine range smaller than 1 μm. Two distinct Hall-Petch slopes were found, associated with the coarse grain size specimen exhibiting continuous yielding and the fine grain sized specimen exhibiting discontinuous yielding. The dramatic drop in the uniform elongation was found to occur when the grain size became below 1 μm. This dramatic drop was attributed to the early plastic instability associated with the occurrence of the discontinuous yielding behavior in the fine grained specimens, which could be explained by using the Hall-Petch analysis for the yield and flow stresses. By applying post-annealing cold rolling, the yielding behavior was changed from the discontinuous type to the continuous type, and the uniform elongation of the specimen increased. Since it has been found that discontinuous yielding is an unique mechanical behavior of various kinds of materials with fine grain sizes, it can be concluded that the yielding behavior has a significant importance on the ductility of the UFG materials.

References

[1] Hall EO (1951) The deformation and ageing of mild steel. *Proc.Phys. Soc. B* 64: 747-753.

[2] Petch NJ (1953) The cleavage strength of polycrystals. *J Iron Steel Inst* 174: 25-28.

[3] Tsuji N, Ito Y, Saito Y, Minamino Y (2002) Strength and ductility of ultrafine grained aluminum and iron produced by ARB and annealing. *Scripta Mater* 47: 893-899.

[4] Huang X, Hansen N, Tsuji N (2006) Hardening by annealing and softening by deformation in nanostructured metals. *Science* 312: 249-251.

[5] Huang X, Kamikawa N, Hansen N (2010) Strengthening mechanisms and optimization of structure and properties in a nanostructured IF steel. *J Mater Sci* 45: 4761-4769

[6] Kidmose J, Lu L, Winther G, Hansen N, Huang X (2012) Strain distribution during tensile deformation of nanostructured aluminum samples. *J Mater Sci* 47: 7901-7907.

[7] An H, Wu S, Zhang Z, Figueiredo RB, Gao N, Langdon TG (2012) Enhanced strength–ductility synergy in nanostructured Cu and Cu–Al alloys processed by high-pressure torsion and subsequent annealing. *Scripta Mater* 66: 227-230.

[8] Yu CY, Kao PW, Chang CP (2005) Transition of tensile deformation behaviors in ultrafine-grained aluminum. *Acta Mater* 53: 4019-4028.

[9] Li Z, Fu L, Fu B, Shan A (2013) Yield point elongation in fine-grained titanium. *Mater Lett* 96: 1-4.

[10] Kamikawa N, PhD thesis, 2005, Osaka University.

[11] Gao S, Chen M, Chen S, Kamikawa N, Shibata A, Tsuji N (2014) Yielding Behavior and Its Effect on Uniform Elongation of Fine Grained IF Steel. *Mater Trans* 55: 73-77.

[12] Cottrell A, Bilby B (1949) Dislocation theory of yielding and strain ageing of iron. *Proc.Phys. Soc. A* 49: 49-62.

[13] Hahn GT (1962) A model for yielding with special reference to the yield-point phenomena of iron and related bcc metals. *Acta Metall* 10: 727-738.

[14] Sabirov I, Estrin Y, Barnett M.R., Timokhina I, Hodgson P.D. (2008) Tensile deformation of an ultrafine-grained aluminium alloy: micro shear banding and grain boundary sliding. *Acta Mater* 56: 2223-2230

[15] Saha R, Ueji R, Tsuji N (2013) Fully recrystallized nanostructure fabricated without severe plastic deformation in high-Mn austenitic steel *Scripta Mater* 68: 813-816

[16] M.A. Meyers, A. Mishra, D.J. Benson Mechanical properties of nanocrystalline materials, *Progress in Materials Science* 51 (2006) p. 427 – 556.

[17] Dongare, A. M., Rajendran, A. M., Lamattina, B., Brenner, D. W., Atomic-Scale Study of Plastic-Yield Criterion in Nanocrystalline Cu at High Strain Rates. (2009). *Metallurgical and Materials Transactions A, 41*(2), 523–531

[18] Armstrong RW, Codd I, Douthwaite RM, Petch NJ (1962) The plastic deformation of polycrystalline aggregates. *Phil. Mag* 7: 45-57.

[19] EO. Hall (1970) Yield Point Phenomena in Metals and Alloys, Springer.

Chapter 4 Role of internal stress in yielding behavior of ultra-fine grain materials: Bauschinger effect in 2N-Al with various mean grain sizes

4.1 Introduction

In Chapter 3, the significant effect of the yield point phenomena on the uniform elongation was demonstrated by using Hall-Petch analysis and DIC technique. Although the yield point phenomena associated with the severe strain localization are not favorable from a viewpoint of practical applications, it is still a fundamentally interesting deformation mechanisms of the metallic material. Extensive researches have been done on the strengthening mechanism of the UFG material, the yield point of the UFG material is still not fully understood. The most widely accepted explanation for the yield point in the UFG material is based on the lack of mobile dislocations, as proposed by Hahn [1]. In Hahn's theory, the yield point in metallic material is due to the abrupt drop in the average dislocation velocity by the sudden multiplication of mobile dislocations. Thus, the materials having a strong stress-dislocation velocity dependence (that is having a high *n* value in equation (1.1)), such as Fe, Mo, V would exhibit yield point if the dislocation velocity significantly decreases. While for the metals such as Cu and Al having small *n* values would not exhibit yield point even during the sudden multiplication of mobile

dislocations. However, previous researches have confirmed the appearance of yield point in various kinds of materials having UFG microstructures, such as Fe [2], Al [2], Cu [3], Ti [4], whose *n* values are greatly different. It seems, therefore, difficult to explain the yield point in UFG materials by Hahn's theory. In addition, Orowan [65] found that the well-known strain-aging effect did not occur in the low carbon steel when the direction of the deformation was reversed after the aging treatment. That was contradicted to the mobile dislocation density theory, since based on Hahn's theory the yield point was expected in both forward and reverse deformation after strain-ageing if the mobile dislocations were substantially locked by the interstitial atoms during the aging treatment. Orowan's results clearly suggested that the yield point phenomena in the low carbon steel was anisotropic. Recent research have also found the anisotropy of the yield point in a low carbon steel as well as in an Al-Mg alloy having conventional grain sizes [6]. It was suggested that the yield point phenomena was also related to the internal stress resulting from the inhomogeneous dislocation structures in the materials [6, 7].

The anisotropic character of the mechanical behavior is drawing more and more attentions in the recent decades. It was firstly realized by J.Bauschinger who found that pre-straining in any direction would introduce an anisotropic effect on the flow stress for further deformation in any other direction in metallic materials, which was so-called Bauschinger effect [8]. Several theories have been proposed to explain the Bauschinger effect, including Seeger's theory related to the dislocation pile-up [9] and Orowan's forest dislocation theory [10]. In those theories, the directionality of the strain hardening is explained by the internal stress arisen from the inhomogeneous dislocation structures. In

the UFG material, several studies found unexpected large internal stresses [11, 12, 13], which should be closely related to the strengthening mechanism in the UFG materials.

In this chapter, the development of the internal stress (back stress) during deformation is measured by the Bauschinger test using pure Al having UFG structures. A huge internal stress is found for the UFG specimens, especially at small strain stages. It is shown that the internal stress is the main contribution to the "extra-hardening" of the UFG specimen shown in Chapter 4. In addition, it is also demonstrated that the yield point phenomena in the UFG specimens (of the UFG pure Al at least) are due to the decrease of the internal stress with increasing the plastic strain increased.

4.2 Experiment procedure

4.2.1 Starting material

A commercial purity Al (JIS-1100) (hereafter refer to as 1100-Al) was used for the present study. The chemical composition of the material is show in **Table 4.1**. The starting material has a mean grain size of 18 μm, as can be seen in the microstructure shown in **Figure 4.1**.

Table 4.1 Chemical composition of the 1100-Al used in chapter study (mass %).

Si	Fe	Cu	Mn	Mg	Cr	Zn	Ti	Al
0.101	0.561	0.1	0.001	0.001	0.005	0.001	0.021	Bal.

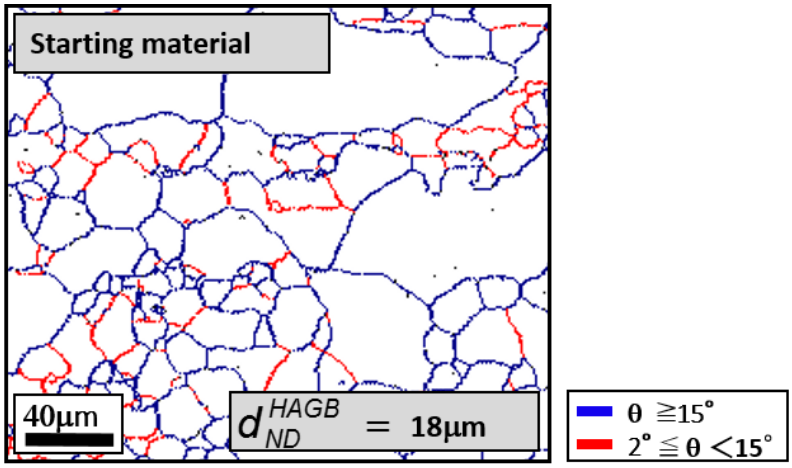

Figure 4.1 EBSD grain boundary map showing the microstructure of the starting material of 1100-Al.

4.2.2 ECAP process

Equal-channel angular pressing (ECAP) process [14] was carried out on the 1100-Al having a shape of round bar having 10 mm in diameter. ECAP is the process in which simple shear deformation is repeatedly imposed on the sample for introducing large amount of plastic deformation (severe plastic deformation). The ECAP facility and procedures used in the present study are schematically illustrated in **Figure 4.2 (a)**. Two channels having a circular cross section with a diameter of 10 mm intersect in the die with an inner corner angle of 90 degrees and a rounded outer corner angle of 20 degrees, as shown in **Figure 4.2 (b)**. The ECAP process was carried out at room temperature by 8 passes with Route-A, during which repeated pressing was conducted without rotation along the extrusion direction between each pass [14]. The equivalent strain in ECAP is defined as [14]:

$$\varepsilon^{ECAP} = \frac{n}{\sqrt{3}}\left\{2\tan^{-1}\left(\frac{\phi}{2}+\frac{\psi}{2}\right)+\phi\sin^{-1}\left(\frac{\phi}{2}+\frac{\psi}{2}\right)\right\} \quad (4.1)$$

Here, n is the number of passes through the dies with inner and outer corner angles of ϕ and ψ. The equivalent strain after 8 passes through the die with ψ=90 and ϕ=20 degrees die in the present case is calculated to be 8.4.

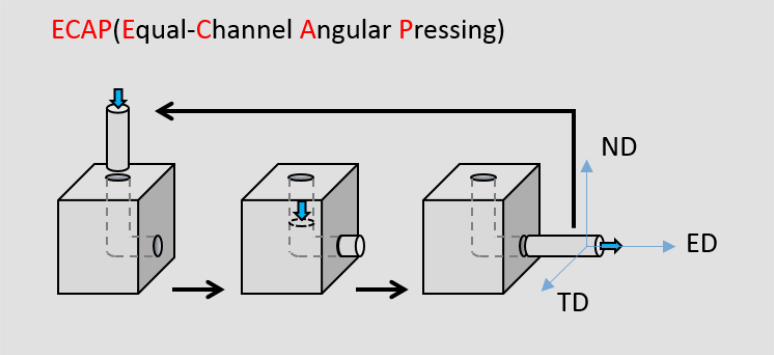

(a)

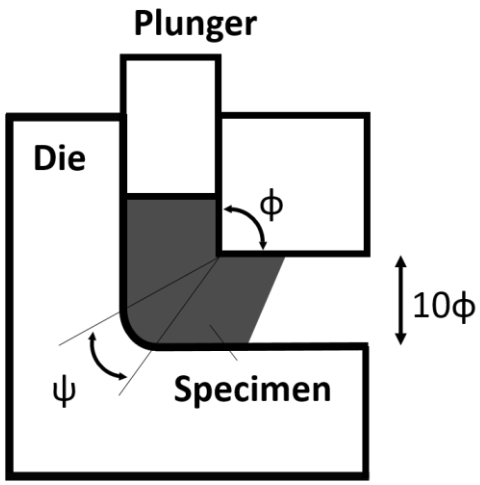

(b)

Figure 4.2 (a) Illustration of the equal-channel angular pressing (ECAP) process and (b) the inner and outer angle of the two channels in the ECAP die.

4.2.3 Microstructure observation

In order to achieve different mean grain sizes, the as-ECAP processed specimens were annealed in an oil bath or in a box-type electric furnace at different temperatures ranging from 100°C to 400°C for various periods. The microstructures were observed from the transverse direction (TD) (**Figure 4.2 (a)**) of the ECAP specimens by SEM-EBSD. The

specimens for the EBSD analysis were prepared by mechanical polishing followed by electropolishing at -30 ºC at a voltage of 12 V in a solution of 30 vol.% nitric acid (HNO_3) and 70 vol.% methanol (CH_3OH). EBSD observation was performed in a field-emission scanning electron microscope (FE-SEM, Phillips FEI XL30S FEG) at an accelerating voltage of 15 kV. For TEM analysis, thin-foil specimens were prepared by twin-jet electopolishing using the same temperature and solution as those for the EBSD specimens. TEM observations were performed in a JEOL-2000EX TEM microscope with a double-tile stage holder at an operating voltage of 200 kV. The TEM microstructures were observed from the TD direction of the ECAP specimens.

4.2.4 XRD measurement

The dislocation densities of the specimens were determined by X-ray diffraction (XRD). The X-ray diffraction was performed using a Rigaku Smart-Lab X-ray diffractometer with Cu Kα radiation. The diffraction patterns of the as-ECAP processed specimens and the specimens subsequently annealed at different temperatures are shown in **Figure 4.3**.

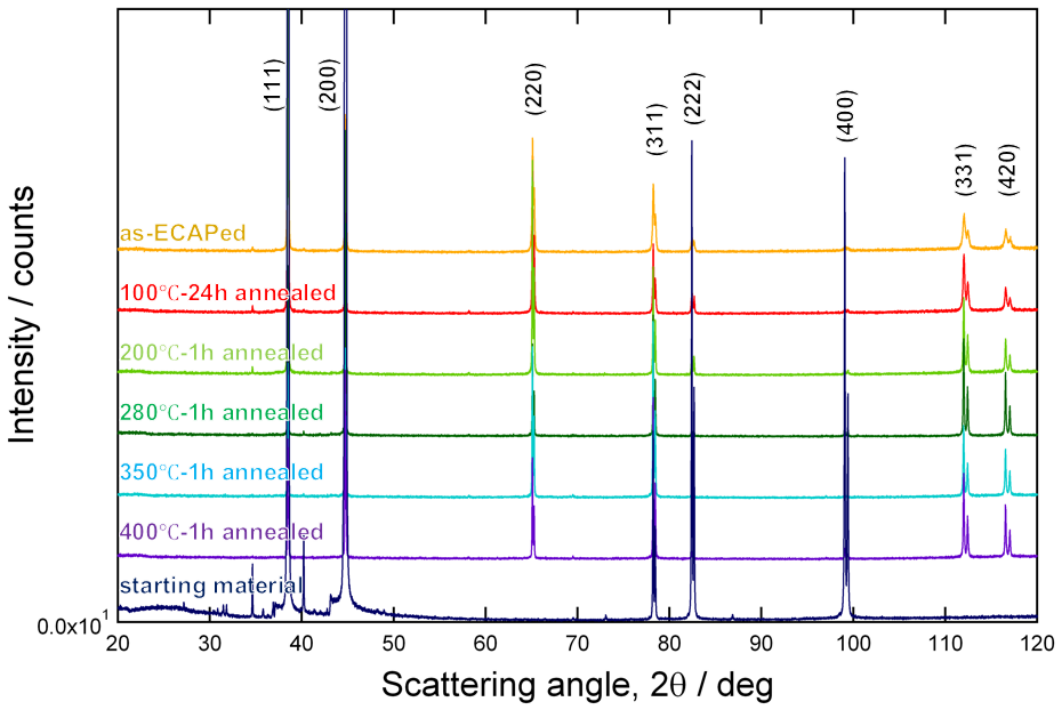

Figure 4.3. Diffraction patterns of the starting material as well as the as-ECAP processed and subsequently annealed specimens.

The dislocation density (ρ) was quantitatively estimated from the XRD pattern using Williamson-Hall method through following equations [15]:

$$\rho = \frac{k\bar{\varepsilon}^2}{Fb^2} \tag{4.2}$$

where *k* and *F* are constant values (16.1 for FCC material and 1, respectively), *b* is the magnitude of Burgers vector (0.286 nm for aluminum), ε is the lattice strain described by {(βcosθ/λ)/(2sinθ/λ)}, β is the full-width at half maximum height (FWHM) of the peaks, λ is the wave length of X-ray and θ is the diffraction angle. **Figure 4.4** shows the Williamson-Hall plots for the as-ECAP processed specimen and the 350°C annealed specimen. In the plot Williamson-Hall plots, the lattice strain ε is obtained by linear

fitting the $\Delta K=\beta\cos\theta/\lambda$ versus $K=2\sin\theta/\lambda$. The dislocation densities evaluated from the XRD results are shown in **Figure 4.15**.

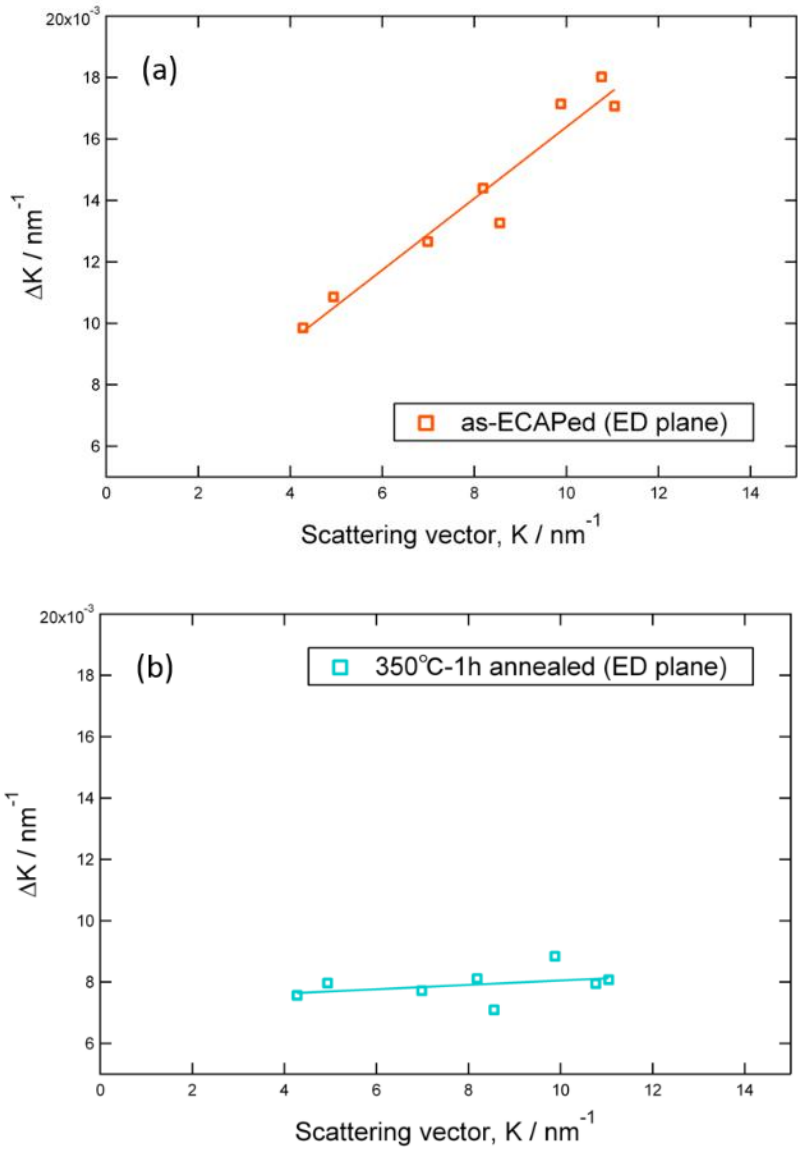

Figure 4.4 Williamson-Hall plots for two specimens (the as-ECAP processed specimen and the ECAP processed and 350C° annealed specimen), from which the lattice strain ε could be obtained by linear fitting.

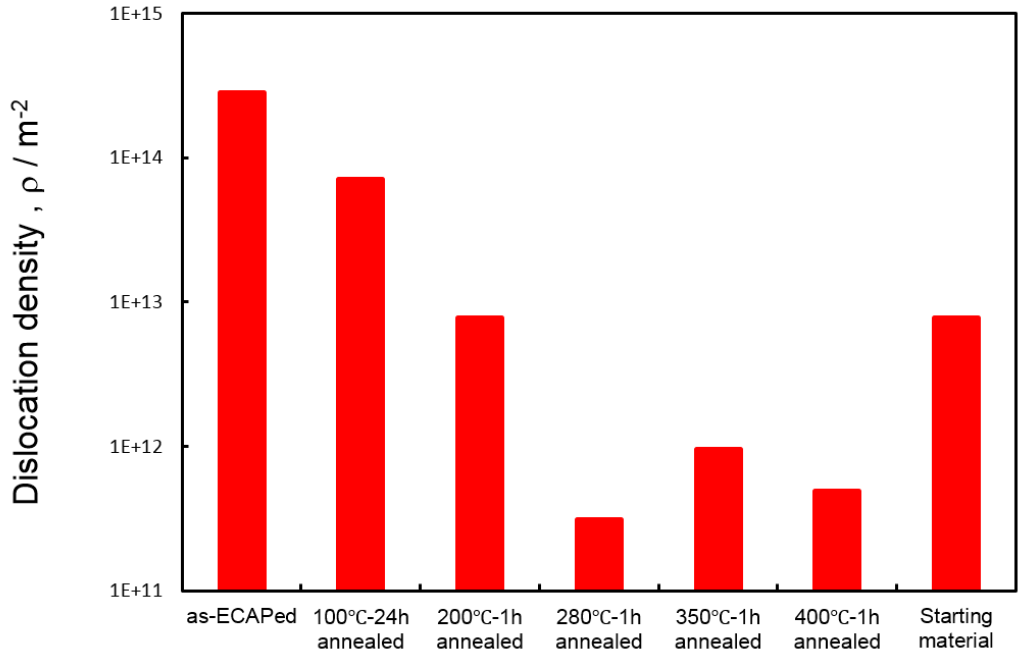

Figure 4.5 The dislocation densities of the as-ECAP processed specimens and the ECAP processed and annealed specimens measured by XRD.

4.2.5 Mechanical test

The annealed specimens were machined into tension/compression test specimens having a dumbbell-shape with a gauge length of 6 mm and gage diameter of 4 mm, as shown in **Figure 4.6**. Tensile test and Bauschinger test were carried out on a fatigue testing machine (Shimadzu Servo-Pulser EHF-LB10kN-10Lmachine) with a screw type jig at room temperature and at an initial strain rate of $5\times10^{-4}s^{-1}$. The tensile axis was parallel to the extrusion direction (ED) of the ECAP process. The displacement of the specimen during the test was precisely measured by an attached strain gauge (KFG-2N-120-C1-23, KYOWA ELECTRONIC). To avoid the early buckling during compression, the jig was fastened to the fatigue test machine by the help of a low-melting point alloy. The setting of the testing system can be seen in **Figure 4.6**. The Bauschinger test was done by first

deforming the specimen to a plastic strain in tension (pre-strain) and then reversing the deformation to the compressive direction. A schematic illustration of the stress-strain curve obtained from the Bauschinger test is shown in **Figure 4.7**. For each grain size, several Bauschinger tests were conducted at different pre-strains in the first tension.

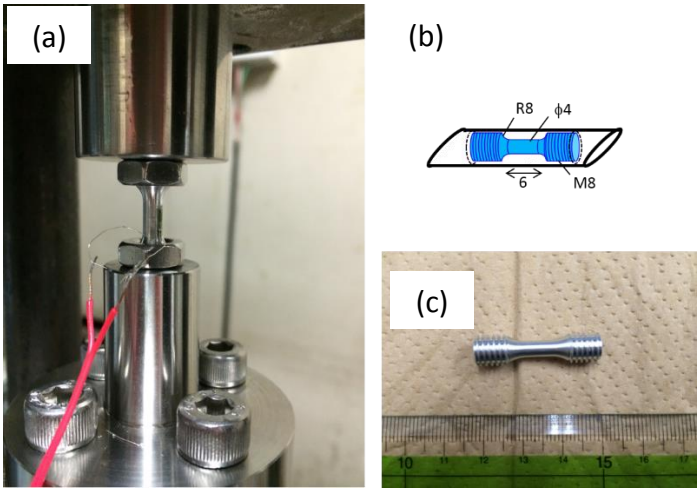

Figure 4.6 Photographs and illustration showing (a) the setting of the Bauschinger test specimen (b) the dimension of the specimen, and (c) the specimen.

The flow stress during plastic straining can be separated into two parts: effective stress and back stress (internal stress). According to the previous study [16], the back stress is (internal stress) usually referred to the stress associated with the long-range interactions between dislocations to overcome obstacles, such as grain boundaries, precipitations. The effective stress is the stress required for dislocations short-range interactions, like friction stress, precipitation hardening and forest hardening. The back stress (internal stress) can be calculated from the tension-compression stress-strain curve, according to the way reported in the previous research [16, 17], as illustrated in **Figure 4.7** and expressed in the following equations:

$$\sigma_e = \frac{(\sigma - \sigma_R)}{2} + \frac{\sigma^*}{2} \tag{4.2}$$

$$\sigma_{Back} = \sigma - \sigma_e \tag{4.3}$$

where σ is the flow stress, σ_{Back} the back stress, σ^* the thermal part of the flow stress, σ_e the effective stress, σ_R the yield stress in the reverse direction. The reverse yield stress is obtained as the stress at a plastic strain offset equal to 5×10^{-5} (0.005%).

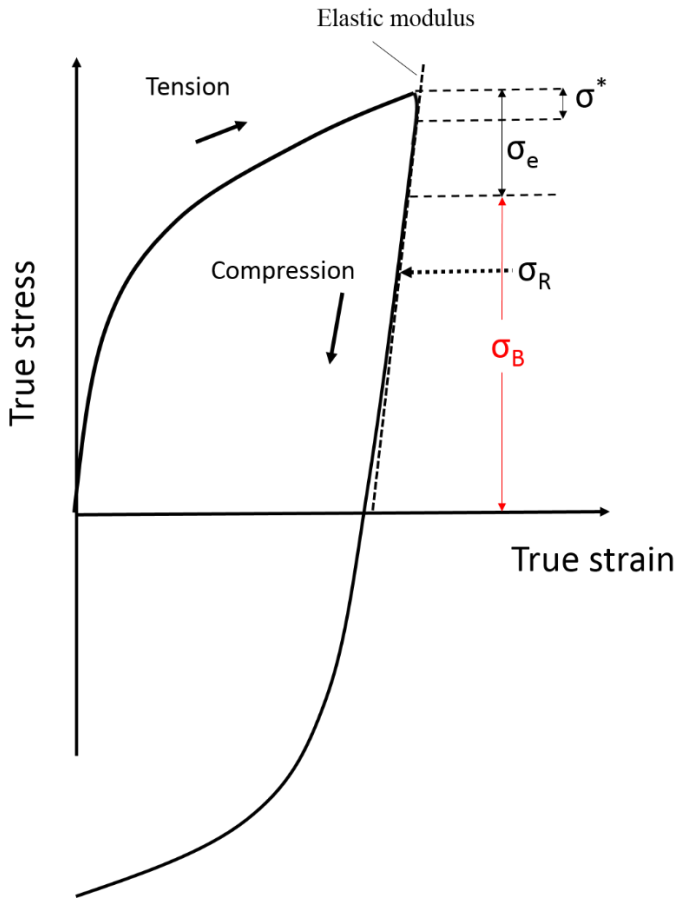

Figure 4.7 Illustration showing the measurement way of the back stress (σ_{Back}) from the tension-compression test.

4.3 Results

4.3.1 Microstructure

The grain boundary map of the starting specimen, ECAP processed specimen and the specimen ECAP processed and subsequently annealed at different temperatures for 1 hour are shown in **Figure 4.8**. The mean grain sizes were measured as the mean interval of the high angle grain boundaries (HAGB) along the ND direction. As can be seen, various mean grain sizes were obtained through the ECAP and subsequent annealing process.

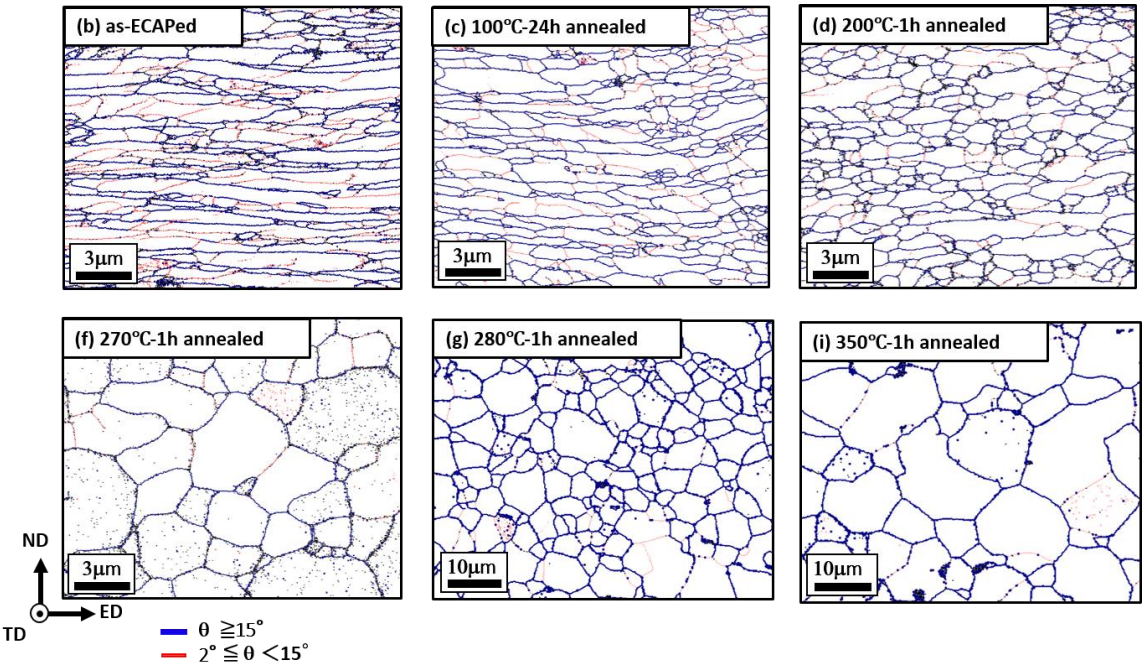

Figure 4.8 EBSD grain boundary maps of the specimens having mean grain sizes of (a) 0.56 μm (as-ECAP processed), (b) 0.51 μm (ECAP processed and 100°C annealed), (c) 0.6 μm (ECAP processed and 200°C annealed),(d)1.5 μm (ECAP processed and 270°C annealed), (e)3.8 μm (ECAP processed and 280°C annealed) and (f) 6.0 μm(ECAP processed and 350°C annealed).

4.3.2 Mechanical behavior

4.3.2.1 Monotonic tensile test

Monotonic tensile stress-strain curves of the specimens having different mean grain sizes are shown in **Figure 4.9**. The yield strength greatly increased by decreasing the mean grain size. Meanwhile the uniform elongation gradually decreased as the mean grain size decreased down to 2.0 μm, and then abruptly dropped to less than 2%. It is noteworthy that the specimens having the grain sizes larger than 3.8 μm exhibited continuous yielding, while a yield point phenomena appears when the mean grain size is smaller than 3.8 μm. A distinct yield drop, followed by a region of a stress plateau can be clearly observed in the specimen having the grain size of 1.5 μm (in pink color). Lüders band deformation was also observed on the specimen surface during the tensile test of the round-bar specimens. As the mean grain size becomes smaller than 1.5 μm, necking immediately occur after the yield point. Severe shear band deformation was observed on the surface of those specimens whose grain size was smaller than 1.5 μm, as shown in **Figure 4.10**.

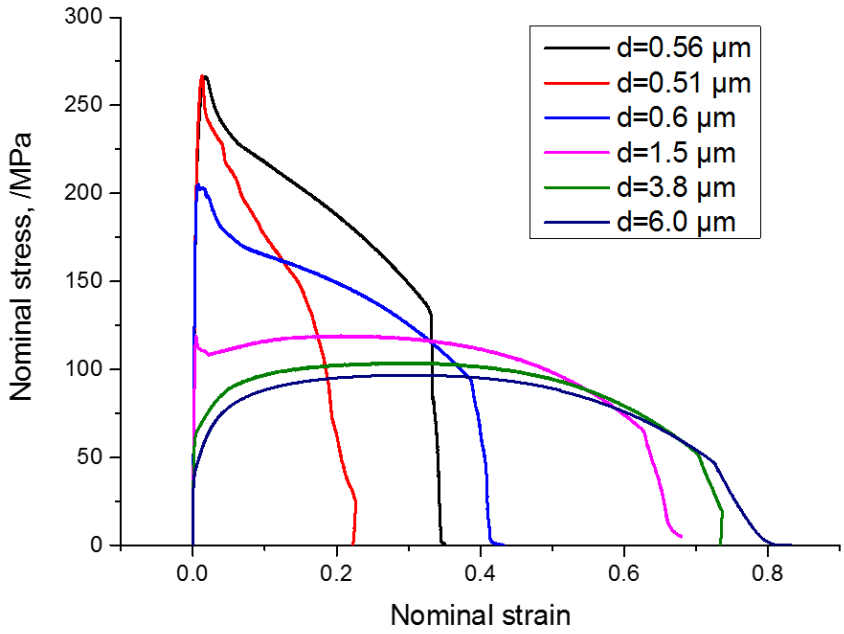

Figure 4.9 Monotonic tensile stress-strain curves of the as-ECAP processed specimen (d=0.56 μm) and subsequently annealed specimens having different mean grain sizes ranging from 0.56 μm to 6 μm.

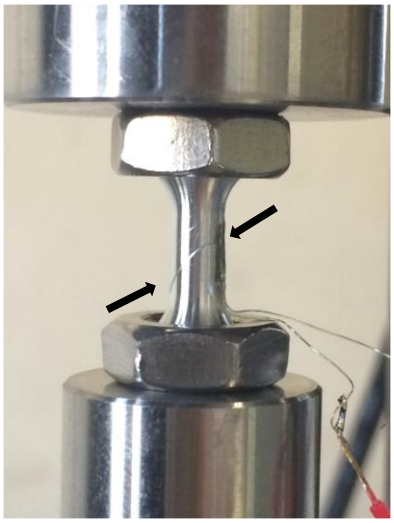

Figure 4.10 Surface morphology of the specimen having the grain size of 0.6 μm, after the tensile test. Severe shear bands (localized deformation) can be seen.

The stress-strain curves at a small strain stage of **Figure 4.9** are exaggerated and shown in **Figure 4.11**. The specimen annealed at 100°C having a mean grain size of 0.51 μm

showed an even higher yield stress than the as-ECAP processed specimen, which should be attributed to the "hardening by annealing" behavior in the ultra-fine grain materials [18]. It should be also noted that the flow stress deviated from the elastic modulus (E=69GPa) at a very early stage in the specimens showing the yield point phenomena. In other words, a certain amount of plastic deformation has already occurred before the macroscopic yield point in those specimens.

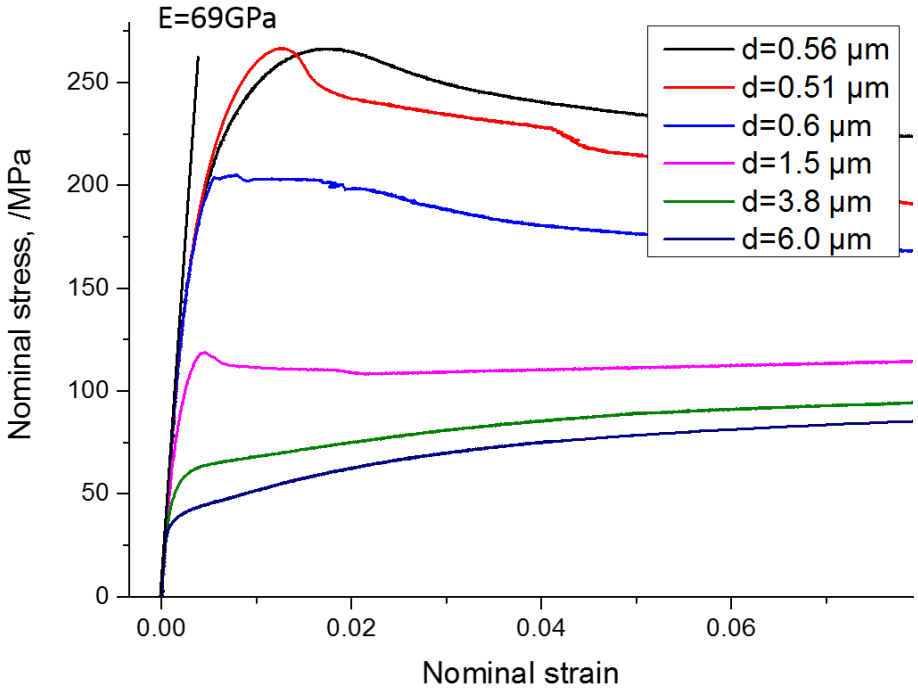

Figure 4.11 Tensile stress-strain curves at small strain range of the specimens having various mean grain sizes. The elastic modulus of the pure Al is also given in the figure so that the plastic strain before the macroscopic yield point can be realized.

Monotonic compression tests were also conducted for the specimen having each grain size before the Bauschinger test, in order to examine the asymmetry of tension-

compression yield stress. It was confirmed that there was almost no difference between the compressive yield stress and the tensile yield stress for all the grain sizes.

4.3.2.2 The Hall-Petch relationship

Yield stress obtained from the tensile test is plotted as a function of $d^{-1/2}$ in **Figure 4.12** (Hall-Petch plot). The 0.2% offset proof stress was taken as the yield stress. The Hall-Petch relationship for conventionally coarse grain sized 2N-Al [19] is also plotted in a dashed line. It can be seen that the yield stress of the specimen having the grain size of 6.0 μm is almost on the line of the conventional Hall-Petch relationship of Al. As the mean grain size decreases to be smaller than 6.0 μm, the yield stress starts to positively deviate. It is seen that another distinct Hall-Petch relationship is recognized depending on the average grain size range, with the different values of k_y and σ_0. In the fine grain size range (d = 0.5 ~ 3.8 μm), a very high k_y value (160MPa· $\mu m^{1/2}$) and a negative σ_0 (-30MPa) are obtained. This is the so-called "extra-hardening" which has been also observed in fine grained IF steel in **Figure 3.4** in Chapter 3.

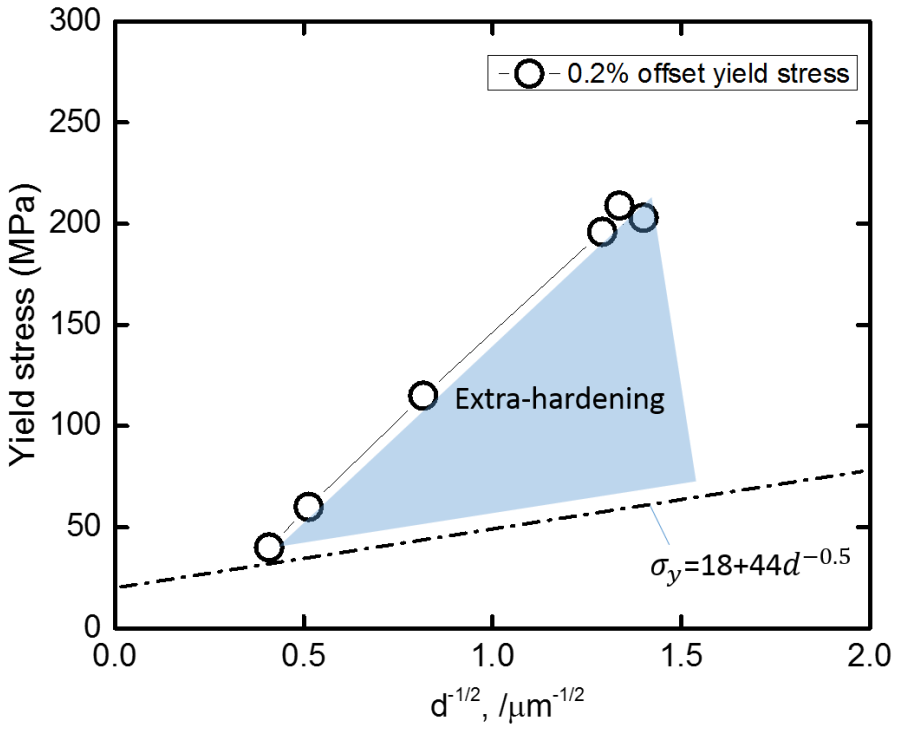

Figure 4.12 Yield stress of the 2N-Al specimens plotted as a function of inverse square root of the mean grain size (Hall-Petch plot). The Hall-Petch relationship obtained by the conventionally coarse grain sized Al [19] is shown by the dashed line and the extra-hardening region is emphasized by the blue color.

4.2.3.3 Bauschinger tests

Stress-strain curves obtained from the monotonic tensile test and Bauschinger tests of the specimen having the coarse grain size (d=3.8 μm) are displayed in **Figure 4.13 (a)**. The stress-strain curves at small strain range is enlarged in **Figure 4.13 (b)**, in which the measured back stress is also shown. It is seen that as the pre-strain (e_1) increases from around 0.001 to 0.008, the flow stress increases from 50 MPa to 70 MPa and the back stress increases from 22 MPa to 44 MPa. The increase in the flow stress (20MPa) is almost equal

to the increase in the back stress (22MPa). The stress-strain curves and enlarged stress-strain curves of the as-ECAP processed specimen having UFG microstructure (d=0.51 μm) are shown in **Figure 4.14 (a)** and **(b)**, respectively. It can be seen in **Figure 4.14 (b)** that as the pre-strain (e_1) increases from 0.002 to 0.008, the flow stress increases from 150 MPa to 250 MPa and the back stress increases from 85MPa to 165MPa. Similarly, the increase in the back stress (80MPa) contributes to the most of the increase in the flow stress (100 MPa). By comparing the back stress value in the two specimens having different grain sizes, it can be realized that the increasing in the flow stress, in other words, the strain hardening at early stages of the tensile test, mostly comes from the increasing in the back stress in both coarse grain sized specimen and UFG specimen. On the other hand, the back stress is significantly higher in the UFG material than that in the coarse grain sized material.

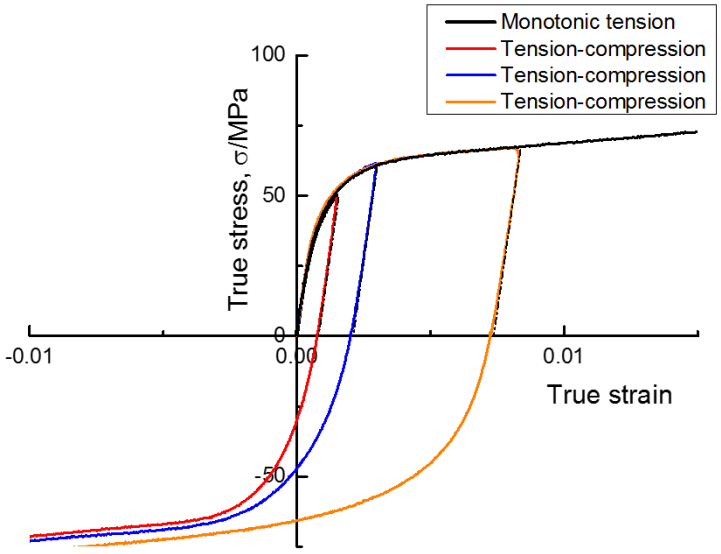

(a)

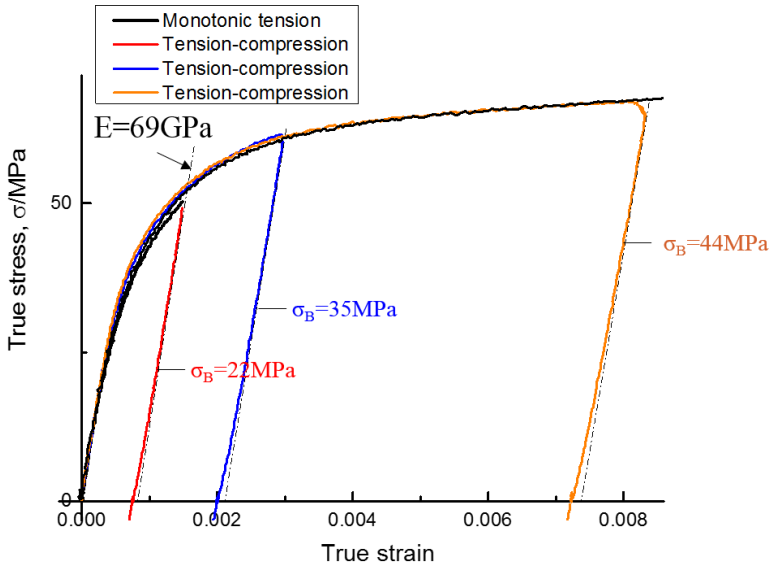

(b)

Figure 4.13 (a) Monotonic tensile stress-strain curve and stress-strain curves obtained from the Bauschinger tests of the specimen having d=3.8 μm. (b) Enlarged stress-strain curves in the small strain range. The value of back stresses are indicated in **(b)** and elastic modulus of pure Al (E=69GPa) is indicated on the unloading parts by the dashed lines.

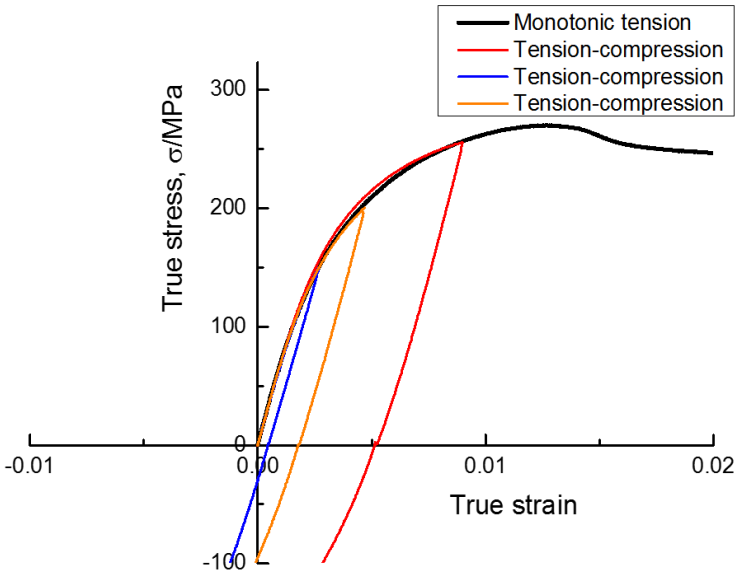

(a)

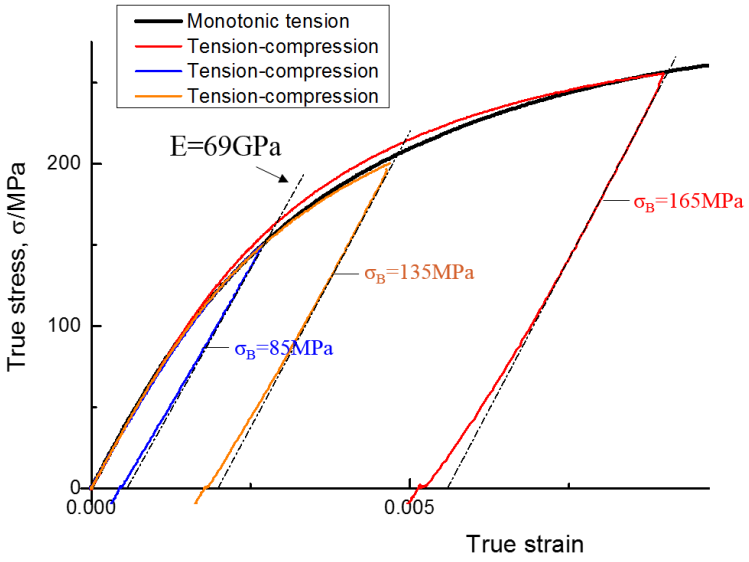

(b)

Figure 4.14 (a) Monotonic tensile stress-strain curve and stress-strain curves obtained from the Bauschinger tests of the as-ECAP specimen having d=0.51 μm. (b) Enlarged stress-strain curves in the small strain range. The value of back stresses are indicated in **(b)** and elastic modulus of pure Al (E=69GPa) is indicated on the unloading parts by the dashed lines.

In **Figure 4.15**, the measured back stresses are plotted as a function of the pre-plastic strain in the first tension for the specimens having various grain sizes. It can be observed that the back stress becomes higher when the mean grain size decreases at any identical plastic pre-strain. In the pre-strain range $\varepsilon=0\sim0.005$ and $\varepsilon=0.03\sim0.07$, the back stress monotonically increases with increasing the pre-strain. The difference in the back stress between the specimens having various mean grain sizes is significantly large at the small pre-strain range ($\varepsilon=0\sim0.005$), compared with that in the relatively large pre-strain range ($\varepsilon=0.03\sim0.07$), indicating a strong grain size dependence of the back stress in the small pre-strain range ($\varepsilon=0\sim0.005$) and a weak dependence of the back stress in the large pre-strain range ($\varepsilon=0.03\sim0.07$).

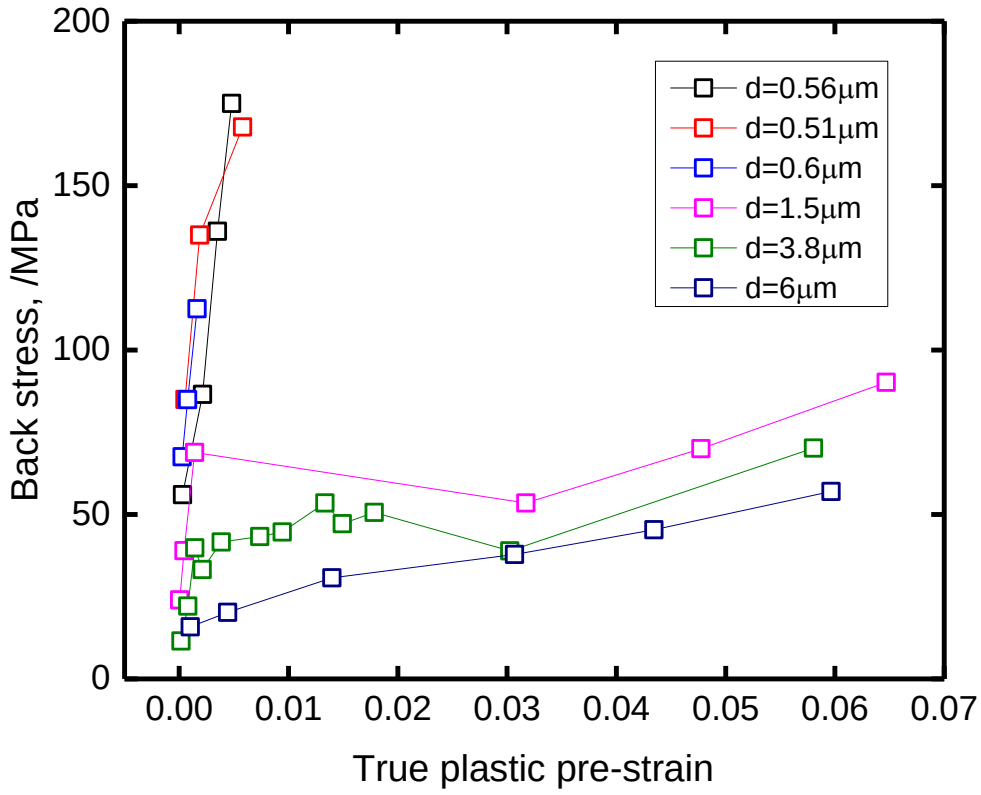

Figure 4.15 The back stress measured form the stress-strain curve of the specimens having different mean grain sizes, plotted as a function of the pre-plastic strain (e_1) in the true strain.

It is very interesting that in the coarse grain sized specimens (d=3.8 μm and d=1.5 μm) the back stress firstly increased, then decreased and increased again with increasing the pre-strain in a small strain stage ($\varepsilon < 0.04$). For the specimen having d=1.5 μm, the Bauschinger test could not be done in the pre-strain of $\varepsilon=0.0015 \sim 0.03$ because during which the inhomogeneous deformation was induced by Lüders bands. However, it still can be realized that the back stress monotonically increases before the macroscopic yield point and decreases just after the propagation of the Lüders band.

In the specimen having the grain size of 3.8 μm, the back stress continuously decreases as the pre-strain increases in the strain range of $\varepsilon=0.012\sim0.03$, although the flow stress in tension monotonically increases with increasing the plastic strain.

For the specimens having ultra-fine grain sizes ($d=0.51 \sim 0.6$ μm), the Bauschinger tests could be only conducted at the pre-strain smaller than the macroscopic necking strain, because of the difficulty in the measurement arose with the early strain localization following to macroscopic necking.

4.3 Discussion

4.3.1 Yield point phenomenon and Hall-Petch relation

The yield point phenomenon is usually found in BCC metals such as low carbon steels, Mo, W and in a few FCC metals such as brass (Cu-Zn) and Al-Mg. The yield point phenomenon has been attributed to the release of dislocations from the atmosphere formed by impurity or alloying elements, as proposed by Cottrell in the early days. Later on, based on the Johnston-Gilman theory, Hahn [1] proposed that a sudden dislocation multiplication could also cause the yield point phenomenon, which does not necessarily require dislocation locking mechanism. In Hahn's theory, one of the two necessary conditions are required for the material to exhibit the yield point: either the material has an extremely low dislocation density, and/or the material shows a high sensitivity of the flow stress on dislocation velocity.

In recent decades, it has been shown by many studies that the interstitial free (IF) steel [2], 2N-Al [2], 4N-Al [19], commercial purity Cu [3] and many other metals and alloys can also exhibit the yield point behaviors when the grain size is refined to the UFG range [4], although it is well known that their conventional grain sized counter-parts do not exhibit yield point. Some of those UFG materials, such as commercial purity Al and Cu, do not necessarily satisfied neither Cottrell's theory nor Hahn's theory, due to the lack of impurity atmosphere or having a very low stress-dislocation velocity sensitivity. Thus, it is reasonable to consider that the yield point behavior in those UFG materials is likely due to a grain size effect rather than the dislocation locking mechanism or the velocity dependent flow stress.

The yield point phenomena in the UFG materials are sometimes called “early plastic instability” [20] (although this phrase is usually referred to the macroscopic necking phenomena in the as-deformed materials in the SPD community [14]) and has usually been explained by the poor capability of strain hardening in the UFG materials, coming from the absorption of the dislocations by the large amount of grain boundaries.

In addition, it has been found that the yield stress of the UFG materials is much higher than that predicted by extrapolating the Hall-Petch relationship from conventionally coarse grain size range to UFG range, which is so-called “extra-hardening” . The mechanism of the extra-hardening is still unclear, although it is believed by many researchers that it should be related to the scarcity of the dislocation sources in the UFG materials [18]. It has been concluded in Chapter 3 that the extra-hardening is in close accordance with the appearance of the yield point phenomena in the UFG IF steel. Similar work has been done by Kamikawa by using the 2N-Al and 4N-Al having various grain sizes fabricated by ARB and subsequent annealing processes and the same conclusion was obtained [19], the extra-hardening in the fine grain sized 2N-Al and 4N-Al corresponds to the appearance of the yield point phenomena and the abrupt decrease in the uniform elongation is due to the severe strain localization induced by the yield point. It is thus believed that for the 2N-Al in the present case the extra-hardening also corresponds with the appearance of the yield point phenomena.

4.3.2 Extra-hardening and the back stress

The present results show that the back stress exhibits a very strong grain size dependence in the small strain region and a weak dependence in the large strain region. In

addition, the value of the back stress is significantly higher in the UFG specimens than that in the coarse grain sized specimens. The dependence on the grain size and the amount of the pre-strain is very similar to that of the yield stress. Therefore, it is considered that extra-hardening should be closely related to the back stress in the small strain range.

Because of the limited number of the Bauschinger test specimens, the value of the back stress exactly at 0.2% plastic pre-strain is lacked. However, the back stress at 0.2% plastic strain can be roughly estimated in **Figure 4.16** showing a good linearity with the plastic pre-strain in the small strain range. The estimated back stresses of different specimen at 0.2% plastic strain are plotted in the Hall-Petch plot, as shown in **Figure 4.17**. The red bars represents the amount of the back stress estimated for each specimen from **Figure 4.16**. It is interesting that the amount of the back stress and the degree of the extra-hardening have a good correlation. It is, therefore, likely that the extra-hardening is mainly due to the dramatic increase of the back stress at small strains during the tensile test. The back stress of the as-ECAP processed specimen (d= 0.51 μm) is lower than that of the low temperature annealed specimens (d=0.56 and 0.6 μm), possibly due to the higher dislocation densities retained specimens. This result also suggests that the "hardening by annealing" behavior of the UFG material is closely related to the increase of the back stress.

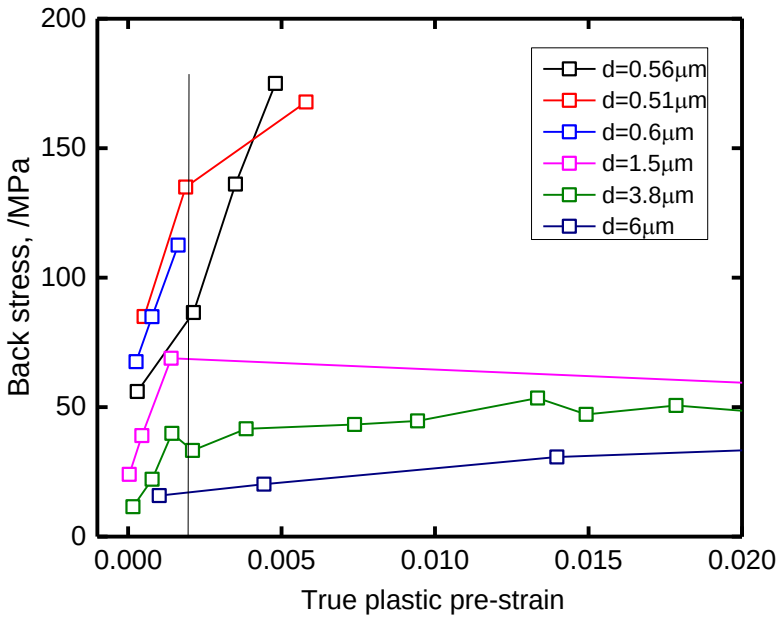

Figure 4.16 Experimentally obtained back stresses at small plastic pre-strain region (0-0.02). The back stresses at the pre-strain of 0.002 of the specimens can be estimated from this figure.

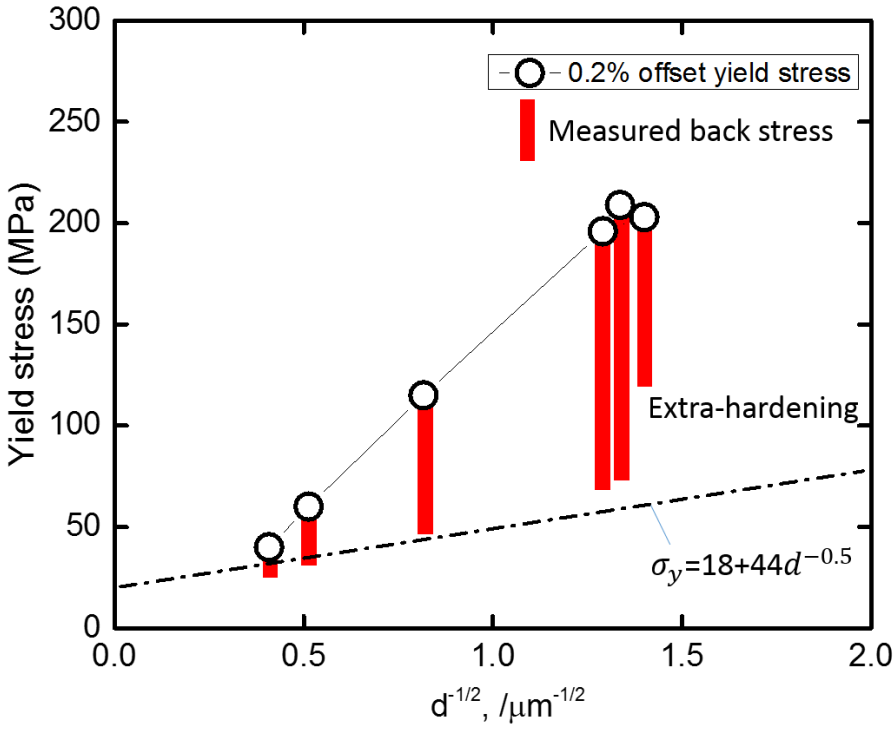

Figure 4.17. The back stresses at 0.2% pre-strain estimated from Figure 4.15 are indicated as the red bars in the Hall-Petch plot. The 0.2% proof stress obtained from the monotonic tensile test for the specimens are also plotted. The Hall-Petch relationship obtained in the conventionally coarse grain sized specimens is also given.

4.3.3 Yield point phenomena and "hardening-softening-hardening" of the back stress

It was very interesting to note in **Figure 4.15** that for the specimen having d=1.5 μm and d=3.8 μm, the back stress firstly increased, then decreased, and increased again as the pre-strain increased in the small-strain range (ε=0 ~ 0.03), exhibiting an "increase-decrease-increase" behavior. Meanwhile, in this small pre-strain range the flow stress of

the specimen having d=3.8 μm monotonically increased. Even for the specimen having d=1.5 μm, which exhibited the yield point phenomena, the flow stress right after the propagation of the Lüders band was higher than that just before the yield point, while the corresponding back stress was smaller after the Lüders band propagation than it is before the yield point. This result indicates that a part of the flow stress even decreases in the small strain range, although the overall flow stress increases with increasing the plastic strain.

From **Figure 4.15**, it can be realized that the evolution of the back stress with the plastic pre-strain can be divided into three stages:

Stage 1 ($\varepsilon=0 \sim 0.01$): the back stress greatly increases with increasing the plastic pre-strain. The level of the back stress strongly depends on the grain size of the material: it is dramatically larger in the specimens having fine grain sizes than that in the ones having coarse grain sizes. The hardening rate of the back stress with pre-strain is significantly higher in this stage than those in the later stages.

Stage 2 ($\varepsilon=0.01\sim 0.03$): the evolution of the back stress starts to behave different depending on the grain size. For the specimens having coarse grain sizes, the back stress is still increasing in this strain range, although the hardening rate starts to decrease, as can be seen in the specimen having d=6 μm in **Figure 4.15**. For the specimens having relative finer grain sizes (d=1.5 and 3.8 μm), the back stress firstly increases and then decreases. For the specimens having grain sizes smaller than 1.5 μm, the back stress could not be measured because of the highly localized plastic strain (necking).

Stage 3 ($\varepsilon=0.03\sim 0.07$): the back stress monotonically increases at a smaller rate with the increasing in the pre-strain, compared with that in the stage 1. The back stress of the specimens having grain sizes smaller than 1.5 μm could not be measured due to necking.

From the above categorization, it is realized that the extra-hardening measured by the 0.2% proof stress in the small grain sized specimens occurs in the stage 1 during which the back stress greatly increases (hardening). In the stage 2 the hardening rate of the back stress decreases and the back stress itself decreases as grain size becomes smaller (softening). In the stage 3 the increase in the back stress is measured in the specimens having the grain sizes larger than 1.5 μm (hardening). Thus, it is reasonable to expect that the decrease of the back stress (softening) in the stage 2 becomes more significant as the grain size decreases to be smaller than 1.5 μm, although unfortunately the decrease of the back stress cannot be measured because of the yield point and subsequent necking. For the same reason, it is believed that the hardening of the back stress followed by the softening could not be measured. The significant decrease in the back stress may lead to the decreasing in the overall flow stress and cause the macroscopic strain localization, such as the yield point phenomena observed in the specimens having the grain sizes smaller than 1.5 μm. Therefore, it is considered that the reason of the yield point phenomena in the UFG 2N-Al is different from that explained by the mobile dislocation theory proposed by Hahn. In Hahn's theory, the yield drop is due to the abrupt decrease in the effective stress caused by the dislocation velocity dependence of the flow stress, while in the present case the yield drop is likely due to the decrease in the back stress (internal stress). The origin of the back stress is discussed in the next section.

4.3.4 Origin of the huge back stress

In the previous section, the important characteristics of the back stress were found: firstly, the back stress exhibits a strong grain size dependence in the stage 1 and a weak grain size

dependence in the stage 2. Secondly, it shows a softening in the stage 2 when the mean grain size is smaller than a critical size.

It is known from the previous researches [16, 17] that the back stress developed during deformation in the polycrystalline material is a long-range internal stress, mainly originating from dislocation interactions with inhomogeneous microstructures, for example, the grain boundary and the dislocation cell structure. Feaugas [16] found that at in the SUS316L stainless steel, the back stress at small strain range originated from the intergranular stress between the neighbouring grains while at larger strain range it originates from the intragranular stress arises from dislocation structures in the grain interior, such as dislocation walls and bundles. A high hardening rate in the back stress was measured at a small strain range and a low hardening rate was measured in a large strain range in Feaugas's research, which is quite similar to the present results of 2N-Al.

TEM microstructures of the as-ECAP processed and annealed 2N-Al specimens are shown in **Figure 4.18**. Relatively "clean" microstructures are realized in the specimens having ultrafine grain sizes, in which the grains have some dislocations in the grain interior but no dislocation walls and bundles are observed. Although the back stress was measured after a certain amount of plastic pre-strain, the microstructure should not change significantly from those shown in **Figure 4.18**, as the plastic pre-strain applied is very small ($\varepsilon=0 \sim 0.01$). Lloyd [21] also showed that in the Al-Mg with ultrafine grain size there were no dislocation substructures forming right after the yield point but only few dislocations in the grain interior. Therefore, it is considered that the huge back stress in the ultrafine grain sized specimens at the small range is not from dislocation substructures. Instead, the huge back stress is likely due to the intergranular stress originating from the

interaction between the dislocation pile-up and grain boundaries. During tensile deformation, the pre-existing dislocations would be blocked by the grain boundaries and pilling up against grain boundaries. The back stress given by the dislocation pile-up can dramatically increase with increasing of the number of the pile-up dislocations or with decreasing the pile-up length, according to the following equation:

$$\tau = \frac{n\mu b}{(1-\upsilon)\pi D} \tag{4.3}$$

where τ is the shear stress on the front dislocation, μ the shear modulus, b the Burgers vector and n the number of the pile-up dislocations and D the grain size (pile-up length). It is seen that a large shear stress can be developed by decreasing the grain size or increasing the number of the pile-up dislocations. Therefore, a huge back stress in the UFG materials can be expected from the dislocation pile-up even at small plastic strain, which contributes to the extra-hardening.

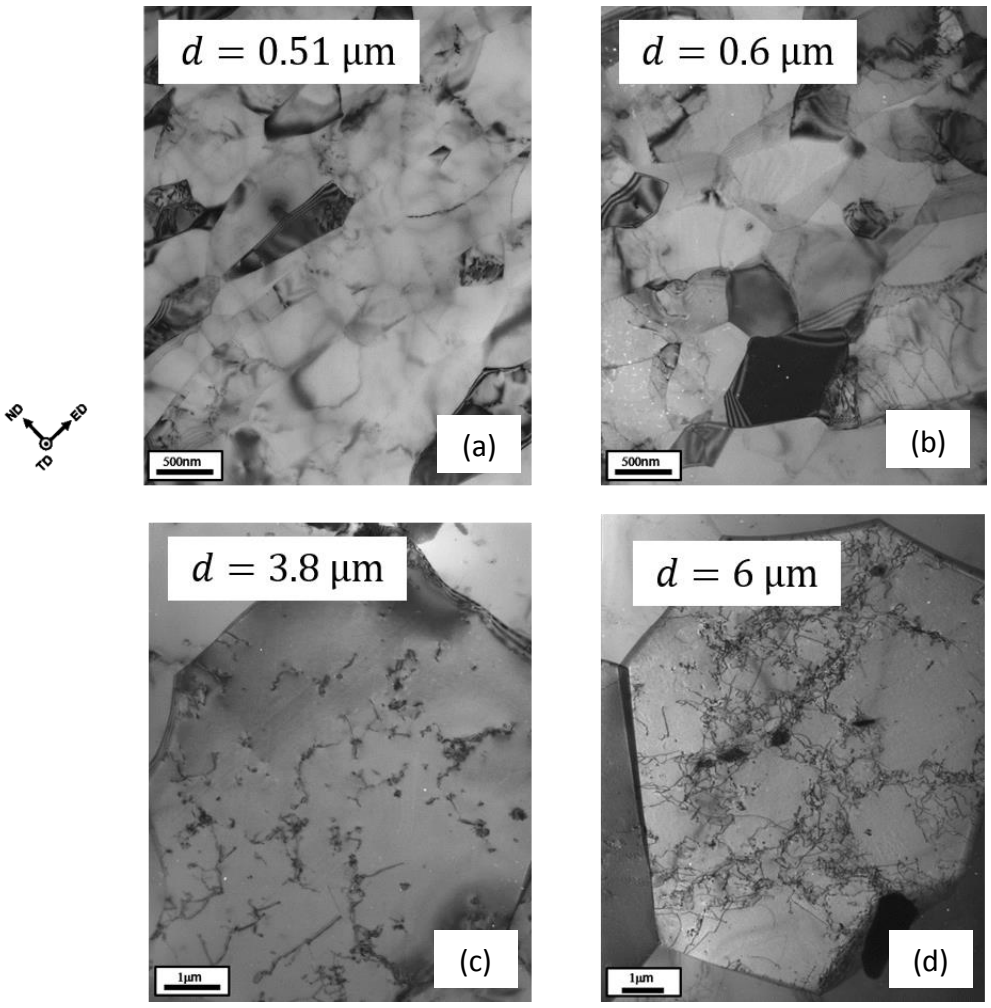

Figure 4.18. Microstructures of the specimen having grain size (a)d=0.51 μm (b) d=0.6 μm (c) d=3.8 μm (d) d=6 μm, observed by TEM.

On the other hand, the decrease of the back stress (softening) in the stage 2 can be understood from the decrease of the intergranular stress at grain boundaries. In the stage 2, the dislocation pile-up would activate the dislocation sources in the neighboring grain or on the grain boundaries so as to decrease the stress concentration, resulting in a decreasing in the intergranular back stress. Sinclair [22] proposed a physical model for the strain hardening behavior of the fine grain sized copper based on the dislocation pile-up and

forest dislocation hardening. He believed that the initial high work hardening rate of the UFG specimen was due to the accumulation of the pile-up dislocations. As the plastic strain increases, the stress fields of those dislocation pile-ups would have a chance to be "screened", namely dislocations with opposite sign would decrease the stress field of the dislocation pile-up. At the beginning of plastic deformation, the dislocation density is relatively small, so that the stress field due to the pile-up dislocations can dramatically increases. When the plastic strain increases to some certain level, the stress-field of the pile-up dislocations would be sufficiently screened – resulting in a decrease in the back stress. It should be emphasized that by any stress relaxation process on the grain boundaries, either the screening of the stress field, or activation of dislocation sources, or cross-slip occurring at the head of the dislocation pile-up, the intergranular back stress can decrease, causing the softening in the stage 2.

In the stage 3, the back stress starts to increase again, mainly rising from the formation of the inhomogeneous submicrostructures in the grain interior, such as dislocation walls and bundles, or even low angle grain boundaries. For the specimens having coarse grain sizes, for example, d=3.8 μm and d=6 μm in the present case, the decrease of the hardening rate of the back stress in the stage 1 is quite small, thus the overall strain hardening in the flow stress occurs. For the specimens having finer grain sizes, for example, d= 1.5 μm, the decreasing of the back stress hardening rate in stage 2 becomes more, leading to the softening in the global flow stress and causing the yield point phenomenon and Lüders deformation. For the specimen having much finer grain sizes, such as the specimens having d smaller than 1 μm in the present case, decreasing of the back stress in stage 2 is so large that the following back stress hardening in stage 3 cannot compensate the softening

occurred in the stage 2, and then a significant yield drop occurs in tensile deformation, leading to an immediate necking to failure.

4.4 Conclusion

By the tension-compression test, a significantly large back stress was measured in the specimens with ultra-fine grain (UFG) sizes, compared with that in the coarse grain sized specimens. It was demonstrated that the large back stress was the main contribution to the extra-hardening occurred in the UFG materials.

The back stress firstly increased, then decreased and increased again with the increase of the pre-strain at a very beginning of the plastic deformation (plastic strain smaller than 3%) in the relatively coarse grain-sized specimens. This result gave a possible explanation of the dramatic loss in the uniform elongation, or early plastic instability, of the UFG materials: the decrease of the back stress at early plastic strain stage significantly lowers the overall strain hardening rate of the material, resulting in a drop in the uniform elongation.

Reference

[1] Hahn, G. (1962). A model for yielding with special reference to the yield-point phenomena of iron and related bcc metals. *Acta Metallurgica*, *10*, 727.

[2] Tsuji N, Ito Y, Saito Y, Minamino Y (2002) Strength and ductility of ultrafine grained aluminum and iron produced by ARB and annealing. Scripta Mater 47: 893-899.

[3] An H, Wu S, Zhang Z, Figueiredo RB, Gao N, Langdon TG (2012) Enhanced strength–ductility synergy in nanostructured Cu and Cu–Al alloys processed by high-pressure torsion and subsequent annealing. Scripta Mater 66: 227-230.

[4] Li Z, Fu L, Fu B, Shan A (2013) Yield point elongation in fine-grained titanium. Mater Lett 96: 1-4.

[5] E. Orowan, Internal Stress and Fatigue in Metals, Elsevier (1958), p.59.

[6] Saada, G., Kruml, T. (2012). Removal of plastic instabilities by reversal of the applied stress. *Philosophical Magazine*, 1–16.

[7] Taupin, V., Varadhan, S., Fressengeas, C., & Beaudoin, a. J. (2008). Directionality of yield point in strain-aged steels: The role of polar dislocations. *Acta Materialia*, *56*(13), 3002–3010.

[8] A. Abel, Historical Perspectives and Some of the Main Features of the Bauschinger Effect, Mater. Forum, 1987, 10, 11-26.

[9] A.Seeger, ‘’Kristallplastizität, Handbuch der Physik, band Ⅶ/2 (1958) [Springer-verlag].

[10] E. Orowan, ‘’Internal Stress and Fatigue in Metals’’, Elsevier (1958), p.59.

[11] Kaneko, Y., Hayashi, S., Vinogradov, A. (2013). Cyclic Response of SUS316L Stainless Steel Processed by ECAP, *54*(9), 1612–1618.

[12] Wu, X., Yang, M., Yuan, F., Wu, G., Wei, Y., Huang, X., Zhu, Y. (2015). Heterogeneous lamella structure unites ultrafine-grain strength with coarse-grain ductility, 1–6.

[13] Li, L., Van Petegem, S., Van Swygenhoven, H., Anderson, P. M. (2012). Slip-induced intergranular stress redistribution in nanocrystalline Ni. *Acta Materialia*, *60*(20), 7001–7010.

[14] Azushima, A., Kopp, R., Korhonen, A., Yang, D. Y., Micari, F., Lahoti, G. D., Yanagida, A. (2008). Severe plastic deformation (SPD) processes for metals. *CIRP Annals - Manufacturing Technology*, *57*(2), 716–735.

[15] G. K. Williamson and W. H. Hall. Acta Metall. 1 (1953), 22-31.

[16] Feaugas, X. (1999). On the origin of the tensile flow stress in the stainless steel AISI 316L at 300 K: back stress and effective stress. *Acta Materialia*, *47*(13), 3617–3632. doi:10.1016/S1359-6454(99)00222-0

[17] Feaugas, X., Haddou, H. (2007). Effects of grain size on dislocation organization and internal stresses developed under tensile loading in fcc metals. *Philosophical Magazine*, *87*(7), 989–1018.

[18] Huang X, Hansen N, Tsuji N (2006) Hardening by annealing and softening by deformation in nanostructured metals. Science 312: 249-251.

[19] Kamikawa N, PhD thesis, 2005, Osaka University.

[20] Vinogradov, A. (2015). Mechanical Properties of Ultrafine-Grained Metals: New Challenges and Perspectives. *Advanced Engineering Materials*, n/a–n/a. doi:10.1002/adem.201500177

[21] Lloyd, D. J., Jin, H. (2013). Inhomogeneous yielding and work hardening of a fine grained Al–Mg alloy. *Materials Science and Engineering: A*, *585*, 455–459.

[22] Sinclair, C. W., Poole, W. J., & Bréchet, Y. (2006). A model for the grain size dependent work hardening of copper. *Scripta Materialia*, *55*(8), 739–742.

Chapter 5 Conclusion

The present study investigated the yield point phenomena in the polycrystalline materials having fine grain sizes, with a special focus on the UFG IF steel and 2N-Al fabricated by SPD and subsequent annealing processes. A good correspondence between the yield point phenomena and the extra-hardening in the Hall-Petch relationship was experimentally found in the UFG materials. Moreover, it was shown by the DIC analysis that the yield point phenomena played a very important role in the ductility of the UFG IF steel. An unexpected high internal stress was found in the UFG 2N-Al by the tension-compression test, which was considered to be responsible for the extra-hardening phenomena. The yield point phenomena in the UFG Al was related to the decreasing of the internal stress during plastic deformation.

In Chapter 1 of the thesis, the background and purpose of the study were introduced.

In Chapter 2, the effect of interstitial impurity atoms on the yielding behaviors of an ultra-low carbon steel was studied. Cold rolling and subsequent annealing were carried out on an ultra-low carbon steel containing 11 ppm carbon and 8 ppm nitrogen in order to obtain the specimens having different mean grain sizes ranging from 15 μm ~ 50 μm. After annealing, the specimens were either water-cooled (WC) or air-cooled (AC) to room temperature. Tensile test revealed that the WC specimen exhibited continuous yielding while the AC specimens exhibited discontinuous yielding. The strain-ageing experiment was carried out on the specimen and it was confirmed that the discontinuous yielding was due to the dislocation locking mechanism by interstitial atoms such as carbon and nitrogen

in the material. The difference in the yielding behavior between the WC and AC specimens was attributed to the different state of interstitial atoms changed by the cooling methods. In addition, it was found that the Hall-Petch slope, k_y, was significantly higher in the AC specimens exhibiting discontinuous yielding than that in the WC specimens. Relation between the yielding behavior and the Hall-Petch relationship was discussed based on the physical model of the Hall-Petch relationship.

In Chapter 3, the grain size effect on the yielding behavior and the uniform elongation was studied by using an interstitial free (IF) steel, in which the interstitial atoms were substantially scavenged by adding Ti. Accumulative roll-bonding (ARB) process and subsequent annealing were applied to the IF steel to fabricate the specimens having various mean grain sizes from conventional range (larger than tens micron-meters) to ultrafine range. It was found by the tensile test that discontinuous yielding appeared even in the IF steel when the mean grain size was decreased to smaller than 2 μm. The yield stress showed an "extra-hardening". Namely, it became higher than that predicted by the Hall-Petch relationship extrapolated from the conventionally coarse grain size range. The extra-hardening shows a good correspondence with the appearance of the discontinuous yielding. In addition, the uniform elongation of the material abruptly decreased to less than 2% when the mean grain size was smaller than 1 μm. By the digital image correlation (DIC) analysis, it was found that the dramatic drop in the uniform elongation in the UFG range was due to the severe strain localization caused by the discontinuous yielding.

In Chapter 4 the mechanism of the yield point phenomena and the extra-hardening in the UFG materials were investigated. A 99%-purity Al (2N-Al) having various mean grain sizes was fabricated by the equal-channel angular pressing (ECAP) and subsequently

annealing process. It was found that the discontinuous yielding and extra-hardening also appeared in the 2N-Al when the mean grain size of the material decreased to smaller than 3.8 μm. Tension-compression Bauschinger test was carried out on the dumbbell-shaped 2N-Al specimens in order to measure the internal stress during plastic deformation. It was found that the internal stress was significantly higher in the specimens having fine grain sizes than that was in the coarse grain sized specimens. It was considered that the extra-hardening in the UFG specimen was due to the significantly high internal stress and the yield point phenomena in the UFG Al was attributed to the decrease of the internal stress. The reason of the high internal stress is believed to be given by the dislocation pile-up against grain boundaries in the UFG material.

The present work investigated the yield point phenomena in ultrafine grained polycrystalline materials in details and deepened the understanding of the grain size effect on the strength and ductility of the materials. More theoretical and experimental works on the interaction between the dislocation and grain boundary is expected to be done in the future. From the aspect of the practical use of the UFG materials, further research works are required on how to diminish the yield point phenomena and enhance the tensile ductility of the materials having ultra-fine grain sizes.

ACKNOWLEDGEMENTS

My deepest gratitude goes first to my supervisor, Professor Nobuhiro Tsuji, for his excellent scientific guidance and constant supports through my master and doctor course. I also would like to express my gratitude to Dr. Akinobu Shibata and Dr. Daisuke Terada, who have patiently instructed me and helped me a lot with experiments; Professor Zenji Horita of Kyushu University and Professor Yoshihisa Kaneko of Osaka City University who kindly providing me the access to their experimental equipments; Professor Yasuharu Shirai and Professor Haruyuki Inui, for evaluating my dissertation and giving their valuable advices. Professor Ronald W. Armstrong of University of Maryland, Dr. Xiaoxu Huang of Technical University of Denmark (DTU) and Dr. Naoya Kamikawa of Hirosaki University are to be thanked for the fruitful discussions on the subjects of yielding behavior and Hall-Petch relationship through these years.

I am greatly indebted to Ms. Akiko Koike, the secretary of our laboratory, who always kindly helped me for various affairs. In addition, I am thankful to all of my laboratory members for their kind help and support.

The financial support from the doctor fellowship (2015 ~ 2016) of the Japan Society for the Promotion of Science (JSPS) is greatly appreciated.

At last, I wish to thank my parents, for their constant love and support at all times.

LIST OF PUBLICATIONS

International journal paper

1) Si Gao, Meichuan Chen, Mohit Joshi, Akinobu Shibata, Nobuhiro Tsuji, "Yielding Behavior and Its Effect on the Uniform Elongation in IF Steel with Various Grain Sizes", ***Journal of Materials Science***, Volume 49, Issue 19, pp 6536-6542, 2014

2) Si Gao, Akinobu Shibata, Meichuan Chen, Nokeun Park, Nobuhiro Tsuji,"Correlation between Continuous / Discontinuous Yielding and Hall-Petch Slope in High Purity Iron", ***Materials Transactions***, Vol.55, pp.69-72, 2014

3) Si Gao, Meichuan Chen, Shuai Chen, Naoya Kamikawa, Akinobu Shibata, Nobuhiro Tsuji, "Yielding Behavior and Its Effect on Uniform Elongation of Fine Grained IF Steel",***Materials Transactions***, Vol.55, pp. 73-77, 2014

4) Shuai Chen, Akinobu Shibata, Si Gao, Nobuhiro Tsuji, "Formation of Fully Annealed Nanocrystalline Austenite in Fe-Ni-C Alloy",***Materials Transactions***, Vol. 55, pp. 223-226, 2014

5) Sunisa Khamsuk, Nokeun Park, Si Gao, Daisuke Terada, Hiroki Adachi and Nobuhiro Tsuji,"Mechanical Properties of Bulk Ultrafine Grained Aluminum Fabricated by Torsion Deformation at Various Temperatures and Strain Rates",***Materials Transactions***, Vol.55, pp.106-113, 2014

(2) International proceeding papers

1)S.Gao, M.Chen, N. Kamikawa, A.Shibata, N.Tsuji, "Yielding behavior and Hall-Petch relation in fine grained IF steel" *Proceedings: 35th Risoe International Symposium on Materials Science*, (2014)

2)Si Gao, Akinobu Shibata, Nobuhiro Tsuji, "Yielding Behaviors and Hall-Petch Coefficient in Pure Iron", *Proceedings: 35th Risoe International Symposium on Materials Science*, (2012)

3) Hongxing Li, Si Gao, Yanzhong Tian, Daisuke Terada, Akinobu Shibata, Nobuhiro Tsuji. "Influence of Tempering on Mechanical Properties of Ferrite and Martensite Dual Phase Steel", *Materials Today: Proceedings*, 2, pp.667-671, (2015)

4) Shuai Chen, Akinobu Shibata, Lijia Zhao, Si Gao, Yanzhong Tian, Nobuhiro Tsuji,"Microstructural evolution of metastable austenitic steel during high-pressure torsion and subsequent heat treatment", *IOP J. Materials Science and Engineering*, Volume 63, (2014)

5) Mohit Joshi, Yuko Fukuta, Si Gao, Nokeun Park, Daisuke Terada and Nobuhiro Tsuji, "Fabrication of fine recrystallized grains and their mechanical property in HPT processed pure magnesium", *IOP J. Materials Science and Engineering*, Volume 63, (2014)

(3) Presentations in international conference

1) S.Gao, M.Chen, A.Shibata, N. Kamikawa, N.Tsuji, "Strain localization during tensile test of IF steel with various grain sizes", *17th International Conference on the Strength of Materials* (ICSMA 17), Brno (Czech Republic), August 2015. (Oral presentation)

2) S.Gao, M.Chen, N. Kamikawa, A.Shibata, N.Tsuji, "Yielding behavior and Hall-Petch relation in fine grained IF steel",*35th Risoe International Symposium on Materials Science*, Roskilde (Denmark), September 2014. (Oral presentation)

3) Si Gao, Meichuan Chen, Mohit Joshi, Akinobu Shibata, Nobuhiro Tsuji"Yielding Behavior and Its Effect on the Uniform Elongation in IF Steel with Various Grain Sizes",*TMS 2014 Annual meeting*, San Diego (USA), February 2014. (Oral presentation)

4) Si Gao, Meichuan Chen, Shuai Chen, Naoya Kamikawa, Akinobu Shibata, Nobuhiro Tsuji"Yielding Behavior and Its Effect on Uniform Elongation of Fine Grained IF Steel",*International Symposium on Strength of Fine Grained Materials - 60 years anniversary of Hall-Petch relationship*, Tokyo, Japan, July 2013. (Oral presentation)

5) Si Gao, Akinobu Shibata, Nobuhiro Tsuji, "Yielding Behaviors and Hall-Petch Coefficient in Pure Iron", *33rd Risoe International Symposium on Materials Science*, Roskilde (Denmark), September 2012. (Oral presentation),

6) Si Gao, Akinobu Shibata, Nobuhiro Tsuji, "Yielding Behaviors and Hall-Petch Relationship in Pure Iron", *International symposium on Bulk Nano Metals*, Kyoto (Japan), June 2012. (Poster presentation)

7) Shuai Chen, Akinobu Shibata, Lijia Zhao, Si Gao, Yanzhong Tian, Nobuhiro Tsuji"Microstructural evolution of metastable austenitic steel during high-pressure torsion and subsequent heat treatment", *The 6th International Conference on Nanomaterials by Severe Plastic Deformation (NanoSPD6)*, Metz, France, July 2014

8) Mohit Joshi, Yuko Fukuta, Si Gao, Nokeun Park, Daisuke Terada and Nobuhiro Tsuji, "Fabrication of fine recrystallized grains and their mechanical property in HPT processed pure magnesium", *The 6th International Conference on Nanomaterials by Severe Plastic Deformation (NanoSPD6)*, Metz, France, July 2014,

9) Meichuan Chen, Si Gao, Akinobu Shibata, Daisuke Terada and Nobuhiro Tsuji, ‘‘Correlation between Deformation-Induced Martensitic Transformation and Mechanical Properties in TRIP Phenomenon’’, *AIST International Symposium on New Developments in Advanced High Strength Sheet Steels*, Colorado (U.S.A), June 2013.

10) Meichuan Chen, Si Gao, Akinobu Shibata, Daisuke Terada and Nobuhiro Tsuji, ‘‘Characteristics of Deformation Induced Martensite in SUS304 Austenitic Stainless Steel Deformed at RT and -60°C’’, *The 8th Pacific Rim International Conference on Advanced Materials and Processing (PRICM-8),* Hawaii (U.S.A), August 2013.

11) Hongxing Li, Si Gao, Yanzhong Tian, Daisuke Terada, Akinobu Shibata, Nobuhiro Tsuji. “Influence of Tempering on Mechanical Properties of Ferrite and Martensite Dual Phase Steel”, *ICOMAT2014,* Bilbao, Spain. July 2014,

(4) Presentations in domestic conference

1) Si Gao, M.Joshi, 紙川 尚也,柴田 曉伸, 辻 伸泰, “Strain localization during tensile test of IF steel with various grain sizes”, 日本金属鉄鋼協会春季講演大会 2015, 東京大学, 2015 年 3 月

2) S. Gao, M. Chen, J. Mohit, 柴田 曉伸, 辻 伸泰, “Yielding Behavior and Its Effect on the Uniform Elongation in IF Steel with Various Grain Sizes”, 日本金属鉄鋼協会秋季講演大会, 名古屋大学, 2014 年 9 月

3) 紙川尚也、Si Gao、辻　伸泰,”超微細粒金属材料における不連続降伏と異常 Hall-Petch 強化”,日本鉄鋼協会春季講演大会 2014, 東京工業大学, 2014 年 3 月

4) Si Gao, 柴田暁伸, 辻　伸泰, “Yielding Behaviors and Hall-Petch Relationship in Pure Iron”, 『日本金属鉄鋼協会春季講演大会 2012』, 横浜国立大学, 2012 年 3 月.